Jan Mayen

Aeromagnetic Survey 2011/2012 – JAS-12

Part A: acquisition and processing

L. Gernigon, J. Koziel & A. Nasuti

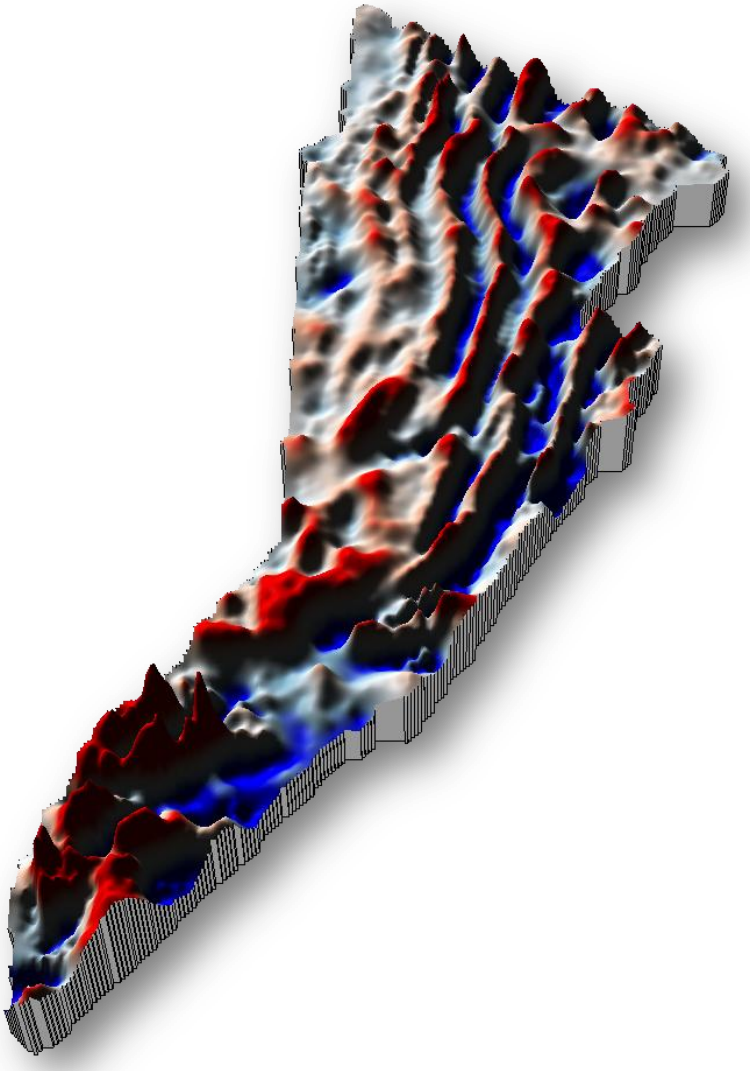

NGU Report. 2012.069. Jan Mayen Aeromagnetic Survey JAS-12 – Part A: acquisition and processing.

NGU Report 2012.69

Jan Mayen Aeromagnetic Survey JAS-12 – Part A: acquisition and processing.

Geological Survey of Norway (NGU)
N-7441 Trondheim, Norway
Tel.: 47 73 90 40 00
Telefax 47 73 92 16 20

REPORT

<table>
<tr><td colspan="2">Report no: 2012.069</td><td>ISSN 0800-3416</td><td colspan="2">Grading: Confidential to December 2017</td></tr>
<tr><td colspan="5">Title:
Jan Mayen Aeromagnetic Survey JAS-12 – Part A: Acquisition, processing.</td></tr>
<tr><td colspan="3">Authors:
Laurent Gernigon, Janusz Koziel and Aziz Nasuti</td><td colspan="2">Clients:
ISOR, Orkustofnun, Norwegian Petroleum Directorate</td></tr>
<tr><td colspan="3">Map-sheet name (M=1:250.000)</td><td colspan="2">Map-sheet no. and -name (M=1:50.000)</td></tr>
<tr><td colspan="3">Deposit name and grid-reference:</td><td colspan="2">Number of pages. 116 Price (NOK).
Map enclosures. 0</td></tr>
<tr><td>Fieldworks carried out:
September 2011-June 2012</td><td>Date of report:
15712/2012</td><td>Project no.:
344300</td><td colspan="2">Person responsible:</td></tr>
<tr><td colspan="5">Summary:

A high sensitivity aeromagnetic survey, JAS-12, was carried out in an area of 80.000 km^2 east of the Jan Mayen microcontinent in the western Norway Basin. Data processing comprised spike-removal and data editing, IGRF corrections, statistical and microlevelling. Several potential field maps were produced from the survey area. Examples of various filters applied to the magnetic field have been illustrated.
One of the major results of this survey was a demonstration of modern, high-resolution aeromagnetic data providing an efficient geophysical tool for better re-mapping of the western Norway Basin, poorly constrained in the past. Trend enhancement and a preliminary interpretation of the survey have been carried out. The magnetic chrons and other new oceanic features have been investigated. The JAS-12 dataset constrains the Continent-Ocean transition (COT) of the eastern margin of the Jan Mayen microcontinent and the subsequent spreading history of the Norway Basin. The survey provides new elements to the discussion of the geodynamic evolution of the Norwegian-Greenland Sea and surrounding volcanic margins and microcontinent. This report (Part A) documents the acquisition and the processing of the JAS-12 survey.</td></tr>
<tr><td>Keywords. Geofysikk</td><td>Berggrunnsgeologi</td><td colspan="3">Magnetometri</td></tr>
<tr><td>Kontinentalsokkel</td><td></td><td colspan="3">Fagrapport</td></tr>
<tr><td></td><td></td><td colspan="3"></td></tr>
<tr><td></td><td></td><td colspan="3"></td></tr>
</table>

CONTENTS

Confidentiality and distribution list

This report is confidential until December 2017 with restricted copies and access. It contains some confidential data not only owned by NGU.

2 copy: NGU library (classified)
1 copy: NGU (Laurent Gernigon)
1 copy: NGU (Aziz Nasuti)
2 copy: NPD (Morten Sand)
1 copy: Orkustofnun (Þórarinn Sveinn Arnarson)
1 copy: ISOR (Anett Blischke)

Laurent GERNIGON (project leader) (1 copy)
Norges geologiske undersøkelse (NGU)/Geological Survey of Norway
Visiting address: Leiv Eirikssons vei 39
Postmail address: P.O. Box 6315 Sluppen
7491 Trondheim, NORWAY
laurent.gernigon@ngu.no

Aziz NASUTI (1 copy)
Norges geologiske undersøkelse (NGU)/Geological Survey of Norway
Visiting address: Leiv Eirikssons vei 39
Postmail address: P.O. Box 6315 Sluppen
7491 Trondheim, NORWAY
Aziz.Nasuti@NGU.NO

Þórarinn SVEINN ARNARSON (1 copy)
Verkefnisstjóri/Hydrocarbon Exploration Manager
Orkustofnun/National Energy Authority
Grensásvegi 9, IS-108 Reykjavík
Iceland
thorarinn.sveinn.arnarson@os.is

Anett BLISCHKE (1 copy)
Íslenskar orkurannsóknir / Iceland GeoSurvey
Department of Energy Technology
Rangarvellir, P.O. Box 30, 602 Akureyri
Iceland
Anett.Blischke@isor.is

Morten SAND (2 copy)
Oljedirektoratet/Norwegian Petroleum Directorate
Professor Olav Hanssens vei 10, PB 600, 4003 Stavanger
Norway
Morten.Sand@npd.no

1 INTRODUCTION

Laurent Gernigon

Like several countries (e.g. Australia, Canada, Finland, Sweden, U.S), Norway was one of the first to support a vigorous government-funded program to develop a countrywide, modern, high-resolution aeromagnetic database. This program includes continuous data acquisition, merging and re-processing of data from individual surveys. In this context, the Geological Survey of Norway (NGU) plays a crucial role in maintaining and continuously updating the national potential field database. NGU's most recent aeromagnetic acquisitions proved the need for modern and new data in order to validate and refine the first order geophysical and geologic features of the Norwegian continental shelf and contiguous oceanic domain. Comparing vintage and modern aeromagnetic surveys is like comparing 2D seismic lines from the 70ies with the most advanced 3D surveys and everybody usually agree that modern data provide much more details and significantly improve our geological knowledge. Consequently, NGU has launched a set of re-mapping projects of the Norwegian continental shelf and adjacent oceanic basins with funding from the petroleum industry and governmental institutions. The need for a new generation of high-quality data becomes a reality for both academy and industry.

1.1 Aeromagnetic data and exploration

The delineation of gravity and magnetic anomalies should normally be the first geophysical method to be applied to a new basin or petroleum province being evaluated or re-evaluated. In frontier and under-explored areas, where seismic data are sparse or non-existent, aeromagnetic acquisition still remains the cheapest and easiest way to get and/or refine the geodynamic and structural setting of the study area. Aeromagnetic data can also be useful to plan strategically new seismic and electromagnetic acquisitions and define potential prospects. Large aeromagnetic surveys can be carried out efficiently and safely almost everywhere, in a short period of time and at a reasonable cost.

Also, when integrated with seismic interpretations, gravity, modern aeromagnetic information can reduce the risks of making faulty geological interpretations. Both gravity and magnetic data are independent of seismic data, both physically and from a measurement point of view. A joint interpretation that combines seismic and other potential field data thus produces a synergy that helps to significantly improve and validate the geological and structural interpretation of sedimentary basins (Fig. 1.1, Table 1.1).

Modern aeromagnetic data are usually applied as a relevant complement for basin and geodynamic interpretation in Norway. If the seismic coverage is poor, it can be jointly combined with gravity data to confirm and/or estimate qualitatively and quantitatively the lateral extent of basement features, lava flows, magmatic intrusions, salt structures or sand channels observed throughout sparse seismic sections (Fig. 1.1). High-resolution aeromagnetic surveys also represent relatively

inexpensive tools for 3D mapping of faults and fracture systems propagating through hydrocarbon-bearing sedimentary levels (Table 1).

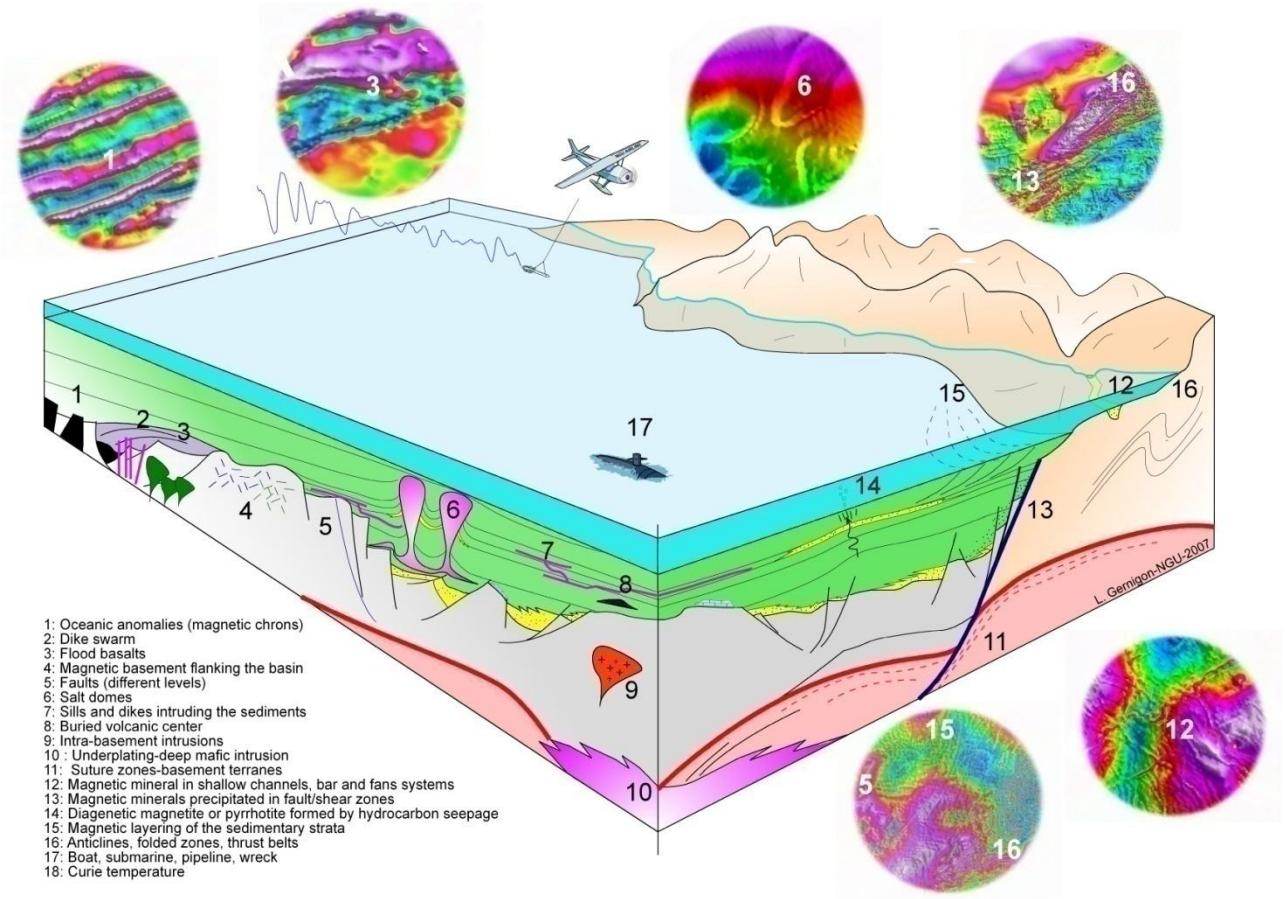

Figure 1.1 3D cartoon and examples of the application of modern NGU aeromagnetic surveys to basin or geodynamic studies. The cartoon illustrates structures and geological units that can cause observable magnetic responses (Gernigon et al. 2007).

A variety of modern techniques to process, display and model the magnetic anomalies are offered for basin analysis. Several magnetic techniques can support the basin analysis and permit to: 1) identify and delineate in depth mafic intrusions and others volcanics, 2) to quantify and evaluate the top of the magnetic basement and infer the location of the thickest sedimentary section, 3) detect subtle intra-sedimentary "micro-magnetic" anomalies and 4) evaluate, to some extent the temperature of the crust (Curie temperature).

WHAT GRAVITY AND MAGNETIC DATA CAN DO FOR YOU
Ten Commandments

1. *Gravity and magnetic surveys are both methods of REMOTE SENSING. They can detect the properties of rocks at a distance - from the air, on the ground or at the sea surface.*
2. *Anomalies and changes in the value of gravity (after allowance for varying elevation and topography) reflect changes in DENSITY.*
3. *Anomalies and changes in the value of the earth's magnetic field (after allowing for changes with time) reflect changes in MAGNETISATION.*
4. *These two properties of rocks are often diagnostic. Taken together they can eliminate many possible geological alternatives and provide fundamental constraints on a geological model.*
5. *Both gravity and magnetic anomalies are a function of the distance between the detector and the sources (rocks). Amplitudes decrease faster with distance for magnetic anomalies therefore they tend to 'see' shallower structures. Both methods, however, provide an INTEGRATED depth spectrum of the sources they are seeing - they see much more than just the surface rocks.*
6. *There are two principal approached to interpretation - PATTERN and SHAPE.*
7. *The PATTERN of a gravity or a magnetic anomaly map is a powerful indicator of how subsurface rocks and formations are distributed. It can provide rapid indications of TRENDS, GRAIN and DISCONTINUITIES. The style of the pattern may be diagnostic of a particular rock sequence or assemblage (for example: sea-floor magnetic anomalies).*
8. *The SHAPE of individual anomalies can be used to determine the shape and position of density of magnetic contrasts (rock units). In theory, there are a number of geometries that will 'fit' a particular anomaly. IN PRACTICE, by using realistic geological or other geophysical controls, anomaly 'fits' will provide REAL NUMERICAL CONSTRAINTS on the anomaly sources.*
9. *However, always understand and appreciate the weaknesses and inaccuracies of the data. Never waste time trying to 'fit' anomalies with greater precision that they were measured at.*
10. *Any final interpretation must satisfy ALL the available geophysical and geological data. Gravity and magnetic anomaly information cannot be ignored. It will not go away. It is real and it is telling us something even if we do not always understand it and even if it appears to be contradicting the surface geology.*

Table 1.1 The Ten Commandments of potential field interpretation (Riddihough, 1986)

1.2 Remapping the Norwegian oceanic domain

Compared to the Norwegian continental shelf or the Barents Sea, the Norwegian oceanic domain is still poorly understood and like other distal margins and frontier areas, scientific interrogations remain. After almost 20 years of under-exploration of the Norwegian oceanic domain, NGU started to re-investigate most of the oceanic domain and the continent-ocean transition in order to get an improved geophysical and geodynamic picture of the Norwegian-Greenland Sea. More precise plate reconstruction and/or advanced basin modelling require such an improved dataset and a complete and modern re-mapping of the oceanic domain is definitively a challenging task.

A detailed account of the spreading history provides crucial information about magmatic production, structures and geodynamics of the oceanic domain. A key element provided by the mapping of the oceanic systems such as the Norway Basin with modern aeromagnetic data is the time. Beginning in the 1950's, geophysicists recognized linear magnetic anomalies (magnetic chrons) across the ocean floor. The discovery of symmetric magnetic anomalies on both sides of mid-oceanic spreading ridges, and the subsequent development of the theory of sea floor spreading confirmed the continental drift theory proposed earlier by Wegener (1924) and revolutionized our understanding of the Earth leading to the theory of plate tectonics established in the late 1960's (Vine and Matthews, 1963).

The correlation between oceanic magnetic anomalies (chrons) and a proper chronostratigraphic scale allows us to constrain accurately the timing of the oceanic accretion. Consequently, we can obtain good age constraints for the oceanic basement and overlying sedimentary sequences. The age of the ocean floor deduced from the magnetic chrons (Cande and Kent 1995) can be used to create a series of palaeotectonic and/or paleogeographic reconstructions. Placed in a time-referenced framework, deformation and movements of first order structures identified from new magnetic data-sets can be evaluated on the basis of several fundamental constraints which provide a means of explaining the tectonic, geological and petroleum evolution of a study area.

Most important, the magnetic pattern can help to locate the ultimate Continental-Oceanic boundary (so-called COB) and delimit the distribution of the pre-breakup sedimentary sequences. In most continental margins, like the mid-Norwegian margin, this issue allows us to define the regional and maximum extend of interesting play concepts. Rift and lithospheric processes in the most distal part of the rifted margin start to be a serious problem as many contributions show that it cannot agree with conventional rift and subsidence prediction models (e.g. McKenzie approach). Advanced modelling suggests that stress and temperature influenced by poorly understood breakup processes and subsequent oceanic spreading can influence the adjacent rifted margin and indirectly its petroleum system. Constraints from the oceanic domain should also provide unambiguous time and petrologic constraints for understanding the thermo-kinematic evolution of rifted margin systems or to calibrate and tie a potential field model.

The first re-investigation of the Norwegian oceanic domain started with the RAS-03 survey along the Lofoten Margin (Olesen et al. 2010) and later with the JAS-05 survey acquired between the

Vøring Marginal High and Jan Mayen in 2005 (Gernigon et al. 2009) and the NB-07 covering the eastern Norway Basin (Gernigon et al. 2008, 2012) (Figs. 1.2, 1.3). These surveys already support our idea that most of the fundamental structures of the Norwegian oceanic basins and adjacent margins have been far from being well constrained and can significantly change our long-believed convictions and inaccurate tectonic and structural models. After analysis of the new datasets, we came up with new challenging hypotheses for the breakup and post-breakup evolution of the mid-Norwegian margin.

One of the first surprising results was probably that some of the "long-believed oceanic fracture zones" simply disappear with such modern datasets. For example, "the Bivrost Fracture Zone" that apparently offset magnetic chrons by 50 km, is just an artefact due to poor quality data (Olesen et al. 2007). When you realise that this trend was used for the last 30 years to guide structural and paleogeographic models offshore Mid-Norway, you may easily imagine the implications of new aeromagnetic acquisitions. Based on the new magnetic compilation and our tectonic analysis of the JAS-05 survey, we also proposed, for example, that a triple junction (ridge-ridge-fracture zone) initiated soon after the breakup between the Vøring Marginal High and the Traill Ø-Vøring igneous complex, now located offshore Greenland (Olesen et al. 2007; Gernigon et al. 2009). In places where a component of opening motion occurs along or close to a pre-existing oceanic transform, magmatic activity could have increased locally along such a "leaky transform" acting as a third branch. This early tectono-magmatic process could be compared to the active and more exotic Azores system, which can be used as a modern analogue to the vintage Norwegian spreading system, initiated 55 Ma ago (Gernigon et al. 2009). This model proposes a younger and post-breakup interpretation of the TraillØ-Vøring igneous complex earlier interpreteted as contemporaneous to the volcanics observed on the Vøring Marginal High by Olesen et al. (2007).

The Norway Basin, particularly investigated in this report is an aborted oceanic basin formed during the onset of breakup between Norway and the coupled Greenland/Jan Mayen conjugate system in the Early Tertiary (~55 Ma ago) (Planke and Eldholm 1994; Saunders et al. 1997; Storey et al. 2007; Karson and Brooks 1999; Jolley et al. 2002; Mjelde et al. 2007; Meyer et al. 2007; Breivik et al. 2006, 2008). The early history of the Norway Basin is traditionally characterized by a first phase of continental breakup resulting in the formation of volcanic margins observed on the mid-Norwegian and Faeroes margins and the proto-Jan Mayen microcontinent, still attached to Greenland at that stage (Talwani and Eldholm, 1977; Nunns, 1982; Skogseid and Eldholm, 1987; Gudlaugsson et al. 1988; Gunnarsson et al. 1989; Kodaira et al. 1998; Gaina et al. 2009; Skogseid, 2000; Breivik, 2012). Around Oligocene time, sea-floor spreading along the Aegir Ridge decreased until it became extinct and the spreading axis "jumped" westwards to initiate the Kolbeinsey Ridge. The relocation of the spreading ridge from the aborted Aegir Ridge to the Kolbeinsey Ridge resulted in the complete separation of the Jan Mayen microcontinent from the Greenland Plate around 25 Ma ago (Unternehr 1982; Kuvaas and Kodaira 1997; Lundin and Doré 2002; Scott et al. 2000; Mosar et al. 2002; Gaina et al. 2009; Gernigon et al., 2012). Based on a previous NB-07 aeromagnetic survey, the structure and spreading evolution of the Norway Basin from the continental oceanic transition region to the extinct Aegir Ridge have been already reinterpreted locally and we proposed a more complex geodynamic history. Our previous interpretation documented a transform margin, an orthogonally rifted segment and an oblique-shear volcanic

margin formed during the onset of breakup between the East Jan Mayen Fracture Zone and the Faeroe Plateau. The detailed fabric of the eastern (part of the) Norway Basin documented by the NB-07 data also indicated that two distinct tectonic phases have reshaped the basin before the cessation of seafloor spreading and abortion of the Aegir Ridge in Late Oligocene (see Gernigon et al. 2009, 2012). After continental breakup, a phase 1 (from 52 to 48 Ma) marks the earliest phase of spreading probably initiated in the central part of the Møre margin. During this period, competing oceanic segments lead to the formation of overlapping systems and pseudo-fault development. We observed a significant change in the Norway Basin's oceanic spreading system in the late Early Eocene and, based on observations from surrounding areas, we suggest that this marked a major tectonic event in the Norwegian-Greenland Sea (Gernigon et al. 2012). During phase 2 (48-28 Ma) of Norway Basin's development, spreading rates decreased, spreading direction changed, and the number of rigid faulting with large displacement increased leading to the formation of new N-S oriented oceanic fracture zones. The fan-shaped development of the spreading system was initiated around C21 (~48-46 Ma) instead of C18-C17 (~40-38 Ma) or C24 (53.3-52.3 Ma) as previously proposed. This new observation also allowed us to refine the tectonic calendar of the Norwegian-Greenland Sea and discuss some implications on the syn- and post-breakup development of the surrounding continental margins and the evolution of the Jan Mayen microcontinent (JMMC). Notably the onset of compression observed in the JMMC and conjugate margin may have initiated during this mid-Eocene reorganisation of the Norway Basin (Gernigon et al. 2012).

1.3 Objective: Jan Mayen aeromagnetic survey 2011/2012 (JAS-12)

The next and natural step of our investigation of the Norwegian and Icelandic oceanic domains was the new aeromagnetic survey JAS-12 situated in the western (part of the) Norway Basin at the edge of the JMMC (Figs. 1.2, 1.3). Other governmental institutions welcomed this initiative and the JAS-12 acquisition was co-funded by Geological Survey of Norway (NGU), the Icelandic National Energy Authority (Orkustofnun) and the Norwegian Petroleum Directorate (NPD). The final compilation will certainly be welcomed by most researchers and explorationists working within the fields of geodynamics and *Geophysics* and should provide a step further to our geodynamic knowledge of the Nordic and Icelandic Seas. It also contributes to a better scientific understanding of the JMMC, outline, geodynamic and tectonic evolution in terms of timing of deformation and definition of its COB.

NGU initiated the JAS-12 project in 2011 with the aim to acquire process and interpret a new aeromagnetic dataset covering the western Norway Basin where magnetic data remained extremely sparse and of poor-quality as suggested by the "gaps" observed in the previous regional compilation. Figure 1.3 underlines the location of the new survey area and illustrates the outline of the few magnetic profiles available in the study area before the new acquisition. Except the JAS-05, NB-07 and NRL-90 survey acquired along the Aegir Ridge in 1990 (Vogt et al. 1980; Jung and Vogt 1997), most of the magnetic profiles in this part of the Norway Basin remain old (70ies–80ies) and mostly inaccurate (Gernigon et al. 2012). In the meantime, modern and more accurate magnetometers, navigation systems and recent advances in processing techniques allow us to seriously improve the quality of aeromagnetic mapping (Luyendyk 1997; Mauring et al. 2002; Reeves 2005; Huang 2008). Modern magnetometers, as used for the more recent NGU surveys,

provide total field measurements of high sensitivity, with virtually no drift and for all intents and purposes can be regarded as giving a reliable reading with a typical noise envelope of ±0.1 nT. The same cannot be said about the old magnetometers from the vintage surveys across the Norwegian-Greenland Sea. They were not absolute and had to be manually calibrated and were sensitive at best to about ±1 nT.

Advances in data acquisition techniques (more sensitive magnetometers, full release of modern Global Positioning Systems, pre-planned drape surveys, etc.), as well as data processing and displaying procedures (such as micro-levelling and advanced gridding techniques), have also significantly improved data quality and resolution, providing levels of detail that are compatible to those derived from seismic recording, well logging and surface geological mapping. Being aware of such major geophysical improvements, the primary objectives of the JAS-12 project were multiple:

1) Provide a better and more reliable and complete magnetic coverage of the Norway Basin.
2) Refine the tectonic and geodynamic setting of this oceanic basin, far from being well understood and often being neglected in the past.
3) Interpret the tectonic framework, basement structure, and lithology from aeromagnetic geophysical results.
4) Correlate and combine these results with the known geology of the study area to aid identification of new structural features.
5) Understand the Continent-Ocean transition (COT) and its implication for continental margins, oceanic segmentation.
6) Constrain the tectonic and geodynamic evolution of the JMMC and conjugate margin (e.g. the mid-Norwegian margin).

The interpretation initiative involves the application of improved processing techniques and cultural source removal from the total magnetic field. In order to enhance the signatures of the basement structures and lithological units, as well as local volcanics lying above the older basement, a number of processed images and interpretations have been produced during this project.

This report documents and summarizes the first part of the JAS-12 project and mostly describes the acquisition, processing and levelling parts the new survey. Filtering techniques and data enhancement methods will be used subsequently for an integrated study of the new survey and a discussion of the most interesting features revealed by this new dataset.

The second report of the JAS-12 (under preparation) will focuses particularly on the geophysical and geological interpretation of the new survey, including also available gravity and released seismic lines, provided by Orkustofnun, ISOR and the Norwegian Petroleum Directory (NPD). It should lead to a preliminary interpretation of the survey area and open discussion dealing with the continental breakup between Norway and the JMMC and the subsequent spreading history of the Norway Basin.

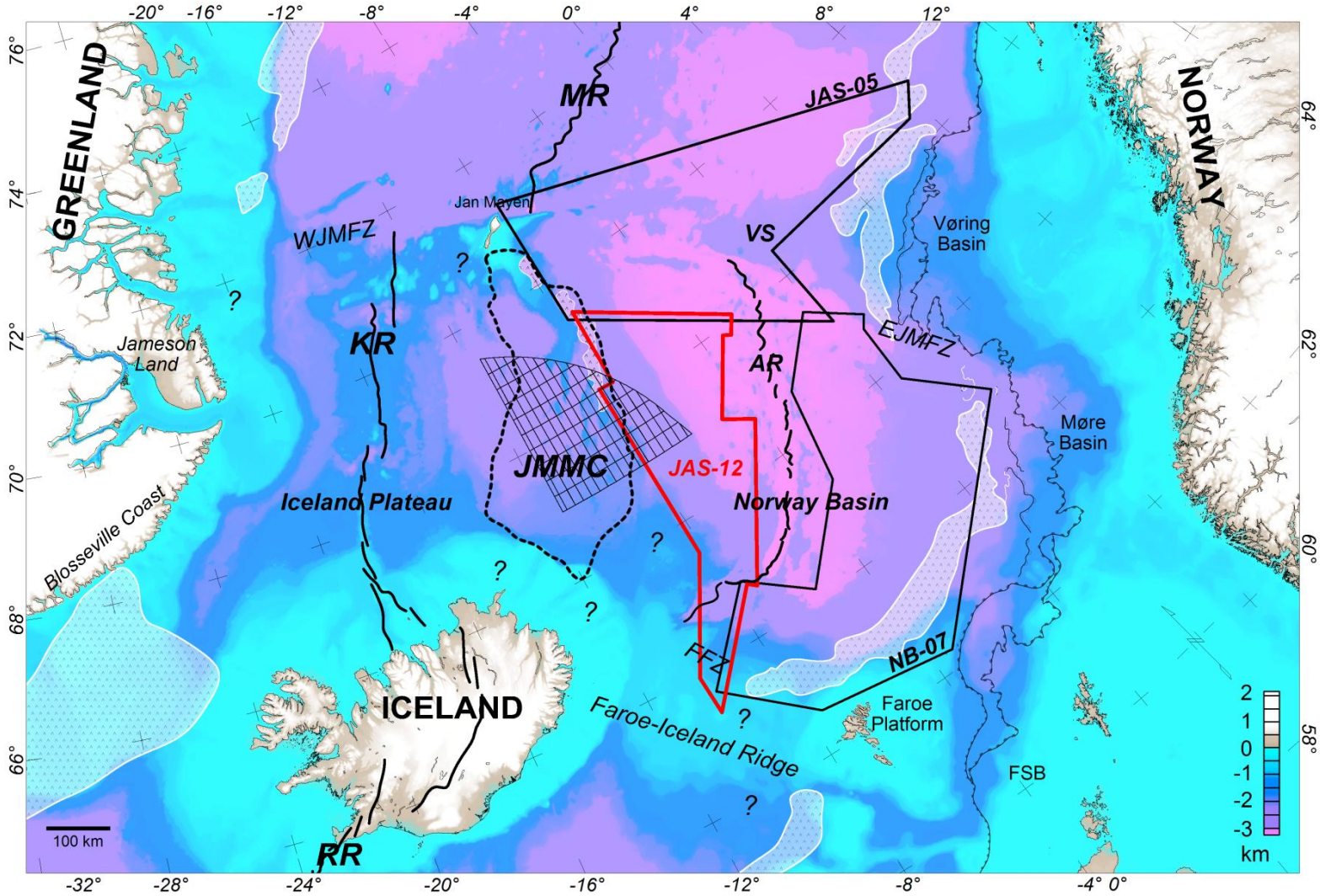

Figure 1.2 Main physiographic features of the Norwegian-Greenland Sea and outline (in red) of the new JAS-12 aeromagnetic survey. The new dataset covers the western part of the Norway Basin between the Jan Mayen microcontinent (JMMC) and the aborted Aegir Ridge (AR). In the central part of the oceanic basin, the Aegir Ridge represents an early spreading centre that aborted during Oligocene. The plate boundary relocated subsequently to the Kolbeinsey Ridge (KR) that is active today. The opening of Iceland Plateau led to the progressive isolation of the Jan Mayen microcontinent located north of Iceland at present day. EJMFZ: East Jan Mayen Fracture Zone; FSB: Faroe-Shetland Basin; MR: Mohn's Ridge; VS: Vøring Spur; WJMFZ: West Jan Mayen Fracture Zone. White outlines represent the Seaward dipping reflectors (SDRS) modified after Berndt et al. (2001) Outline of the inner flows after Gernigon et al. (1999).

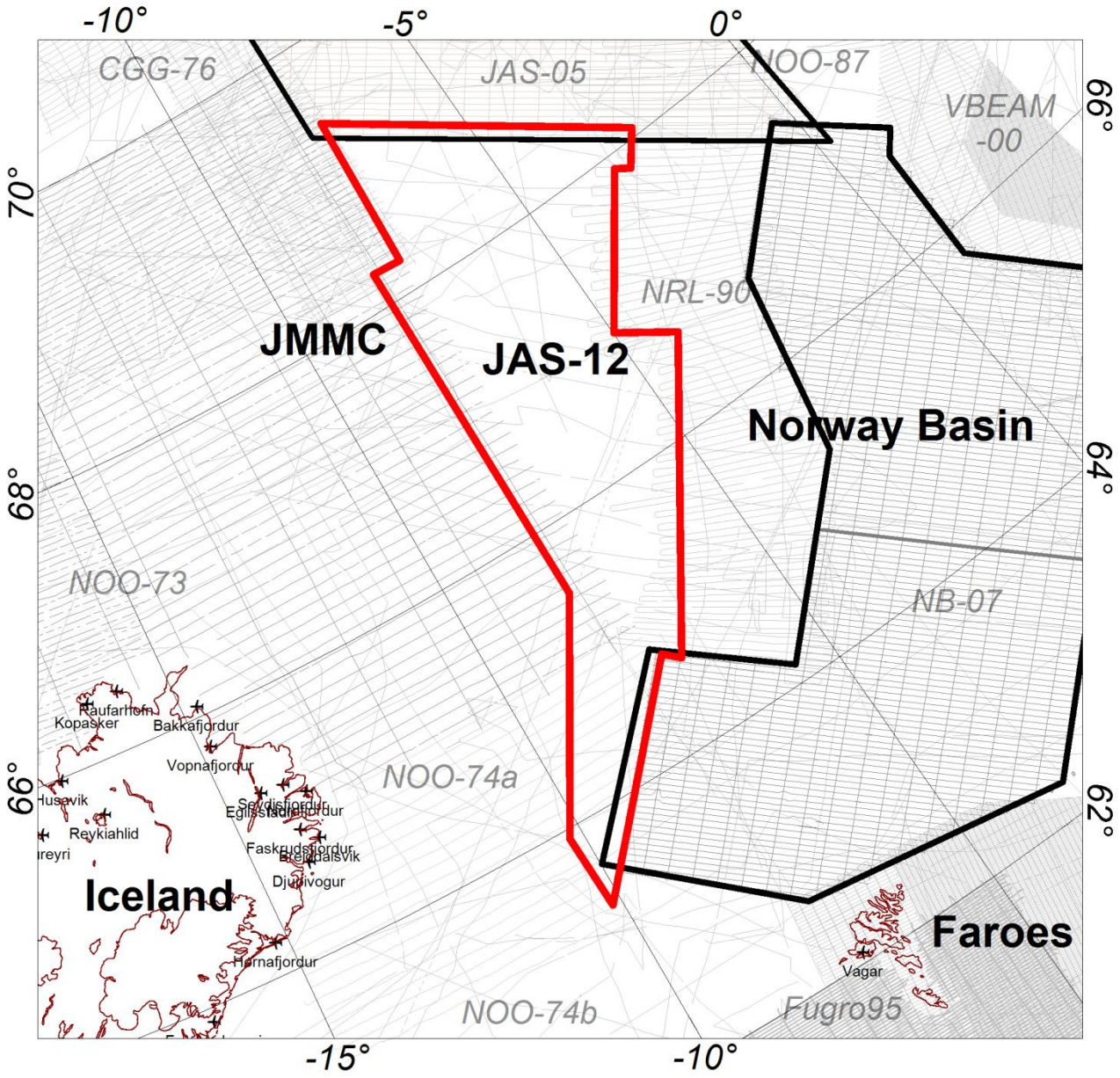

Figure 1.3 Location of the JAS-12 survey area and outline of the previous aeromagnetic surveys surrounding the Norway Basin (Olesen et al. 2006; Olesen et al. 2007; Gernigon et al. 2009; Gernigon et al. 2012). The western part of the Norway Basin was mostly covered by sparse magnetic profiles acquired by the U.S. Naval Research Laboratory (NRL) in the 70ies and 80ies (Jung and Vogt 1997; Verhoef et al. 1997). The aim of the JAS-12 was to fill the profile gaps between JMMC and the NRL-90 survey where the line spacings were really relatively large compared to the surroundings surveys.

2 SURVEY CHARACTERISTICS AND ACQUISITION

Laurent Gernigon and Janusz Koziel

2.1 Survey planning and equipment

The JAS-12 is the most recent high-resolution aeromagnetic survey acquired in the western Norway Basin after more than 30 years of non-magnetic acquisition in the area. As part of the NGU mapping program, the JAS-12 acquisition was carried out during two periods (Tables 2-1, 2.2): a first phase during autumn 2011 (September 15 to October 7) and a final phase during summer 2012 (May 20 to June 6). The first acquisition phase (September 2011) was initiated by Blom Geomatics on behalf of NGU but the survey could not be completed due to increasing icing conditions and bad weather in northern Iceland. For security reasons, the pilot decided to postpone the remaining part of the acquisition. Approximately 25 % of the survey was therefore completed in 2011. At the end of this first phase only 4566 km of aeromagnetic profiles were acquired.

Year	2011			2012												2013							
month	09	10	11	12	01	02	03	04	05	06	07	08	09	10	11	12	01	02	03	04	05	06	07	08
original	Phase1			processing				Report-interpretation																
Final									Phase2			processing				Report-interpretation					?			

Table 2.1 Initial and final JAS-12 survey planning and delivery expectation

The second and final phase of acquisition was carried out and successfully completed during May-June 2012 by the second contractor Fly Taxi Nord (Fig. 2.1). The acquisition was initially planned for approximately 15 days but due to poor weather conditions, some shorter periods with magnetic disturbances and some unexpected administrative issues, the acquisition has been delayed with regard to the initial schedule. In the initial 2011 plan, the use of the Jan Mayen airport was planned to facilitate the coverage in the northern area but in 2012 the military authorities decided not to authorise the civil planes to land on Jan Mayen any longer. The budget was therefore extended due to extra, but not initially planned, ferry flights required to cover the northern area. During the transit flights, Fly taxi Nord managed, nevertheless, to extend the pre-existing flight lines outside the initial survey area.

The airborne magnetic survey was conducted with constant flight-line orientation, usually perpendicular to the regional geological strike, and with a constant line spacing of 6 km x 20 km almost similar to the JAS-05 and NB-07´s configurations (5x20 km) (Fig. 2.2). Table 2.2 defines the coordinates of the original survey area and Table 2.3 summarizes the main characteristics of JAS-12.

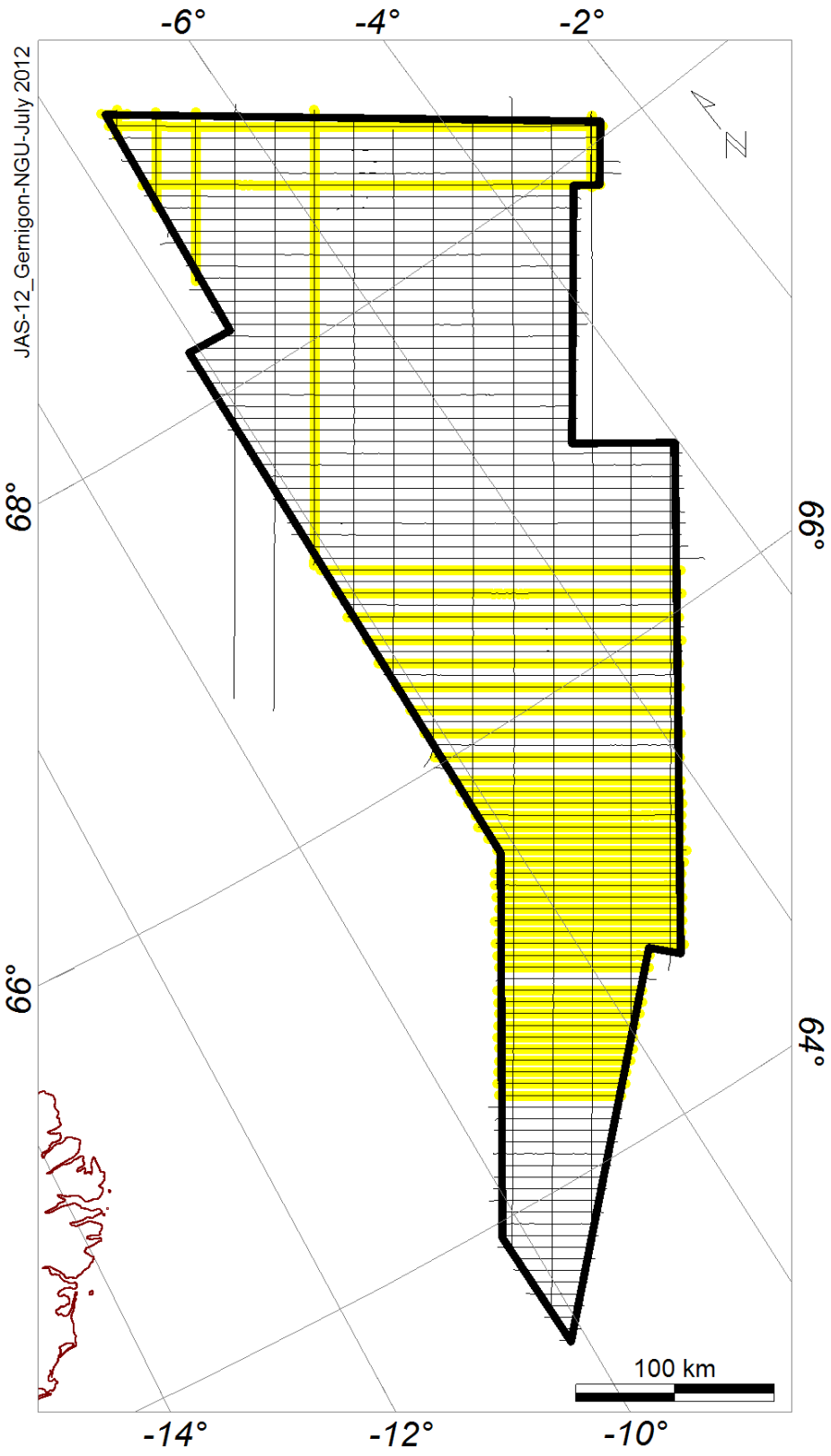

Figure 2.1 Final lines (NW-SE) and tie lines (NE-SW flight configuration) of the JAS-12 survey. The lines underlined by the yellow colour indicate the profiles acquired during the first phase of acquisition in 2011.

Longitude WGS84	*Latitude WGS84*	*X-UTM29 WGS84*	*Y-UTM29 WGS84*
-7.41	69.41	562496.86	7700556.50
-2.48	68.07	771394.83	7564632.98
-2.95	67.84	754290.23	7536931.52
-3.20	67.90	743043.24	7543231.11
-4.99	66.92	675148.92	7428533.38
-4.04	66.65	718953.20	7401499.43
-7.15	64.65	588500.37	7170694.49
-7.39	64.75	576722.80	7181630.01
-10.16	63.35	442174.12	7024777.09
-10.22	63.93	439980.27	7089908.68
-8.16	65.50	538777.08	7264153.36
-8.12	68.26	536247.37	7571717.80
-7.56	68.24	559633.24	7570771.82
-7.41	69.41	562496.86	7700556.50

Table 2.2 Coordinates of the JAS-12 survey area.

The following summary details the essence of the survey program:

Base of operation	Egilsstadir, Iceland
Traverse line spacing and trend	6 km, north – south
Tie line spacing and trend	20 km, east – west
Number of lines	105
Number of tie lines	15
Flying height /sensor altitude	300m (Bloom)/230 m (Fly Taxi Nord).
Speed	~225 km/h
Total line kilometres (original plan)	17.600
Total line kilometres (in contract)	17.600
Total line kilometres (acquired)	18.632 km
Data recorded	Magnetic field intensity, radar altitude and GPS positioning data

Table 2.3 Main characteristics of the JAS-12 survey.

2.2 Project management and personnel on board

From NGU participated:
JAS-12 Project leader: Laurent Gernigon
Contract administration: Odleiv Olesen
Senior engineer: Janusz Koziel (maintenance and installation of the instruments)

From Blom Geomatics participated in 2011 (Phase 1):

Project Manager: Magne Omestad
Captain: Jon Wold,
Co-pilot: Jahn Morten Pettersen

From Fly Taxi Nord participated in 2012 (Phase 2):
Captain: Ronny Thorbjørnsen
Captain: Ole Thorbjørnsen
Co-pilot: Ola Magnus Giæver
Co-pilot: Gard Pettersen
Co-pilot: John Harald Somby

2.3 Equipment and technical specifications

The following equipments were used during the JAS-12 project:

From Blom Geomatics AS (during 2011 Phase 1):

- Aircraft: Piper Navajo PA-31 (registration LN-NP2) (Fig. 2.2)
- Navigation: Applanix POSTrack 510 Flight Management System, with Trimble BD950 GPS receiver. This receiver was set up to output a NMEA-string to the MAG/Grav flight computer
- Altimeter: KING KRA-405 Radar Altimeter.
- Magnetometer: Geometrix G-822 A high-sensitivity magnetometer, installed in a tail stinger.
- Base magnetometer: RMS AADC-II magnetometer compensation system
- Data logging: RMS DGR33A data acquisition system and digital recording system

From Fly Taxi Nord (during 2012 Phase 2):

- Aircraft: Piper Chieftain PA31 with long range fuel tanks (registration. LN-ABZ) from FlyTaxi Nord in Tromsø (Fig. 2.3).
- Navigation: A Topcon Legacy-E, 40 channel GPS receiver combined with an Egnos DGPS correctional receiver (SATREF) with a flight guidance system from Seatex ASA was used for real time differential navigation. The navigation accuracy was better than ±5 m throughout the survey.

- Altimeter: A KING KRA 405 radar altimeter is an integrated instrument of the aircraft and the data were both recorded and shown on the pilot's display. Accuracy of 0.25% with a resolution of 1 foot (0.3058 m).

- Magnetometer: A Scintrex Caesium Vapour MEP 410 high sensitivity magnetometer with a CS-3 sensor was applied in the data acquisition. The noise envelope of the onboard magnetometer was 0.1 nT. Most of the data fell within the limits of ±0.04 nT.

- Base magnetometer: A Scintrex MP-3 and an EnviMag proton magnetometer were used for recording diurnals at the base station at the Egilsstadir airport on the mainland during the last phase of the survey (Fig. 2.4). Data from the base magnetometer were used in planning of flights and to decide on which lines eventually to refly.

- Data logging: A DAS8 data logger, GR33 chart recorder and a HDR150 tape station from RMS Instruments were used to record the different data from the survey.

Figure 2.2 Piper Navajo PA-31 and the Geometrix G-822 high-sensitivity magnetometer, installed in a tail stinger used by Blom Geomatics AS during the first phase of acquisition in 2011.

Figure 2.3 Piper Chieftain from Fly Taxi Nord with the docking cradle for the bird containing a Scintrex Cesium Vapour MEP 410 high-sensitivity magnetometer.

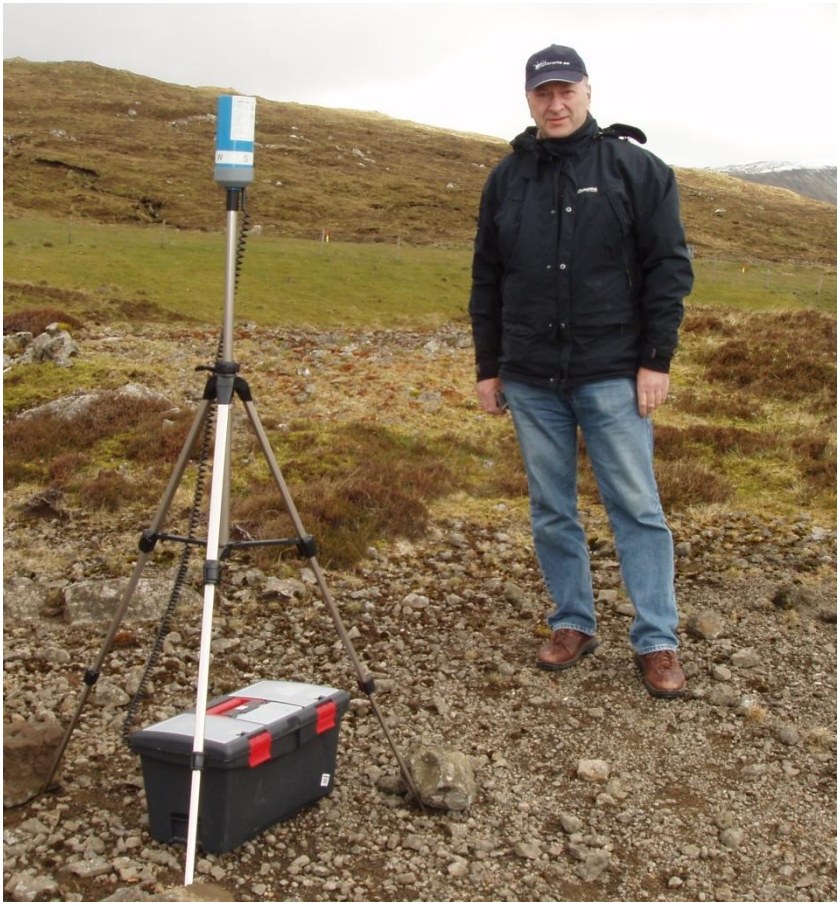

Figure 2.4 Janusz Koziel next to the NGU base station magnetometer.

2.4 Survey characteristics

The JAS-12 area is approximately 630 km long by 250 km and is located between Iceland and the Jan Mayen Fracture Zone (Fig. 1.2). The survey extends from the Continental-Ocean transition of the JMMC eastern margin to the southeast and ends up close to the aborted Aegir Ridge to the east at the edge of the previous NRL-90 survey (Fig. 1.3). During Phase 1, the acquisition was carried out using a Geometrix G-822 high-sensitivity magnetometer, installed in a tail stinger located just behind a Piper Navajo PA-31 (Fig. 2.2). During phase 2, the aeromagnetic survey was carried out using an aeroplane with a Caesium magnetometer installed in a so-called "bird", towed at a sufficient distance from the plane (70 m) to make the plane's magnetic effects negligible (Fig. 2.3). The technical configuration and location of the magnetic sensor explain the difference in flight altitudes shown in Figure 2.5.

The whole area was covered with both profiles and tie-lines (Fig. 2.6). The total survey area represents c. 80.000 km^2 and includes 4.690 km of N-S tie lines profiles and 13.819 km of ordinary E-W line profiles. The aircraft altitude was 300 m in average (1000 feet) (Fig. 2.5). The magnetic sensor was towed approximately 70 m below and behind the aircraft, giving a sensor altitude of app. 230±5 m. The flying speed was 225 km/h and magnetic data were sampled at a rate of 5 Hz, giving a spatial sampling interval of 12-14 m along the lines.

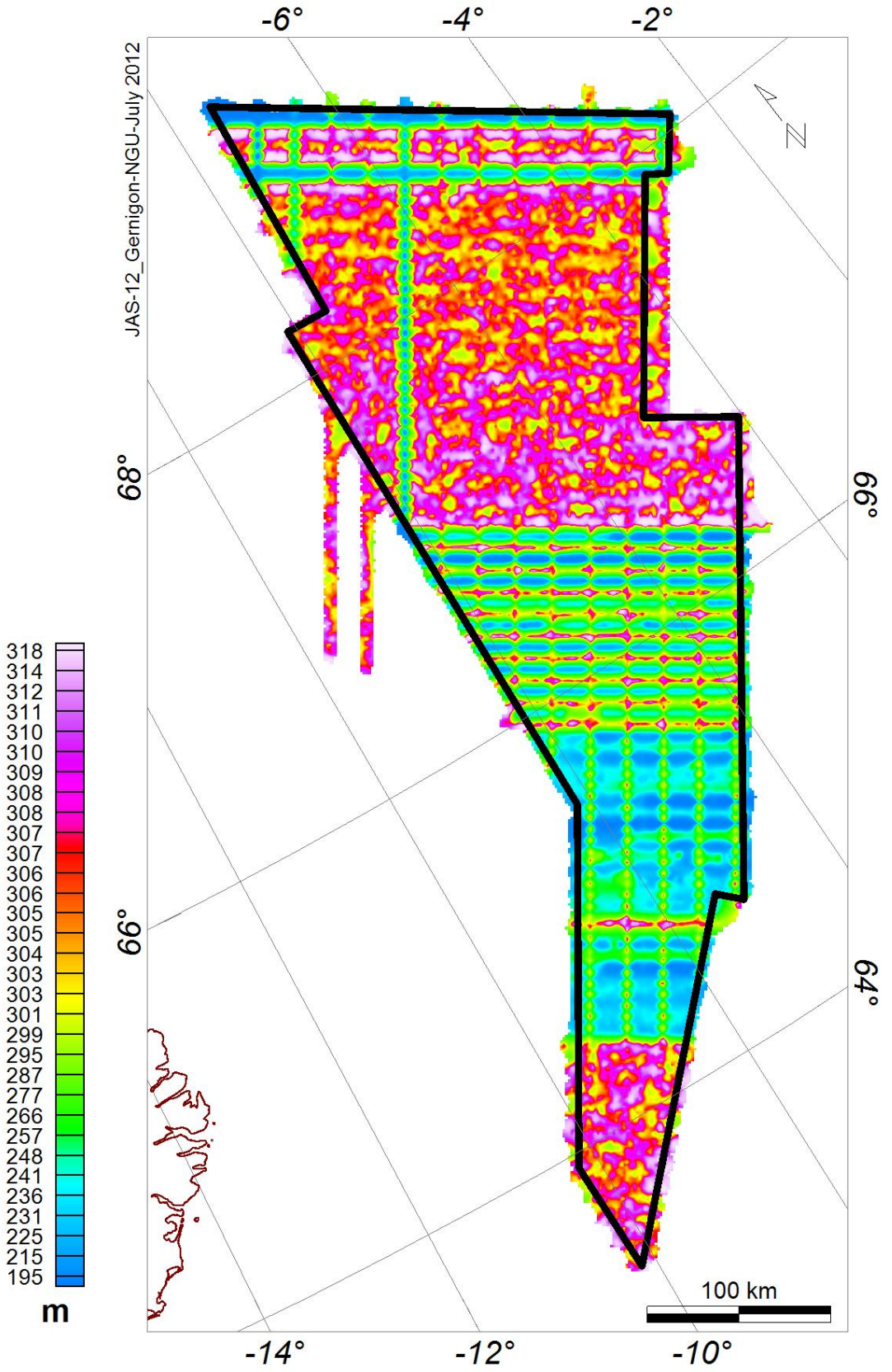

Figure 2.5 Plane altitudes in meters above sea level. Variation of sensor altitude can partly explain minor variation in the raw magnetic field, later corrected by advanced levelling techniques. Also note the altitudes variations recorded during the 2 phases of the JAS-12 acquisition. During Phase 2, the sensor (the "bird") was located 70 below the plane. This explains the major altitudes differences between Phase 1 and Phase 2 observed on this figure.

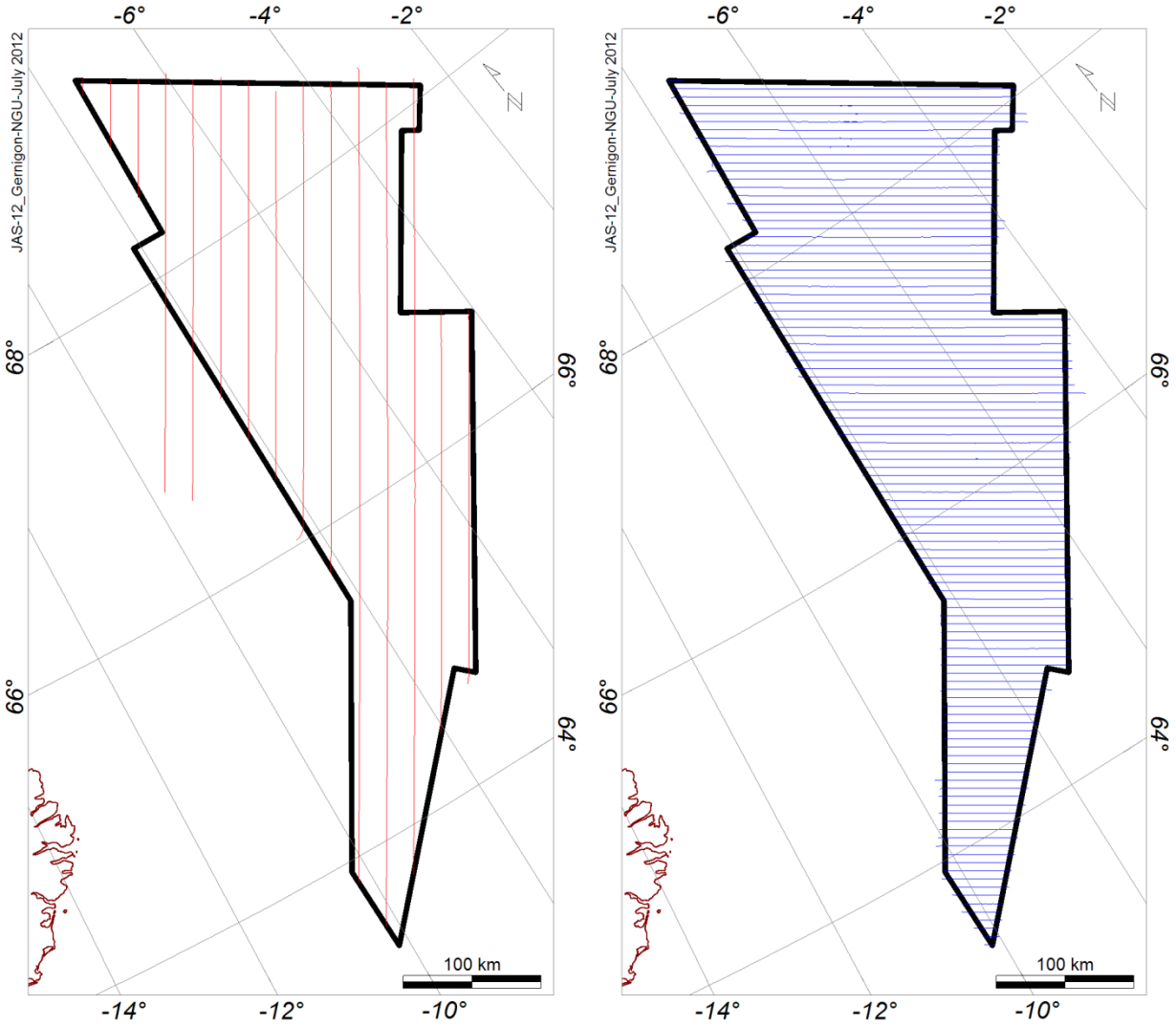

Figure 2.6 Final flight configuration and acquisition of the JAS-12 survey. Outline of the red tie-lines to the left and blue lines to the right. The lines observed outside the initial survey area represent the extra lines acquired during ferry flights.

2.5 Magnetic conditions

The main problem during magnetic acquisition is certainly the diurnal variation of the Earth's magnetic field influenced by solar storms (Fig. 2.7), particularly active at high latitudes (i.e. aurora borealis). It usually causes tie line and regular survey lines to have different readings at the same geographical point (crossover point). Such misfits can produce artefacts during interpolation and consequently erroneous interpretations if no suitable corrections have been applied.

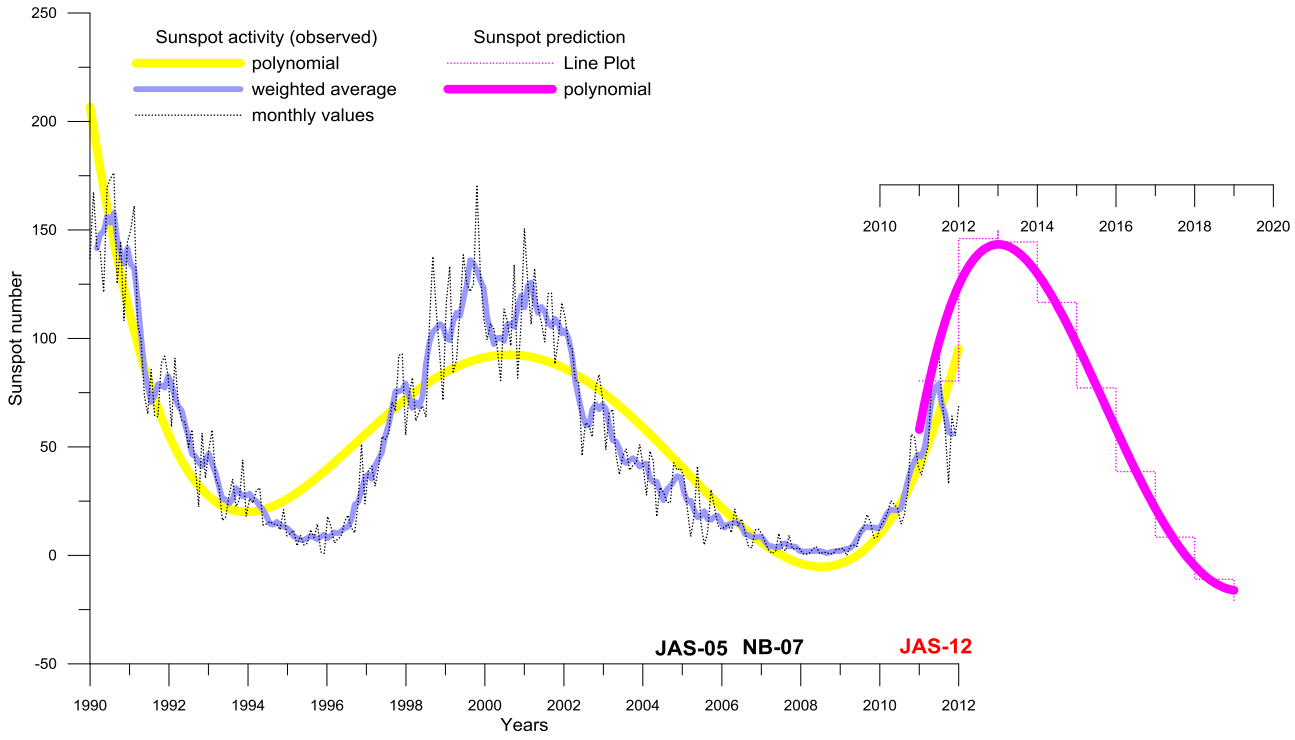

Figure 2.7 Observations and prediction models of sunspot numbers from the US National Oceanic and Asthenospheric Administration (NOOA)(Hathaway et al. 1999). Monthly averages (updated monthly) show that the number of sunspots visible on the sun waxes and wanes with an approximate 11-years mega cycle. The JAS-12 was carried out during a period of increasing solar activity, which represented moderate conditions for the aeromagnetic acquisition. Data Source: http://www.swpc.noaa.gov/ftpdir/weekly/RecentIndices.txt.

If the survey is located close to a base station site, the lines can be directly corrected for diurnal variation. However, most of the offshore acquisition extends far away from land stations and can by experience suffer from different diurnal variation. Efficient statistical algorithms and filtering are usually required to solve this issue and "level" in a proper way all the magnetic profiles (see Chapter 3). Sunspot cycles (Fig. 2.7) strongly influence the geomagnetic field and diurnals. The JAS-12 was acquired during a period of increasing sunspot activity. Solar cycle predictions suggest that the period 2011-2012 coincided with the beginning of a new cycle of magnetic storms providing lower magnetic weather conditions for the JAS-12 acquisition compared to the previous

JAS-05 and NB-07 surveys acquired during almost perfect diurnal conditions. The acquisition has been carried out before the maximum pick expected during the winter of 2013 according the NOAA predictions. At the end, it appears that these diurnal variations had no major disturbing impact on our final dataset notably due to the large amplitudes of the total field anomalies recorded along the JAS-12 survey (mostly oceanic domain) (Fig. 2.8).

The magnetic signature of the airplane also includes 1) its permanent magnetization induced by its motion through the Earth's magnetic field and 2) a component due to the flow of electric current within the plane. The permanent magnetization of the plane varies as the plane changes its orientation leading to heading errors. A magnetic heading test (clover-leaf test) was carried out in June 2005 for the JAS-05 project using the same plane and equipment. The maximum difference of magnetometer readings in the four different directions was negligible: 1.2 nT. We decided not to carry out any new clover-leaf test for the JAS-12 since the equipment was strictly similar.

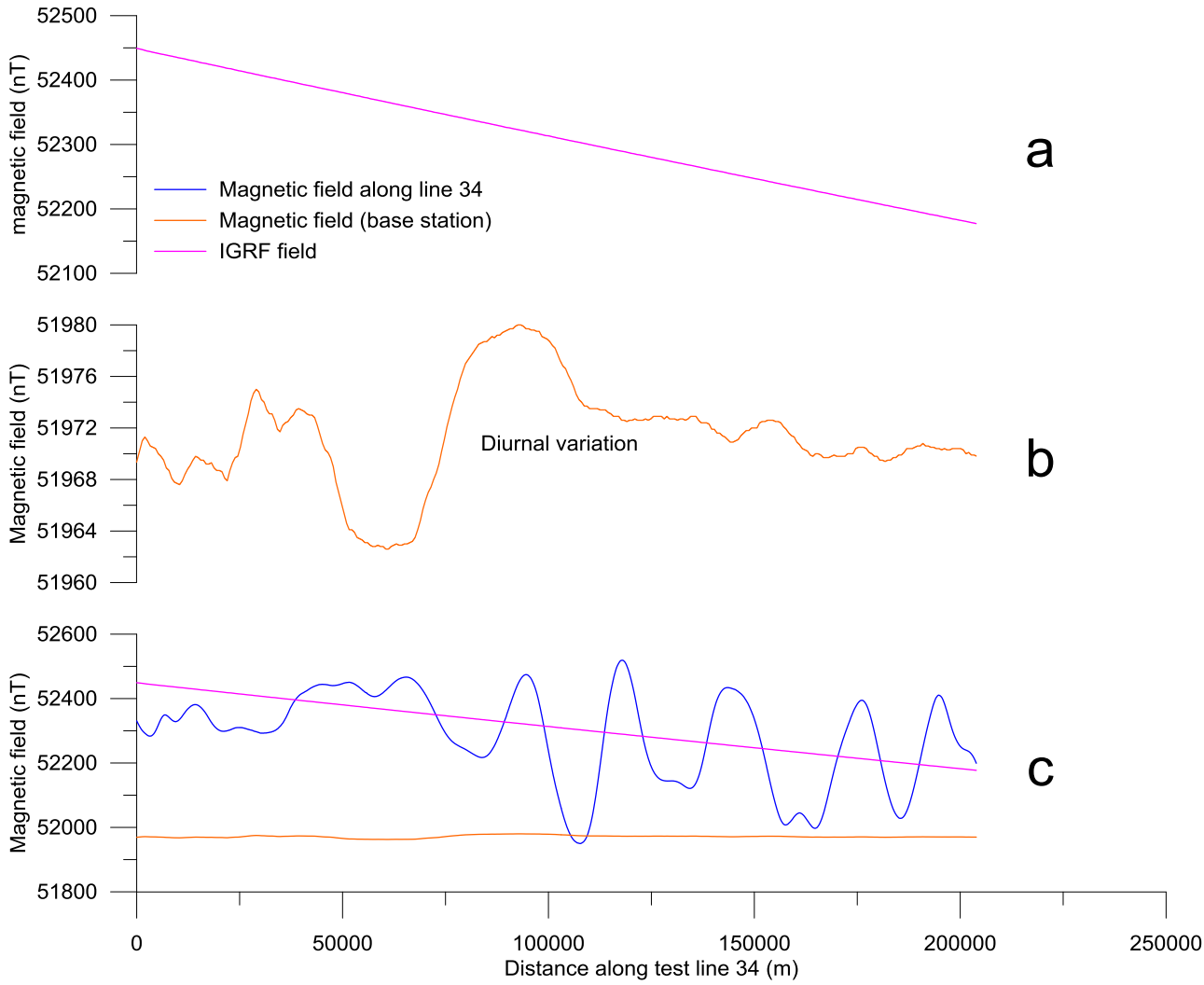

Figure 2.8 Magnetic diurnal along the JAS-12 Profile 34. a) Regional IGRF magnetic field. b) Base magnetometer reading (Rorvik measurements). c) Base magnetometer and uncorrected raw magnetic field from the aeroplane plotted at the same scale for comparison. Note the amplitude differences and the "low" impact of the diurnal variation.

2.6 Map production, projection and archive CD

The Oasis Montaj software (Geosoft 2004) was intensively used for processing and map production. This software package has become a standard for many potential field experts in the mineral and petroleum industry. All database and grids in Geosoft format are provided on the archive USB (NGU USB card attached). The grids are usually presented with or without a shaded relief technique (illumination from the northeast) and a non-linear colour scale. Colour scale and colour distribution for the datasets have been computed using a histogram equalisation technique. We used mostly the Geosoft minimum curvature gridding algorithm to produce the grids displayed in the present report. The grid cell size is mainly 1500x1500 m to fit best the line/tie line configuration of the JAS-12. For practical editing purpose, the JAS-12 maps have been projected in the North Pole Lambert Azimuthal Equal Area (Atlantic) projection using the WGS 84 datum.

For companies that do not use Oasis Montaj specifically. The Oasis Montaj Viewer is a free, easy-to-use software that allows anyone to view, share and print published Geosoft grid (.grd) and very large database (.gdb) files. The viewer can also be used to convert grids and images to a variety of supported data formats, including AutoCAD, ArcView, ER Mapper, TIF and many more. The free software can also be shared and downloaded from http://www.geosoft.com/support/downloads/viewers/oasis-montaj-viewer.

For specific questions do not hesitate to contact NGU (Laurent.gernigon@ngu.no)

3 DATA PROCESSING AND PROFILE LEVELLING

Laurent Gernigon

The raw magnetic profile measurements (Fig. 3.1) should not be used directly for gridding and direct interpretation. The raw dataset required a number of processing steps before production of the final aeromagnetic grid required for interpretation and modelling. Noise filtering and statistical levelling processing were carried out using the professional OASIS Montaj software (Geosoft 2005b). Microlevelling was performed using the MAGMAP FFT package from OASIS Montaj (Geosoft 2005a). The raw data have been processed using standard procedures and methodologies used in many other geophysical surveys (Luyendyk 1997). The various processing steps and standard procedures are outlined below.

3.1 Preliminary noise filtering and basic corrections

3.1.1 Noise filtering

High-frequency noise is usually created as the aeroplane is flying. After acquisition, initial raw data were imported directly into an Oasis Montaj database and subsequently interpolated to a regular grid of 1500x1500 m cells, to check the quality of lines and tie lines (Fig. 3.1). Spikes due to minor noise and artefacts were first removed by non-linear (Naudy) filtering and subsequently smoothed with a light low-pass filter in order to keep the main signal intact.

3.1.2 Systematic lag corrections

Original magnetic profiles were lag-corrected, utilizing the Oasis Montaj processing package (Geosoft 2005a). As part of the processing sequence, lag correction was applied to the JAS-12 data but did not change the data significantly due to negligible variations in values as a function of survey direction.

3.1.3 International Geomagnetic Reference Field (IGRF correction)

As part of the processing, the total magnetic field is computed from the recorded magnetic field after subtraction of the last International Geomagnetic Reference Field (IGRF) model available (Fig. 3.2). The IGRF is a mathematical representation of the undisturbed Earth's geomagnetic field. The International Geomagnetic Reference Field for 2010 (IGRF-2010) was calculated using the Oasis Montaj IGRF tool (Geosoft 2005a). The result of this subtraction isolates the component of the magnetic total field, which is dominated by the magnetic effects from the underlying crustal rocks.

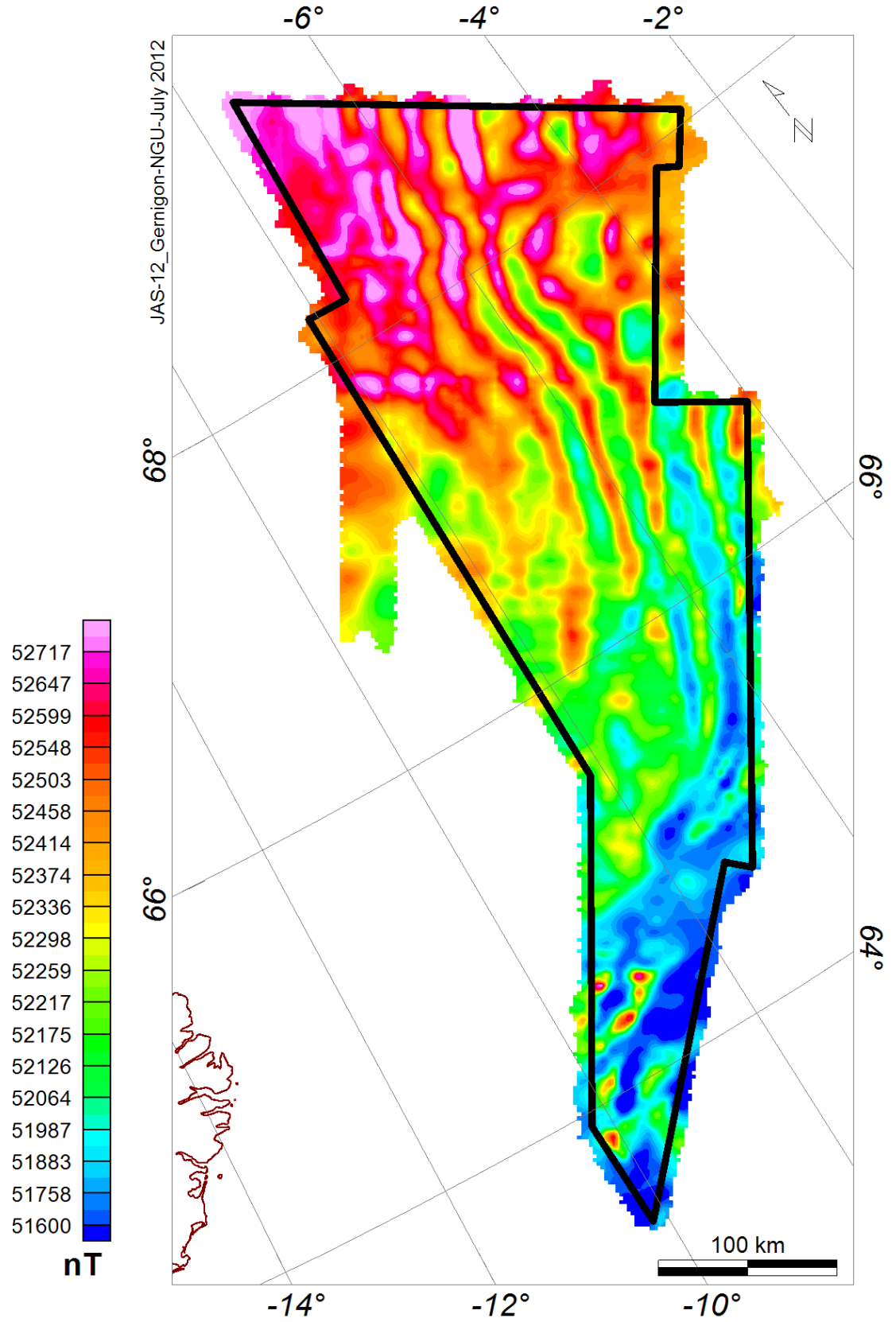

Figure 3.1 Gridding of the raw magnetic profiles (without levelling) by means of the minimum curvature algorithm (grid cell size: 1500x1500 m). Note that few and discrete artefacts are mostly parallel to the profiles due to diurnals. Projection: North Pole Lambert Azimuthal equal area.

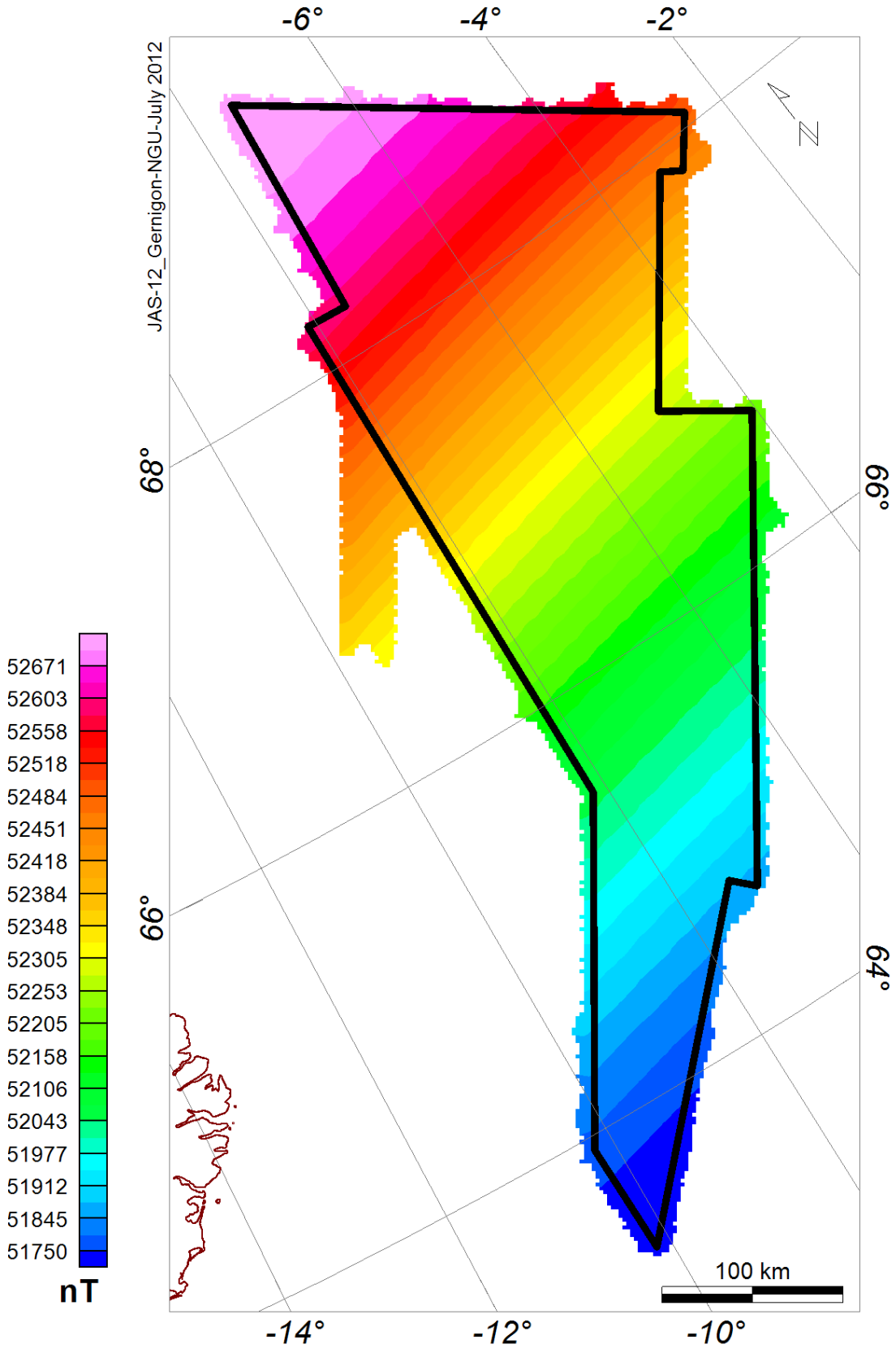

Figure 3.2 IGRF-2010 model along the JAS-12 survey.

3.2 Levelling and microlevelling of the magnetic profiles

3.2.1 Diurnal variation and use of base magnetometer readings

A variety of external, time varying field factors usually influences and causes errors during aeromagnetic acquisition. This includes time variation in the geomagnetic field, altitude variation and magnetic effects of seawater waves. This usually explains the errors at crossover points between line and tie-lines. The most complex and significant problem is probably the diurnal variation of the Earth's magnetic field influenced by the solar wind (Figs. 2.7, 2.8). In polar latitudes, the most famous and spectacular expression of these diurnal effects are the aurora borealis, known to be caused by the collision of charged particles (e.g. electrons), in the magnetosphere with atoms in the Earth's upper atmosphere. Diurnal variations in the magnetic field can cause tie line and regular survey lines to have different readings at the same intersection. Even if they are small these small wavelength artefacts can be visually distracting particularly on image-enhanced displays (Fig. 3.3). Such misfits can produce artefacts during interpolation and consequently erroneous interpretation if no suitable corrections have been applied properly.
The most important reason for this is the time shift in the Earth’s magnetic field variations between the large survey area and the onshore base station. There is normally a spatial difference in amplitude and frequency of these diurnals. Data from the base magnetometer have therefore only been used to assess the quality of individual lines and to make decisions on which lines eventually to re-fly. Due to good magnetic conditions and the large magnetic total field amplitudes observed, no lines have been re-flown.

3.2.2 Statistical levelling

The purpose of "levelling science" is to minimize the residual crossover differences between lines and tie lines in a coherent and statistical way. Proper levelling or micro-levelling algorithms usually require close and proper line spacing and the quality of the final result is most of the time a function of this crucial parameter. The large line spacing of previous surveys did not allow proper levelling and interpolation and produced erroneous or factitious anomalies.

Compared to the previous dataset, the JAS-12 lines/tie lines configuration and resolution allowed us to process and level the data in a proper way to get a reliable and updated magnetic picture of the western Norway Basin and surroundings. After noise removal and lag-corrections, the new aeromagnetic survey was processed using a statistical levelling method by which the discrepancies between the readings at each crossover points were reduced by systematically proportioning them between the tie and line profiles. The levelling method used for our study involved fitting a polynomial to the intersection errors by the method of least squares (Mauring et al. 2002; Reeves, 2005). These polynomials are then subtracted from the original data, reducing the main intersection errors.

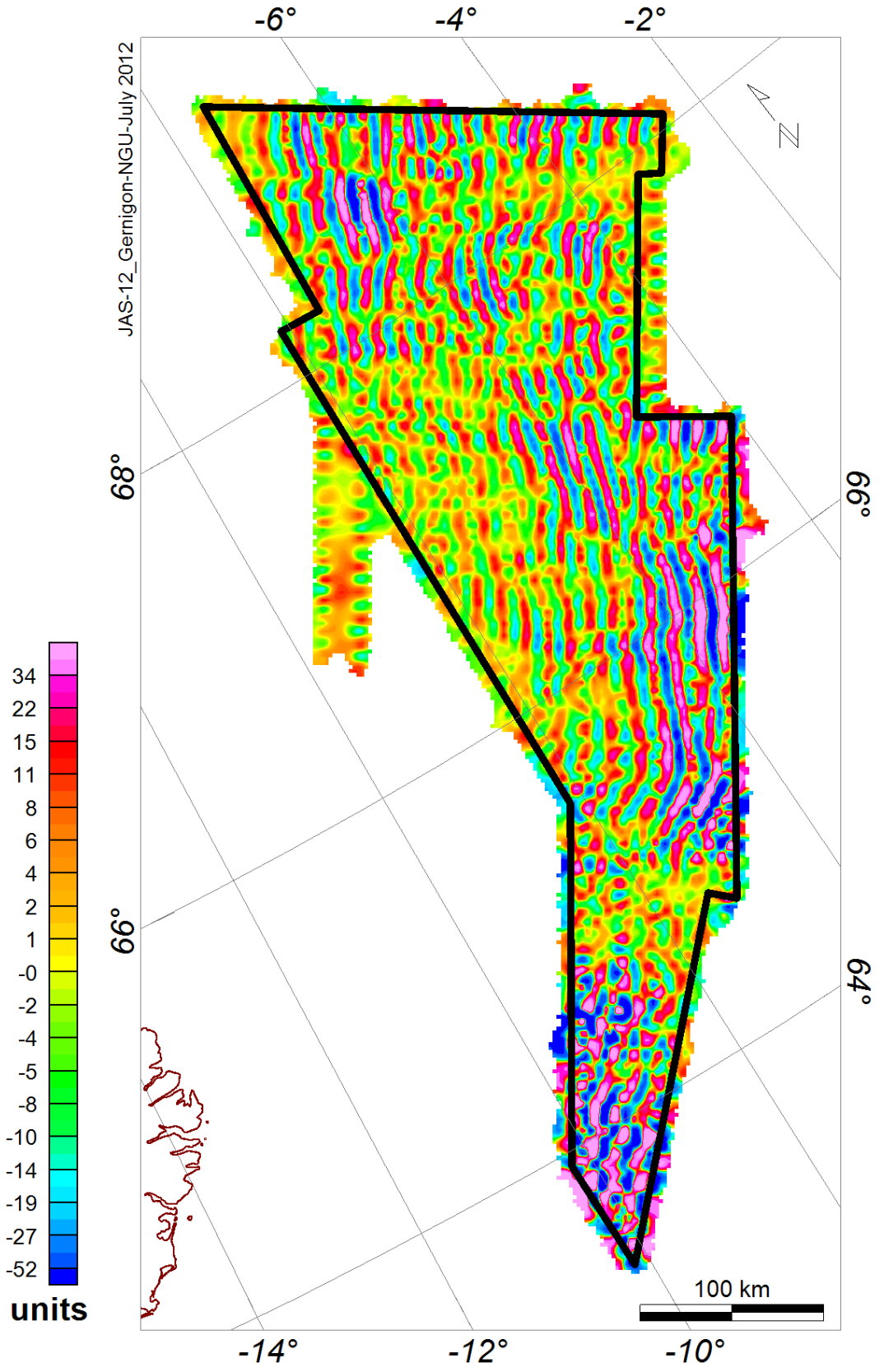

Figure 3.3 High-pass filtering (15 km) of the raw magnetic profiles (without levelling) gridded by means of the minimum curvature algorithm (grid cell size: 1500x1500 m). Note that few levelling errors due to diurnals are mostly parallel to the line profiles. Projection: North Pole Lambert Azimuthal equal area.

We used a first order (linear) trend removal for the levelling of the NE-SW tie-line profiles. The linearly trended tie-lines were subsequently used for full statistical levelling of the survey lines after smoothing of the polynomial fitted mis-lines using a spline algorithm to avoid unwanted distortion of the anomalies (e.g. Mauring et al. 2002).

Levelling was undertaken using the standard statistical levelling method on the tie-lines followed by a statistical levelling of the lines profiles utilising the levelled tie-lines (Geosoft 2005b). We used first a first-order (linear) trend removal in the levelling of the tie-lines. Before running the trend-levelling algorithm, 'suspicious' mis-tie values (outliers) were removed manually before levelling of the tie-lines. The linearly detrended tie-line(s) surface was finally used similarly for the final full levelling of the survey lines (Fig. 3.4). For each outlier removal, gridding has been systematically realised to check the validity of each trial, until we got a reasonable grid. Instead of smoothing, we re-ran several times the full levelling of the lines to further improve the levelling correction. Extreme mis-tie values (outliers) were checked and removed again manually before calculating the next full levelling correction, until convergence was achieved.

We also tried to apply different spline algorithms during the conventional levelling to remove the residual noise, but there were no observable improvements of the resulting grids. Spline and Akima algorithms smoothed the data too much and removed some interesting trends and features, with often small nT variation. The final results were the best compromise between the removal of levelling errors and anomalies preservation. The crossover differences between the raw data and the corrected and levelled version is illustrated in Figure 3.5

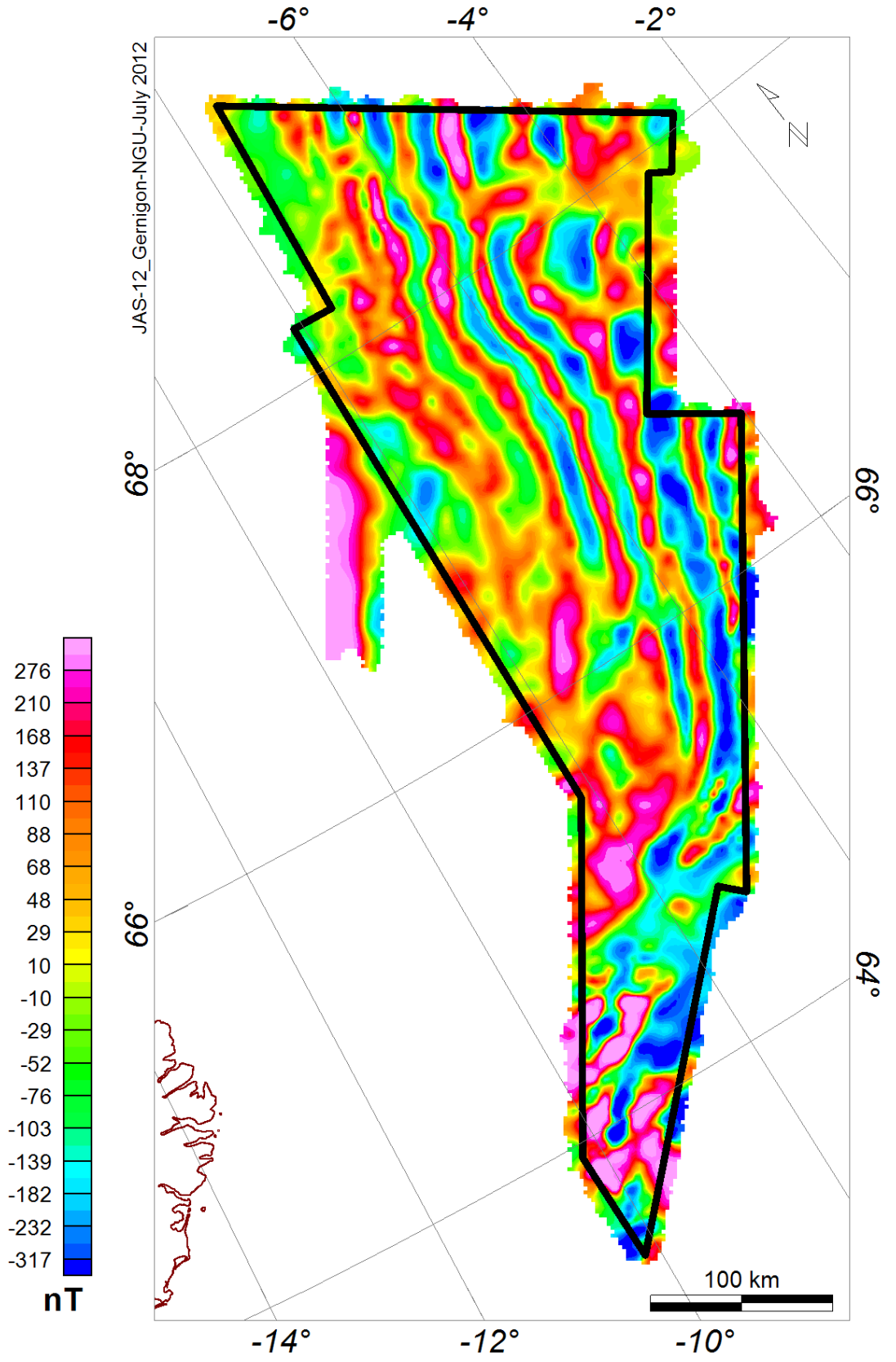

Figure 3-4 Full statistical levelling of the JAS-12 survey, lag-corrected and referred to IGRF-2010. The levelling represents the second step of the levelling approach based on a least-square technique. Final gridding of the line profiles using the minimum curvature algorithm (grid resolution: 1500x1500 m).

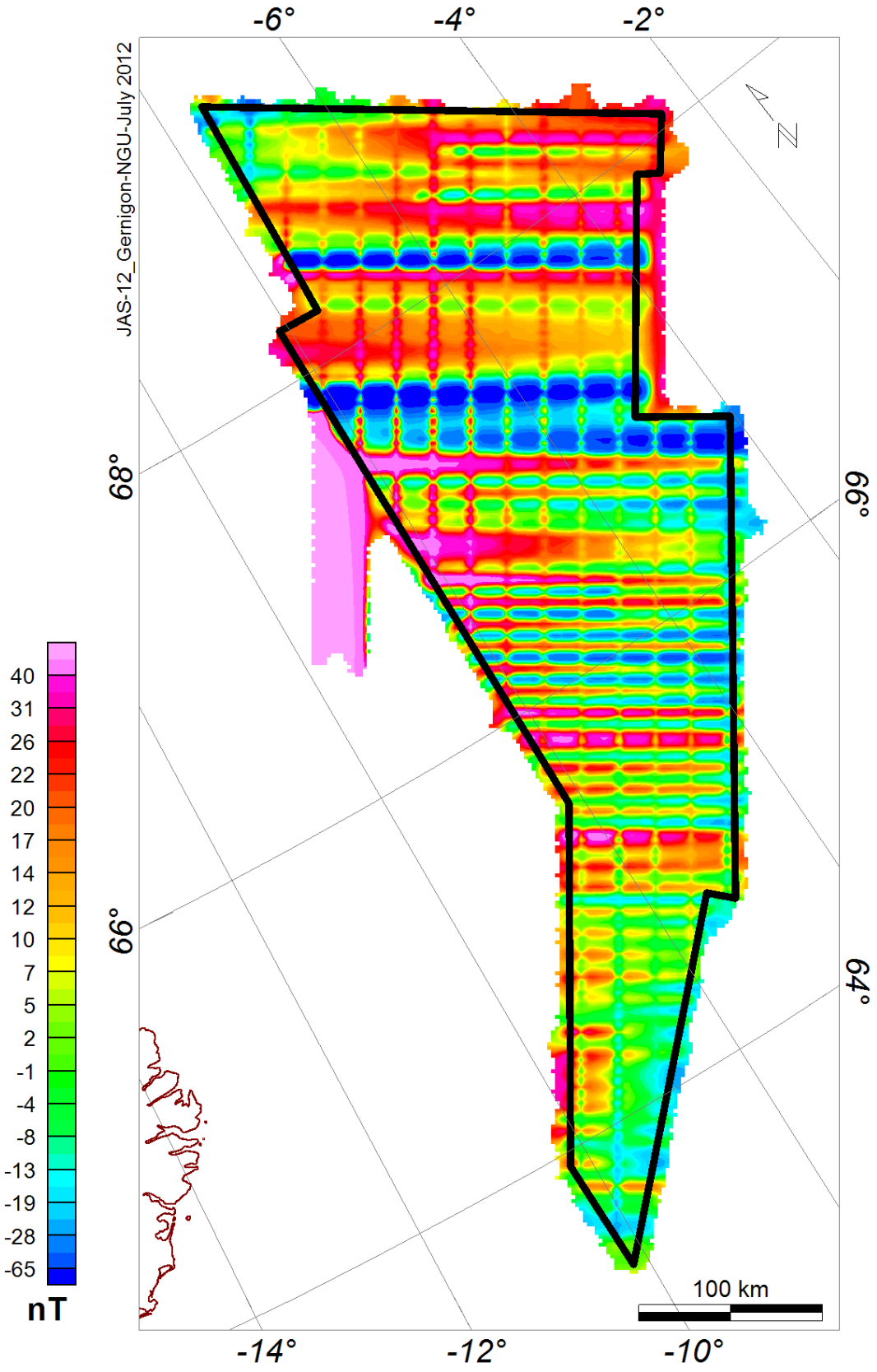

Figure 3.5 Difference between the full statistical levelling and the raw magnetic data. This figure illustrates the diurnal variation observed and subsequently corrected along the lines and tie lines. Gridding of the line profiles using the minimum curvature algorithm (grid resolution: 1500x1500 m).

3.2.3 Micro-levelling

To remove minor ("micro") levelling errors still remaining along parts of some profiles after the statistical levelling, we performed micro-levelling techniques. We tested separately two micro-levelling techniques: 1) the Geosoft micro-levelling approach using a decorrugation technique (Geosoft 2005b) and 2) the moving median filtering method developed at NGU (Mauring et al. 2002, Mauring and Kihle 2006).

The moving median levelling method is described in detail by Mauring and Kihle (2006). A floating median filter was applied to each line. For a given line, the 1D median was determined at each station based on data values within a given distance of the station. We can in the same way find a 2-D median value for a circular area around the station. The difference between the 2D and 1D median value was taken to be the micro-levelling error and was added to the magnetic value at that station after smoothing. This algorithm was particularly efficient to deal with small amplitude variation of the magnetic total field during the previous BAS-06 survey in the Barents Sea (Gernigon et al. 2007a). However, the result along the JAS-12, where amplitudes are significantly higher, was somewhat disappointing as it created high-frequency noise at the end. After several tests, we decided not to consider the result of this moving median levelling method for this survey.

The Geosoft micro levelling has instead been realized using the PGW GX System of the available MAGMAP processing package (Geosoft 2005b). It proved to be more efficient for this specific case where the magnetic anomalies are more prominent. The PGW GX System applies a decorrugation process in the Fourier domain to isolate the levelling corrections before applying them to the original statistically levelled data (Fig. 3.4). The JAS-12 data have been decorrugated to reduce line-to-line levelling errors, which are visible as linear magnetic features parallel to the flight lines (Fig. 3.6). Decorrugation is simply a frequency domain procedure based on a directional cosine filter combined with a Butterworth high-pass filter. During the JAS-12 processing, the Butterworth high-pass filter was set to four times the line spacing to pass wavelengths on the order of two to four line separations. Such a process resulted from a preliminary line-to-line levelling error channel. Afterwards a line-based filter was used to separate the high frequency geophysical signal from the longer wavelength levelling errors. We applied an amplitude limit of 20 nT with a zero amplitude mode in the noise channel allowing a shorter non-linear filter to be applied. The micro-levelling result was finally obtained by subtraction of the levelling error channel (Fig. 3.6) from the original dataset (Figs. 3.5) to produce the final microlevelled channel subsequently gridded using the minimum curvature algorithm (Figs. 3.7, 3.8).

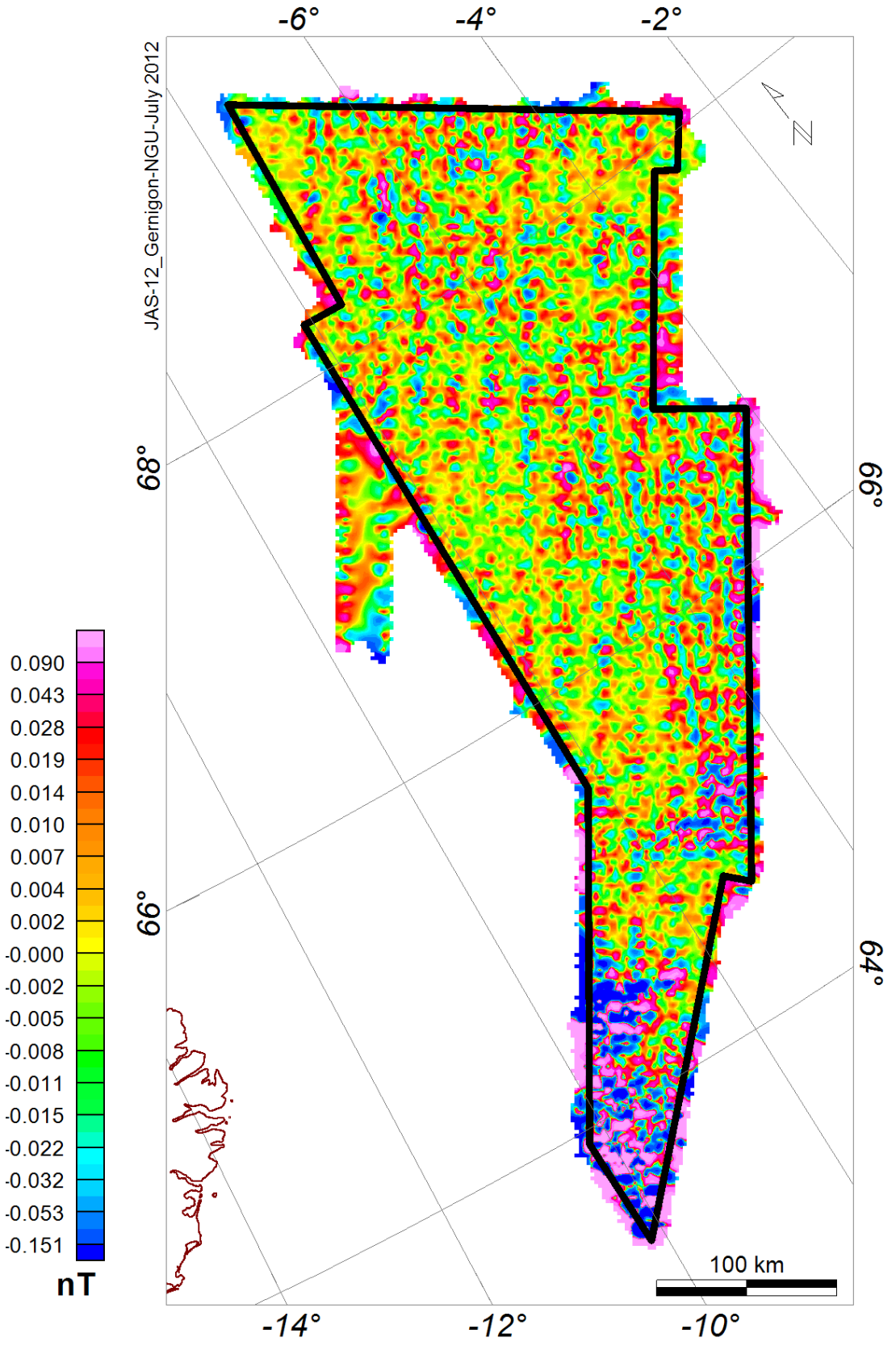

Figure 3.6 Magnetic levelling errors (1500x1500m cell grid spacing). The NW-SE trends represent the remaining microlevelling variations along the pre-existing lines.

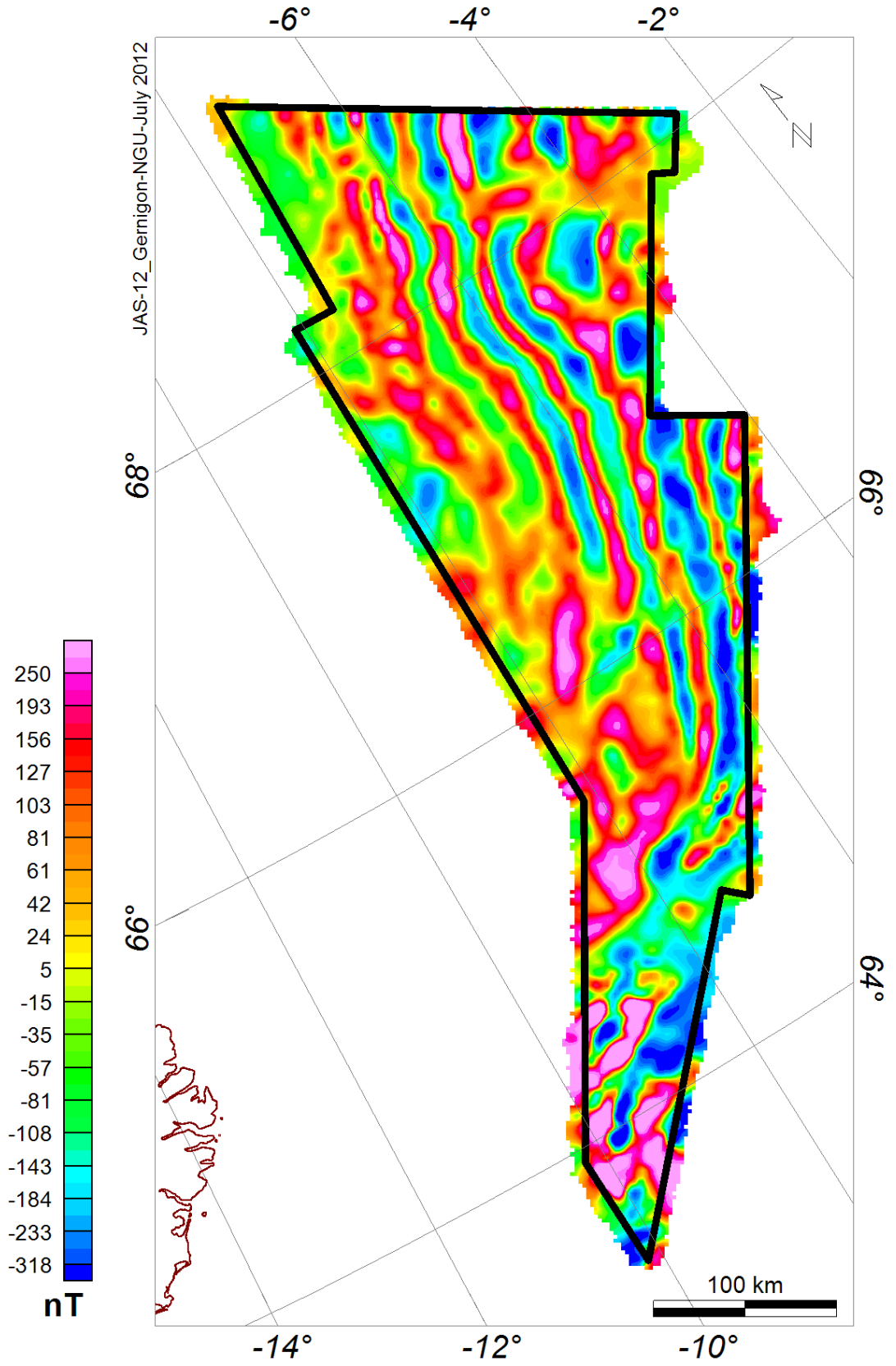

Figure 3.7 Total magnetic field after micro-levelling. Results from the FFT decorrugation technique of Geosoft. 1500x1500m cell spacing was produced using the minimum curvature algorithm. This grid was selected for further filtering presented later in this report.

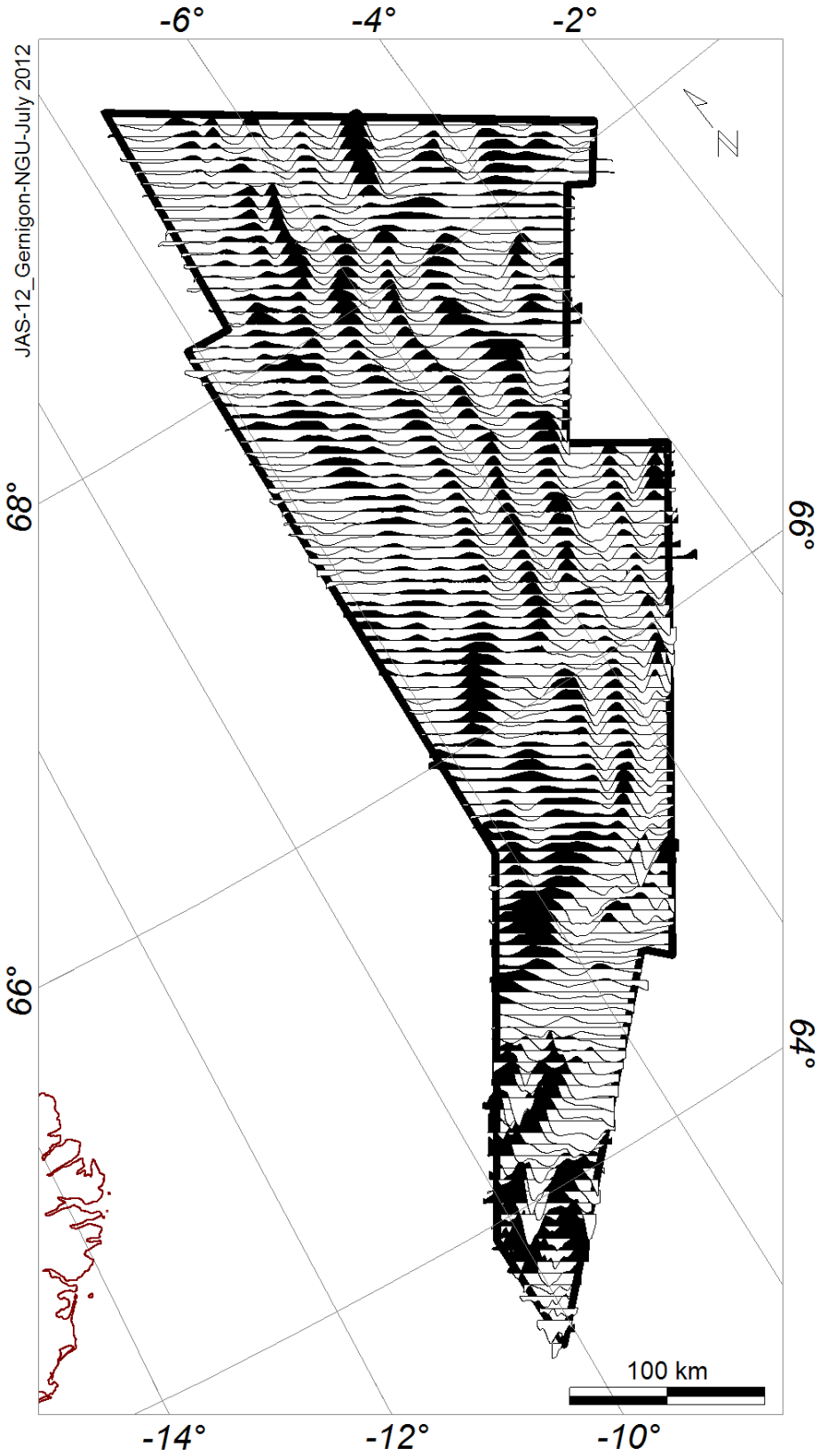

Figure 3.8 Profile map of the final total magnetic field.

3.3 Gridding of the JAS-12 dataset: important comments for interpreters

Most of the magnetic grids presented in this report refer to the minimum curvature gridding technique. The interpolated surface generated by minimum curvature is analogous to a thin, linearly elastic plate passing through each of the data values with a minimum amount of bending. Minimum curvature generates the smoothest possible surface while attempting to honour the data as closely as possible (Briggs 1974; Press et al. 2002). Minimum curvature produces a grid by repeatedly applying an equation over the grid in an attempt of smoothing the grid. Each pass over the grid is counted as one iteration. The grid node values are recalculated until successive changes in the values are less than a pre-defined maximum residual value, or a pre-defined maximum number of iterations is reached (maximum iteration field). The minimum curvature gridding technique is efficient, fast and widely used in the Earth sciences.

However, the minimum curvature is not an exact interpolator and this means that the JAS-12 data are not always honoured exactly after gridding (Fig. 3.7). A full sensitivity study with other gridding techniques was not realised in the present study but the processed profile values still allow interpreters and modellers to regrid the data using other gridding techniques and preferred software as they wish and according to their needs.

Gridding methods like the Kriging technique can be more relevant for specific parts of the survey area. The Kriging algorithm, for example, can be either an exact or a smoothing interpolator depending on the user-specified parameters. It can incorporate anisotropy and underlying trends in an efficient and natural manner and could be used locally to better refine linear magnetic features. The bi-directional gridding algorithm BIGRID was tested but induces artefact in the N-S direction. This may occur because BIGRID first interpolated values along the horizontal direction. One way to properly compare the two-gridding algorithms would be to rotate the lines from NE-SW to the E-W trend first.

Note also that the cell size is critical when it comes to performing image enhancements in the Fourier domain or to define a proper resolution of the dataset. The grid cell size is mostly a function of the line spacing and depth of the magnetic sources (flight altitude+water depth) but is also a function of your needs and observation scale.

Some may consider that a small grid cell size (< 1/5 line spacing) can create high-frequency noise and aliasing (the local "beading effects" along the linear anomalies) but it provides a better depiction of the spatial resolution. However, aliasing produced during the gridding at 500x500 and globally at less than 1500x1500m induces disturbing artefacts during 2D-FFT filtering. For example, downward continuation involves multiplying the Fourier spectrum of the image by an exponential function. This exponential function increases rapidly with frequency and if the cell size is very fine, the very highest frequencies will be substantially amplified. These high frequencies will generally be a mixture of noise (along the line direction) and interpolation effects (in the tie-line direction) and therefore, their amplification is undesirable. Similar initial noise also influences the derivatives and can produce unwanted artefacts. For any Fourier filtering that involves

amplification of high frequencies we urge caution and recommend a cell size no finer than 1/3 to 1/4 of the line spacing. For 2D-FFT manipulation, we rather choose and recommend a grid cell size of 1500 m.

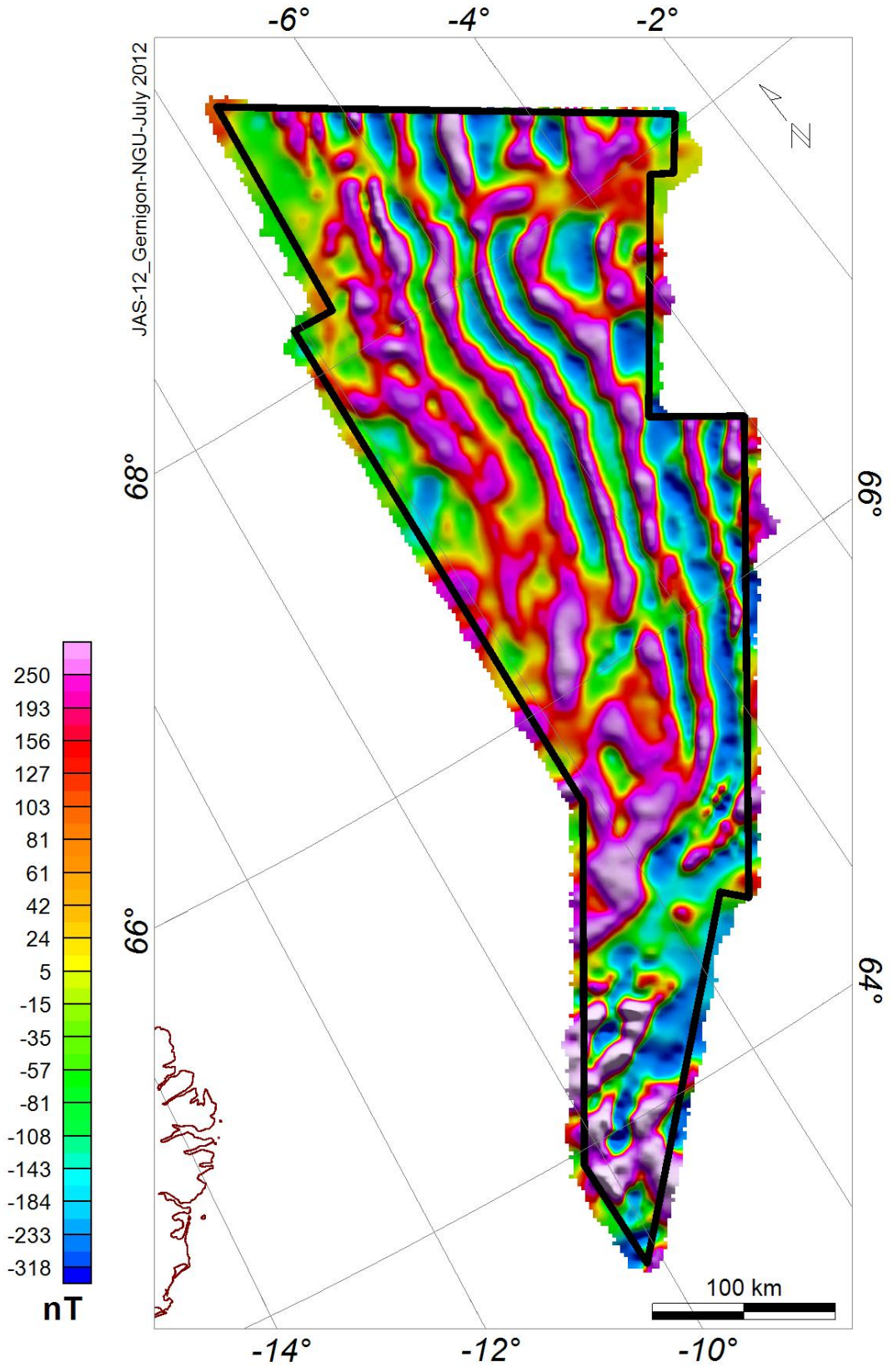

Figure 3.9 Total magnetic field after micro-levelling (colour shaded version). Results using the FFT decorrugation technique (Farraccioli et al., 1998) with a 1500×1500m grid cell spacing. This grid has been used for most of the filtering involving 2D-FFT processing presented in this report.

4 FILTERING TECHNIQUES

Laurent Gernigon

4.1 Potential field and integrated study

As part of the JAS-12 project, potential field filtering techniques are considered as irremediable and complementary for the interpretation of the survey area. It was also a good way to test the validity of other geophysical models and help the seismic interpretation. Relevant filtering has been carried out in order to enhance the main structural changes and magmatic features observed along the JAS-12.

The aim of this section is to briefly present and discuss the different processing techniques used to enhance and model the magnetic data across the JAS-12 survey. Specific and preliminary interpretation based on these grids will be presented in the interpretation report. The filtered grids are also provided in the CDROM.

4.2 Wavelength filtering, frequency content and power spectrum

Magnetic (and gravity) anomalies whose wavelengths are long relative to the dimensions of the geologic objectives of a particular investigation are called regional anomalies. Because shallow geologic features can have large lateral dimensions, one has to be careful, but regional anomalies are usually thought to reflect the effects of relatively deep features. Anomalies whose wavelengths are similar to the dimensions of the geological objectives of a particular investigation are called local anomalies. In the processing of magnetic data, it is usually preferable to attempt to separate the regional and local anomalies prior to interpretation. Magnetic anomalies observed along the JAS-12 survey characterise an amalgamation of sources reflecting the regional field, noise and lateral (density and) magnetic variations within the crust and upper mantle (e.g. Blakely 1995). Measured gravity anomalies, therefore, represent the combination of wavelengths associated with the spatially distributed sources.

During the JAS-12 project, a number of transformation methods have been used after data levelling in order to enhance the main structural and magnetic features. These techniques used to separate regional from local gravity anomalies take many forms and can all be considered as filtering in a general sense (Blakely 1995). Many of these techniques are the same as those employed in enhancing traditional remote sensing imagery, seismic data or processing of digital elevation data (Milligan and Gunn 1997; Mari et al. 2001).

Filters have been applied to the JAS-12 line and/or gridded anomalies which enable us to isolate, interpret or/and enhance the wavelengths of greatest interest, therefore facilitating geological interpretations (e.g. Blakely 1995). The magnetic gridded datasets can be transformed from the space domain into the spectral domain and vice-versa using the Fast Fourier Transform (FFT).

Transformation of the gridded data into the frequency domain is completed by application of a discrete 2D Fourier transform (DFT) (Bhattacharya 1966; Blakely et al. 1995).

For spectral analysis we use the Geosoft MAGMAP Discrete Fourier Transform algorithm (Geosoft 2005a,b,c), which applies the method of Bhattacharyya (1966). The DFT algorithm works fast by exploiting symmetries that are present for images of certain dimensions. The algorithm implemented by Geosoft in Oasis Montaj is explicitly the Winograd DFT (Geosoft 2005c, Winograd 1978). This FFT transformation requires that the image fills an entire rectangle, a condition not met by the JAS-12. Therefore, any survey gaps or irregular edges will also need to be filled with synthetic data. The edge matching and the gap filling were achieved using the maximum entropy algorithm (Burg 1975).

Fourier transforms are usually displayed as 2-D power spectra with a logarithmic stretch applied to the data. The power spectrum of the JAS-12 survey reflects the strength of the sine and cosine components at each frequency (Fig. 4.1). The reason for displaying with a logarithmic stretch is the huge variation in the amplitudes of the different spectral components. Most aeromagnetic datasets are dominated by the lower frequency Fourier components for the deep part of the basin (i.e. magnetic intensity is smooth at an airborne altitude). The maximum and reliable frequencies present in the Fourier domain are a function of the Nyquist number, which again is a function of the spatial grid size, $NX_{max}=1/2\Delta x$ and $NY_{max}=1/2\Delta y$. Any higher frequencies present in the data will appear at lower frequencies and effectively contaminate the spectrum. This phenomenon produces the aliasing problem previously discussed and is an inevitable consequence of discrete sampling when the sampling rate is not sufficiently rapid.

The Fourier transform, $F(u,v)$, of the magnetic signal, $T(x,y)$, defined over a 2-D space is given by:

$$F(u,v) = \int_{-\infty}^{\infty} du \int_{-\infty}^{\infty} dv \cdot T(x,y) \cdot exp[2\pi(ux + vy]$$

If (x,y) are spatial co-ordinates in units of meters, then (u,v) are frequency co-ordinates in units of cycles per meter. In real world applications it is not possible to measure the signal of Interest continuously, nor is it possible to measure it indefinitely. To overcome these difficulties, the Geosoft FFT algorithm usually interpolates our data to a regular grid and then calculates the resulting Fourier transform. With a $N \times M$ spatial grid with cell spacing of Δx and Δy in the x- and y-directions respectively, the FFT is calculated on an $N \times M$ frequency grid with spacing of $\Delta u = 1N\Delta x$ and $\Delta v = 1M\Delta y$

$$F_{jk} = \Delta x \Delta y \sum_{n=1}^{N} \sum_{m=1}^{N} T_{mn} exp\left[2\pi . i \left(\frac{jn}{N} + \frac{km}{M}\right)\right]$$

where

$F_{jk} = F(\frac{j}{N\Delta x}, \frac{k}{M\Delta y})$ and $T_{mn} = T(n\Delta x, m\Delta y)$

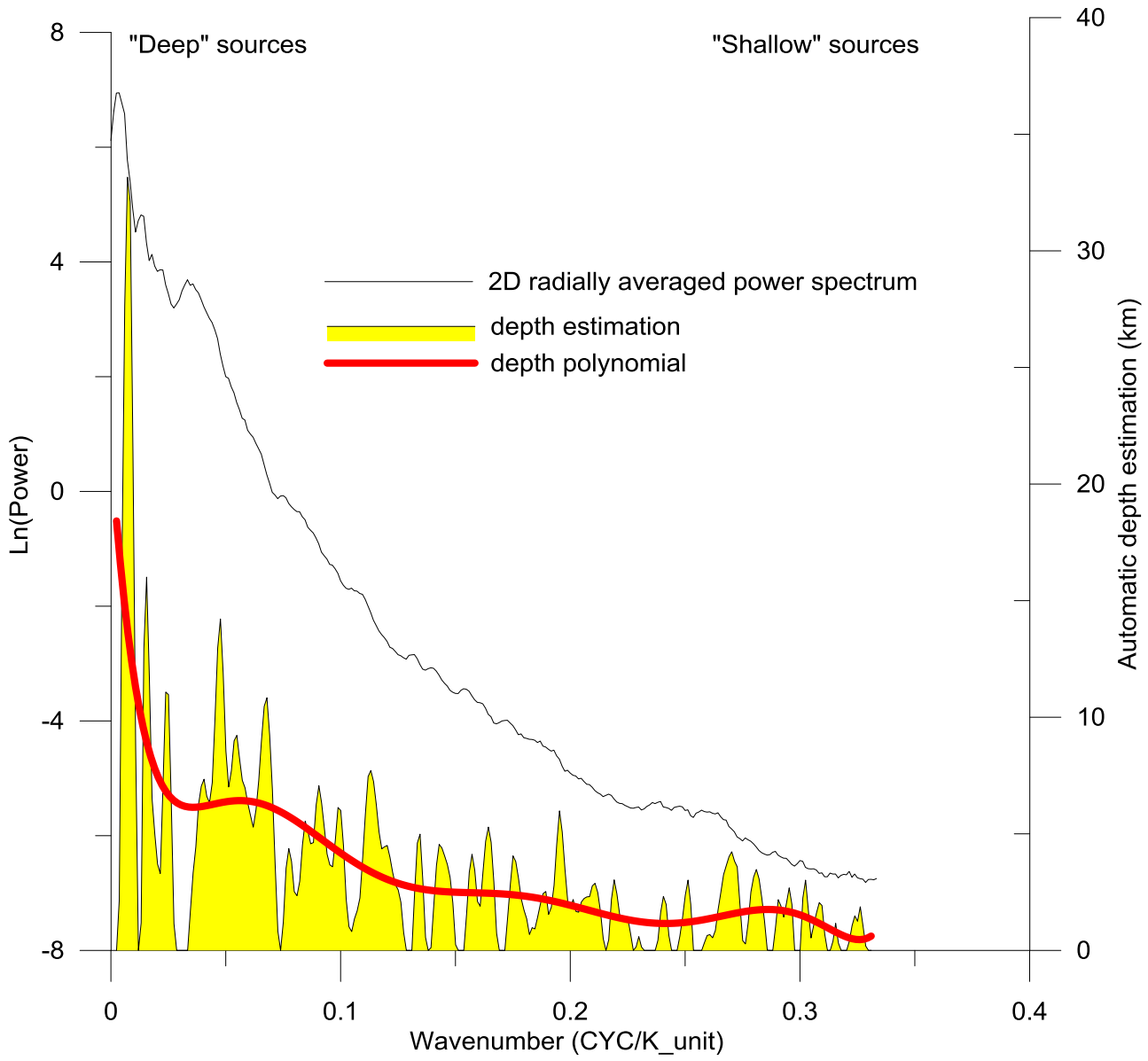

Figure 4.1 Frequency content and averaged power spectra computed for the JAS-12 magnetic total field grid. Steeper slopes increasing to the left of the plot, coincides with the deep-seated contribution. The depth estimate plot bar is an automatic 5 points slope and depth calculation, derived from the spectrum file (only for the 1500x1500 m grid). The polynomial curve (red) is an order 8 orthogonal polynomial calculated thought the depth estimation of the spectrum computed for the 1500x1500 grid size. It can be used to average and highlight the main segment and the statistical magnetic source estimation. The deepest set of sources along the survey is located at ~20 km but most of the sources are located at depths less than 10 km.

4.3 Magnetic sources

A relationship between the power energy spectrum and the depth distribution of magnetic sources can also be roughly investigated before any advanced integrated interpretation is concerned (Fig

4.1). The relationship was demonstrated for a simple magnetic prism by Battacharrya (1966) (Fig. 4.2). He showed that the power energy spectrum of the magnetic total field produced by a synthetic prism (Φ_{prism}) can be approximated as a function depending on depths to the top (z_{top}) and base of the prism (z_{base}) (Fig. 4.2). At medium to high wavenumbers (=long wavelengths):

$$\Phi_{prism}(k) \approx e^{-k.z_{top}} - e^{-k.z_{base}}$$

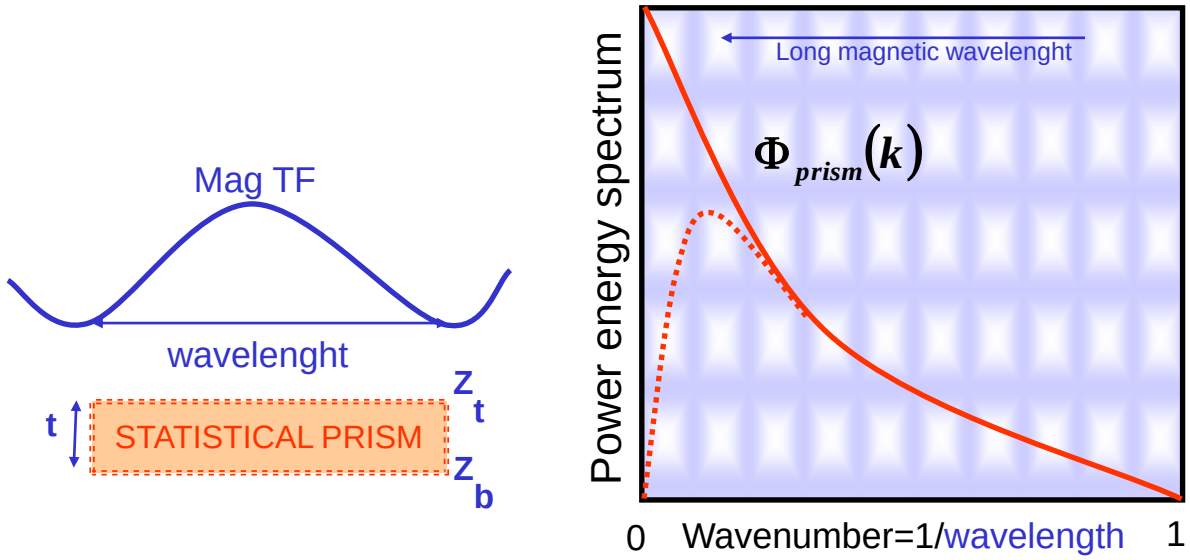

Figure 4-2 Magnetic total field produced by a simple prim (left) and power energy spectrum of this magnetic total field as function of the wavenumbers (k).

This fundamental approach also proposed by Spector and Grant (1970) provides information about the depth to a magnetic source. In their theory, the anomaly is assumed to be produced by a large number of blocks but the parameters describing one of the blocks are assumed to obey probabilities common to an entire set of different sources. The slope of each linear segment provides information about the depth to a magnetic discontinuity and magnetic interface (Spector and Grant 1970).

If we examine the shape of a JAS-12 power spectrum (Fig. 4.1), the "statistical" average depth to an ensemble of sources along the JAS-12 survey can be roughly evaluated using the value of the slope α along the steepest straight segment observed along the radial spectrum divided by 4π. We calculate automatic slopes using a gradient routine along a few adjacent points (Fig. 4.1). Unfortunately, some artefacts at low wavenumbers persist and sometimes wrongly affect this estimation. It should be noted that it is easier and more reasonable to measure the slopes on a printout, as the spectrum is more stretched out. The graphical technique is time-consuming but it makes it easier to identify and validate straight-line segments. Due to graphical uncertainties we estimate an uncertainty of ± 20%, in average for each theoretical depth calculation. This technique allows us a preliminary and quick look at the magnetic source depth distribution of the JAS-12 survey.

4.4 Reduction to the pole (RTP)

The magnetic data were reduced to the pole to properly register and locate the magnetic anomalies spatially above the magnetic bodies within the crust. Inclination and declination were derived from the last IGRF model (Fig. 4.3).

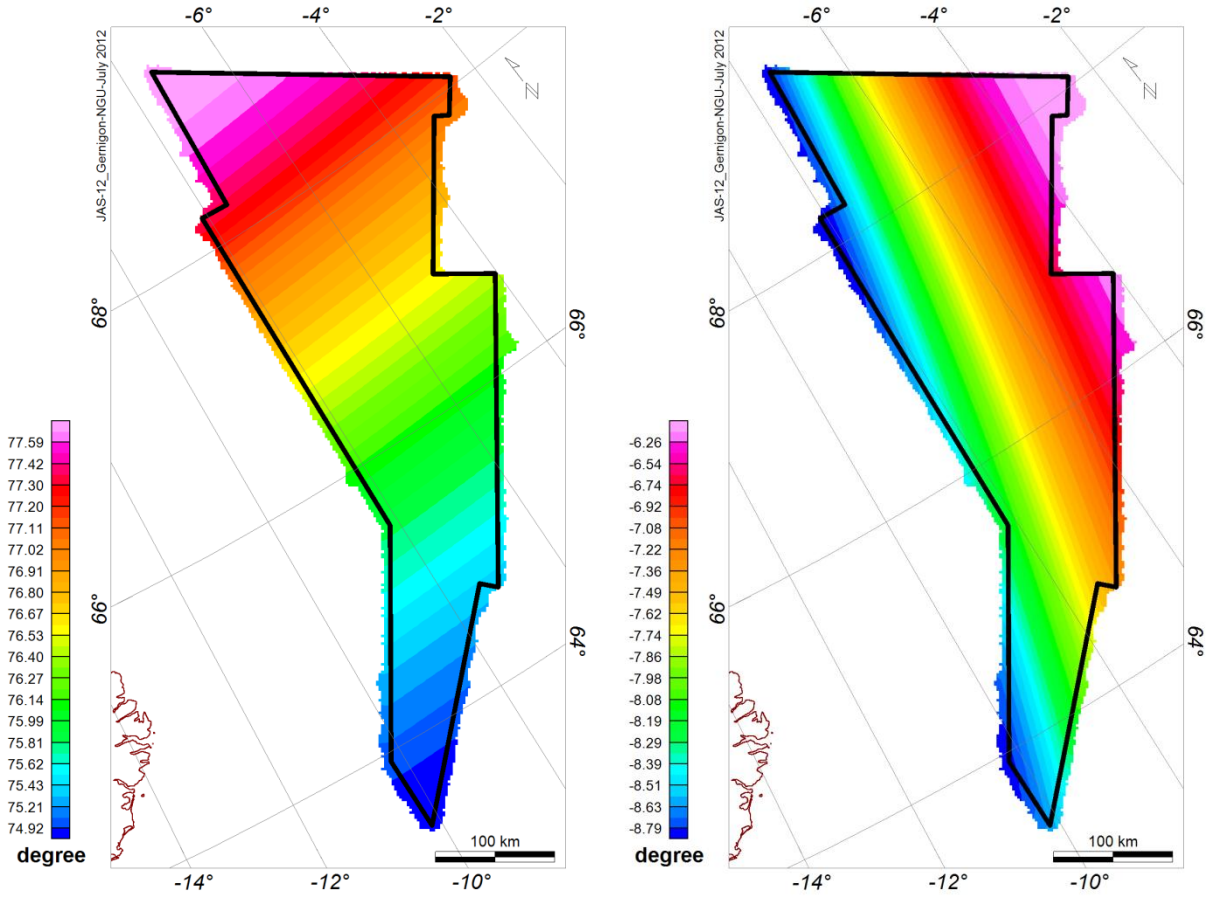

Figure 4.3 Values of inclination (left) and declination (right) of the geomagnetic field in the JAS-12 survey area.

Even if only minor changes can be observed along the JAS-12 at the Norway Basin latitude, the process is usually recommended for the application of magnetic data, and makes magnetic maps more reliable for geological mapping by removing some of the complexity involved in interpreting the anomalies (Blakely 1995).

The RTP is a process involving a phase transformation of the magnetic anomaly, within the Fourier domain. The measured total field anomaly is transformed into the vertical component of the field (Arkani Hamed 1988; Blakely 1995). At the latitude of the JAS-12 survey, we have found that the simplest and most effective technique is the one developed by GEOSOFT in the development of MAGMAP FFT processing (Geosoft 2005c). There are two ways to obtain the reduction to the pole. Running a 1D-FFT filter along each profile or running a 2D-FFT along the magnetic total field grid

(Figs. 4.4, 4.5, 4.6). Assuming that all the observed magnetic field of a study area is due to induced magnetic effects, pole reduction was calculated in the frequency domain using Fourier convolution

$$\mathcal{H}(u,v) = \mathcal{F}(u,v).G(u,v)$$

$\mathcal{F}(u,v)$ is the Fourier transform of the magnetic field and u,v represent the frequencies in units of cycles per meter. The filter operator G(u,v) is simply multiplied by the transform of the grid on an element by element basis and the inverse transformation of $\mathcal{H}(Mu,v)$ is leading to the final RTP grid. The following operators (Grant and Dodds 1972) can be used (Figs. 4.5):

Using the 1D-FFT:

$$G(\theta) = \frac{1}{[\sin^2(I) + i.\cos(I).\cos(D-\theta)]^2}$$

Using the 2D-FFT:

$$G(\theta) = \frac{[\sin^2(I) + i.\cos(I).\cos(D-\theta)]^2}{[\sin^2(I') + i.\cos(I').\cos(D-\theta)].[\sin^2(I) + i.\cos^2 \mathrm{I}.\cos^2(D-\theta)]}$$

Where:
$\theta = \tan^{-1}(\mathrm{u/v})$ is the wavenumber direction
I is the magnetic inclination
I´ is the second magnetic inclination (=0 in this study)
D is the magnetic declination

The assumption following this transformation is that the magnetic bodies are magnetised vertically at the pole and that the anomalies are observed from the pole. Key assumptions are that the magnetization of the source is entirely due to induced magnetization. The phase of the anomaly is therefore transformed into simpler symmetrical shapes that are assumed to lie directly over the magnetic sources (Blakely 1995). This assumption is essential for future mapping and analysis of the magnetic anomalies because it is assumed when applying edge enhancement techniques, that the causative field is vertical. Consequently, some agree that the RTP filtering should be carefully considered. Moreover, it is assumed that both the magnetic field and the magnetization of the crust have constant directions within the study area (Arkani-Hamed 2007).

Statistics	Inclination	Declination	IGRF
Minimum value	74.64°	-9.03°	51654.74
Maximum value	77.97°	-5.40°	52824.75
Mean value	76.47°	-7.61°	52274.89
Standard deviation	0.78°	0.77°	270.97

Table 4-1 IGRF field, minimum, maximum and mean values for inclination and declination observed in the JAS-12 survey.

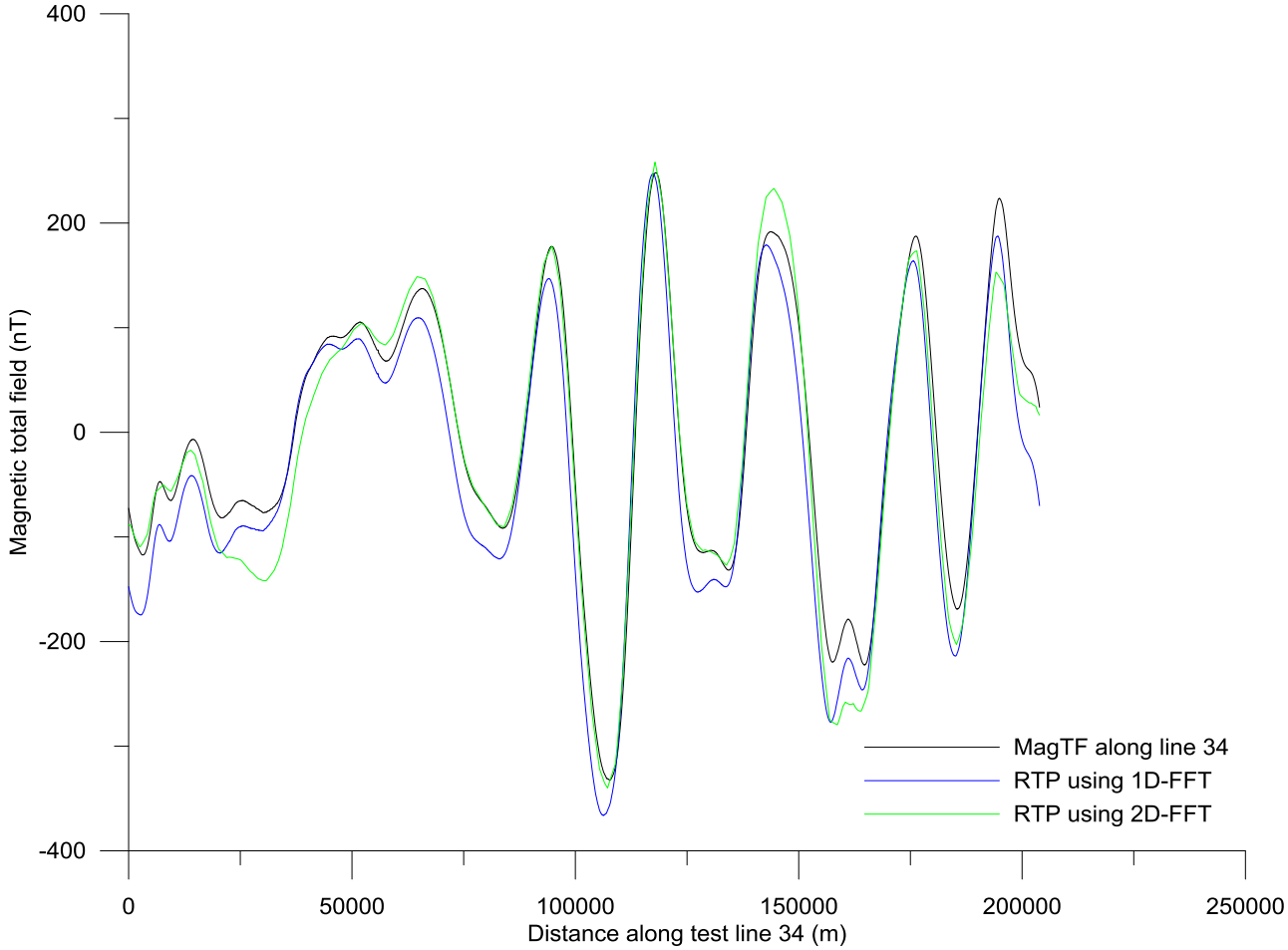

Figure 4-4 Differences between the 1-D and 2D FFT algorithms used to calculate the reduction to the pole along the test line 34 of the JAS-12 survey with the mean values of inclination and declination. The result is compared with the original magnetic total field.

The RTP filtering is also limited for large surveys because each RTP equation does not consider the synchronous variation of both inclination and declination. Each transformation only considers one value for inclinations and declinations. For the RTP transformation, we used the mean values of the inclination and declination (Table 4.1) and Figure 4.6 shows that other values can produce a significantly different RTP signal. This effect needs to be considered during the evaluation of the uncertainties associated with the magnetic chrons interpretation (Figs 4.8, 4.9).

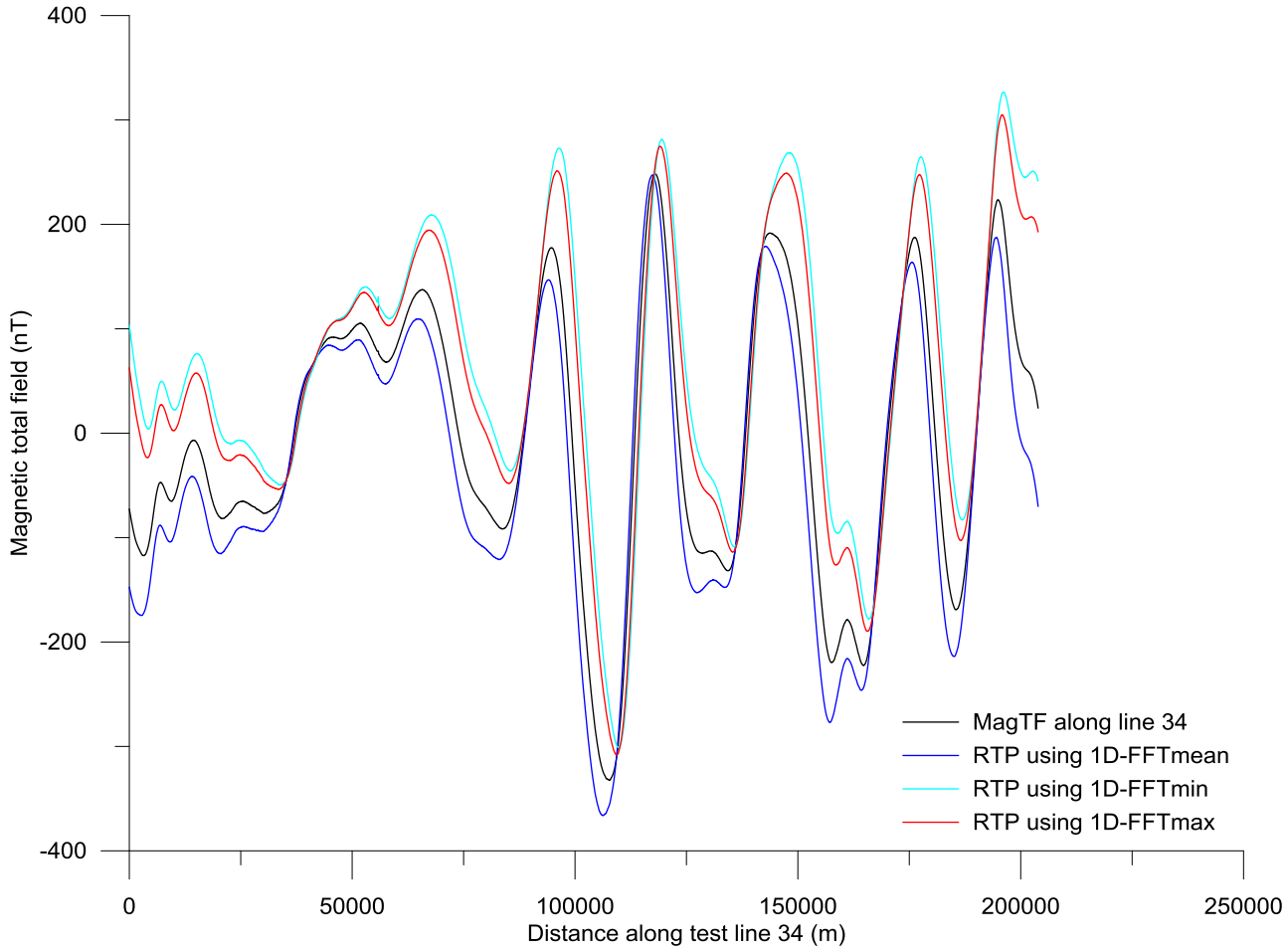

Figure 4.5 Differences between the 1-D FFT algorithms using different inclinations and declinations values (see Table 4.1). RTP transformation assumes only one value for both inclination and declination.

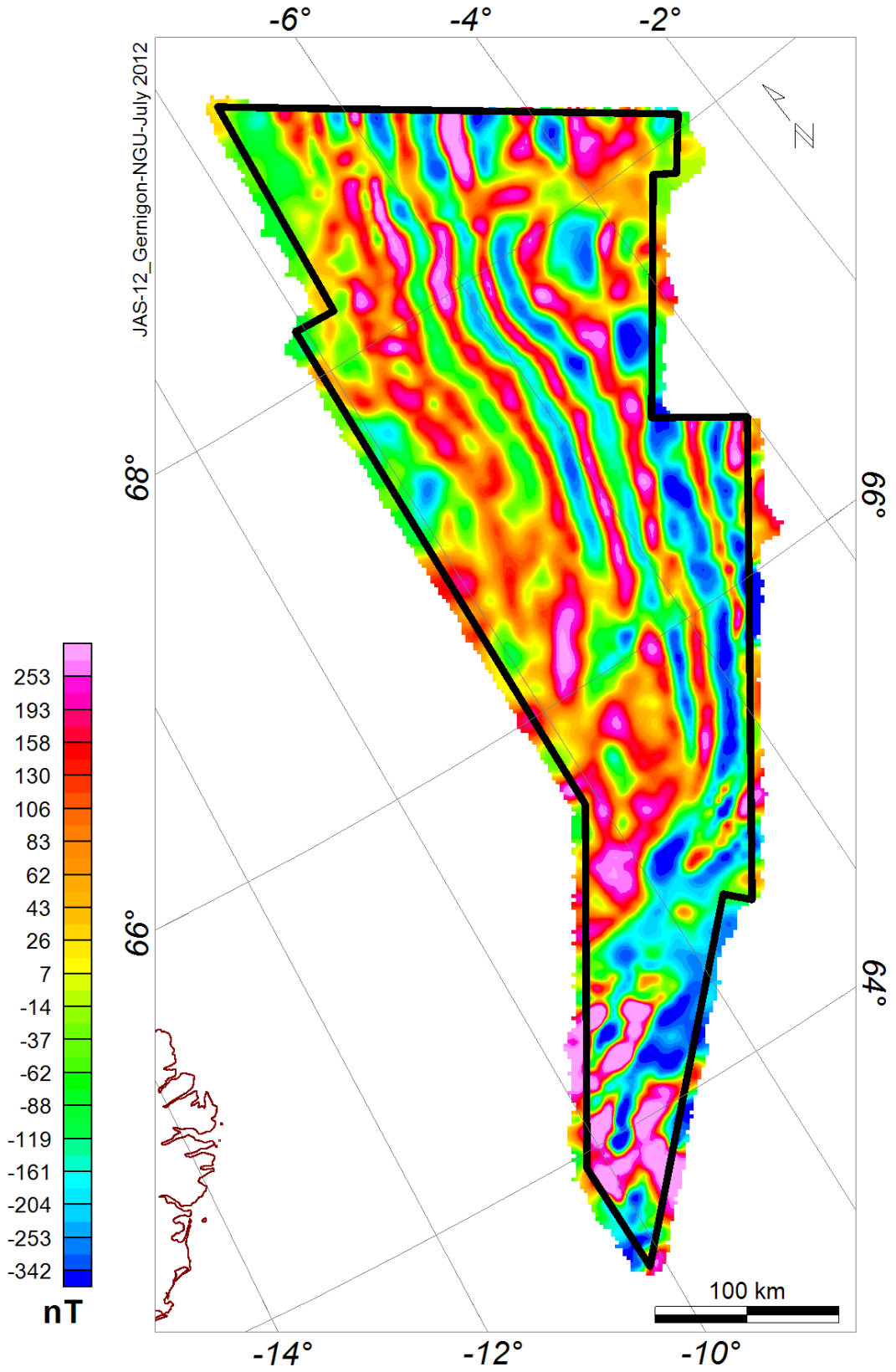

Figure 4.6 Total magnetic field reduced to the pole (Inc: 76.47; Dec: -7.61) carried out using a 2D-FFT filtering. The RTP transforms the anomaly into the one that is related to a vertical magnetization and a vertical Earth's field, i.e. the anomaly that would be observed if the sources were located at the Earth's magnetic north pole. As a result, it removes asymmetries caused by the non-vertical inducing field and places the anomalies more directly over their causative bodies, thus facilitating the interpretation of the magnetic dataset. Note that at the JAS-12 latitude, these changes can be relatively important.

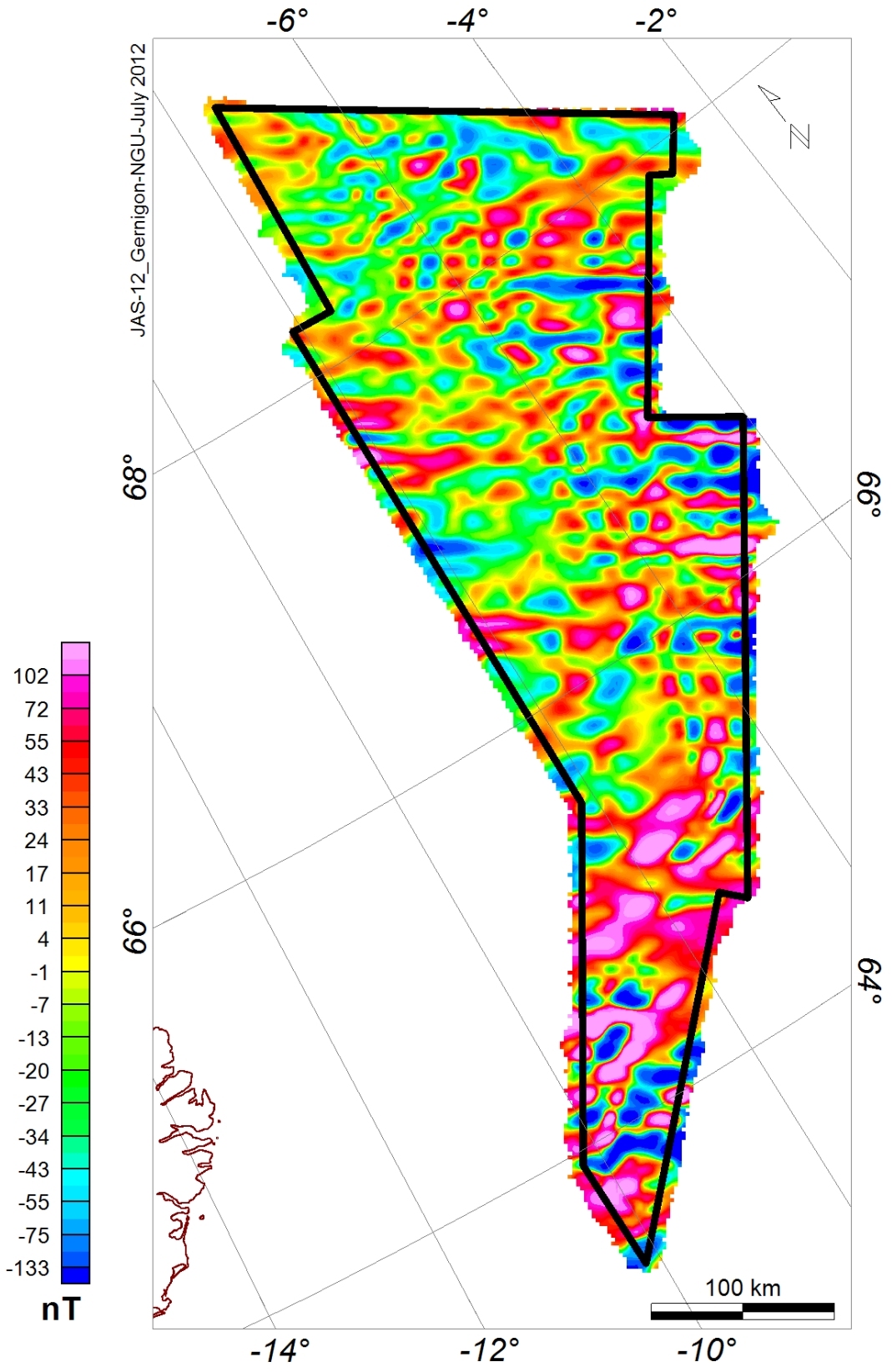

Figure 4.7 Anomalies differences between the total field reduced to the pole and not reduced to the pole.

4.5 Upward continuation

Upward continuation is a low-pass filtering process simulating the result of the survey if it was carried out at a higher elevation (Fig. 4.8). This process is based on the physical fact that the further the observation is from the body causing the anomaly, the broader the anomaly is. Upward continuations to 15 and 30 km have been used for the JAS-12 survey to give indications about the main magnetic and tectonic units in the area (Fig. 4.8). Upward continuation underlines deep crustal blocks or deep sedimentary units of markedly different magnetic composition.

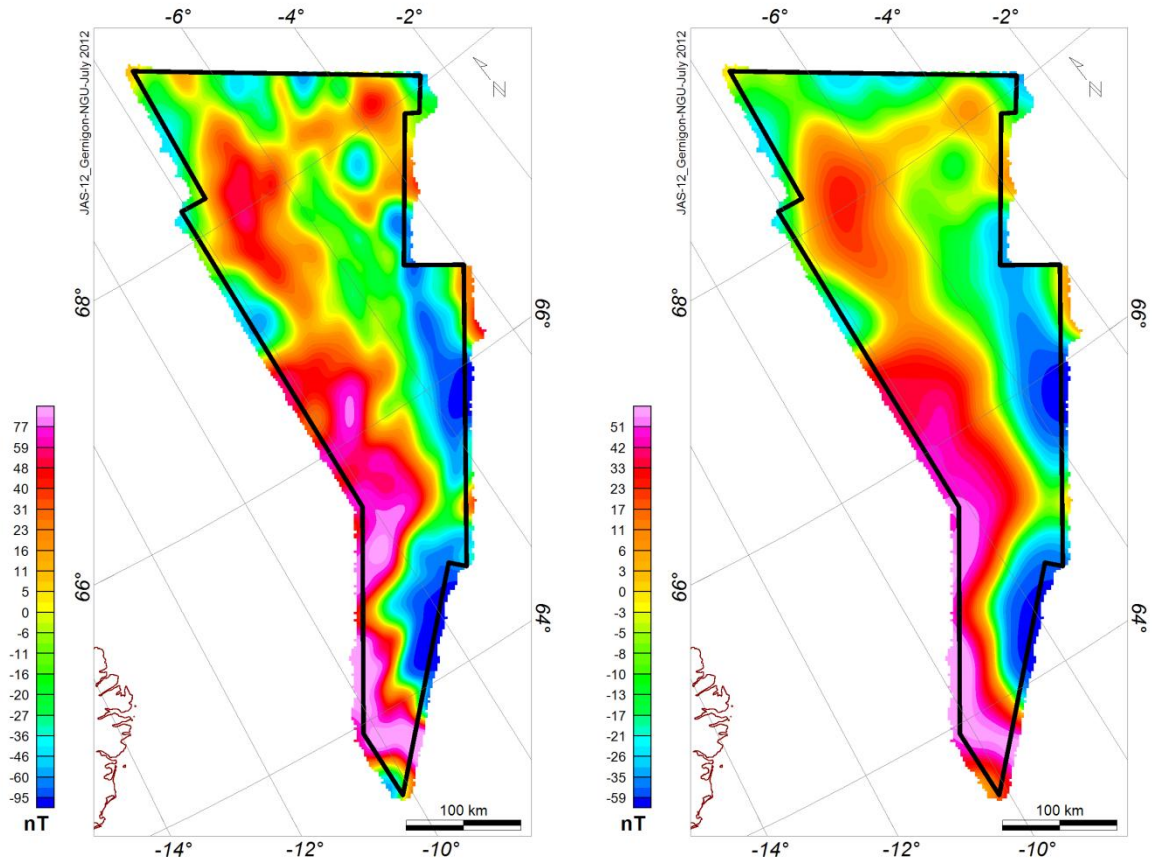

Figure 4.8 Upward continuation of the magnetic total field. On the map to the left an upward continuation of 15 km has been calculated and we have used a similar upward continuation of 30 km on the map to the right. Upward continuation uses wavelength filtering to simulate the appearance of potential-field maps as if the data were recorded at a higher altitude. Large-scale regional anomalies and main crustal patterns are revealed.

4.6 High-pass, low-pass and band-pass filtering

To successfully delineate the shallow crustal feature, it is necessary to distinguish the short wavelength (noise) and long (regional) wavelengths due to deeper sources in order to isolate the wavelengths derived from upper crustal structures.

The regional anomalies can be estimated employing a variety of analytical techniques, including high-pass and low-pass filters (Figs. 4.9, 4.10, 4.11, 4.12, 4.13). The magnetic data were most useful to determine the presence, trends and depth of intrusions, faults and basement structures. High-pass filtering of the data at 50-30 km can be used to highlight sources typically at depths shallower than 10-15 km whereas 20-15 km high-pass filtering will be used for source depths shallower than 5 km (Figs. 4.9, 4.10).

Using band-pass filter (Fig. 4.11), we can also investigate more precisely different ranges of wavelengths and estimated the depth distribution for different set of anomalies using the method of Spector and Grant (1970) to get the depth estimations of the sources assuming that the long wavelengths reflect the deeper sources. Approaches to this problem are generally data- or model-based. Linear segments in the logarithmic power spectrum of the JAS-12 (Fig. 4.1) correspond to different components of the field. The band-pass filtering has been designed to carry out the separation. This approach is used to separate expected basement effects from intra-sedimentary sources and deep versus shallow crustal sources within the JAS-12 magnetic data.

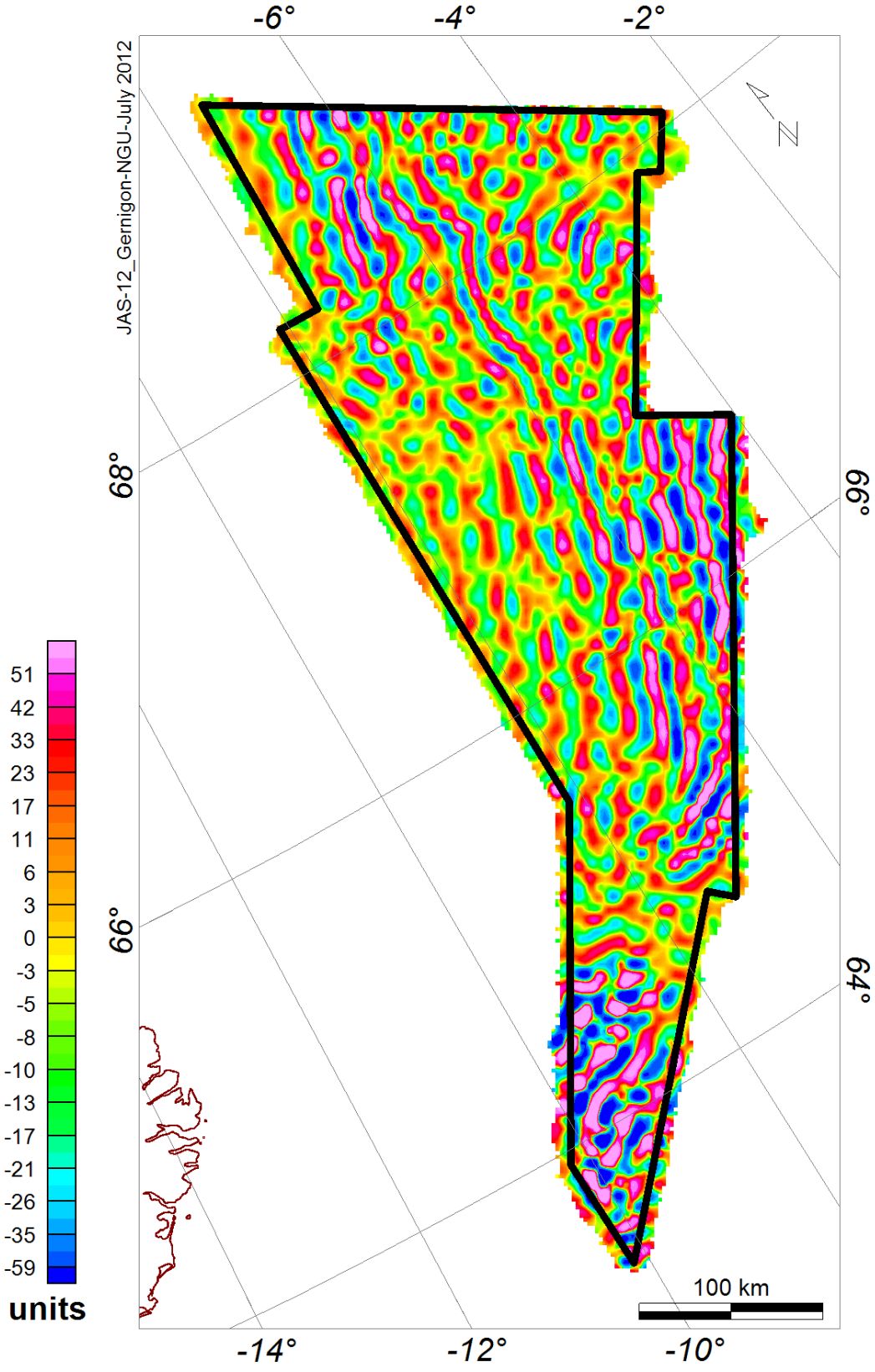

Figure 4.9 High-pass filtering (20km) of the magnetic total field. This filter emphasizes the distribution of the short wavelengths. Grid cell size: 1500x1500m.

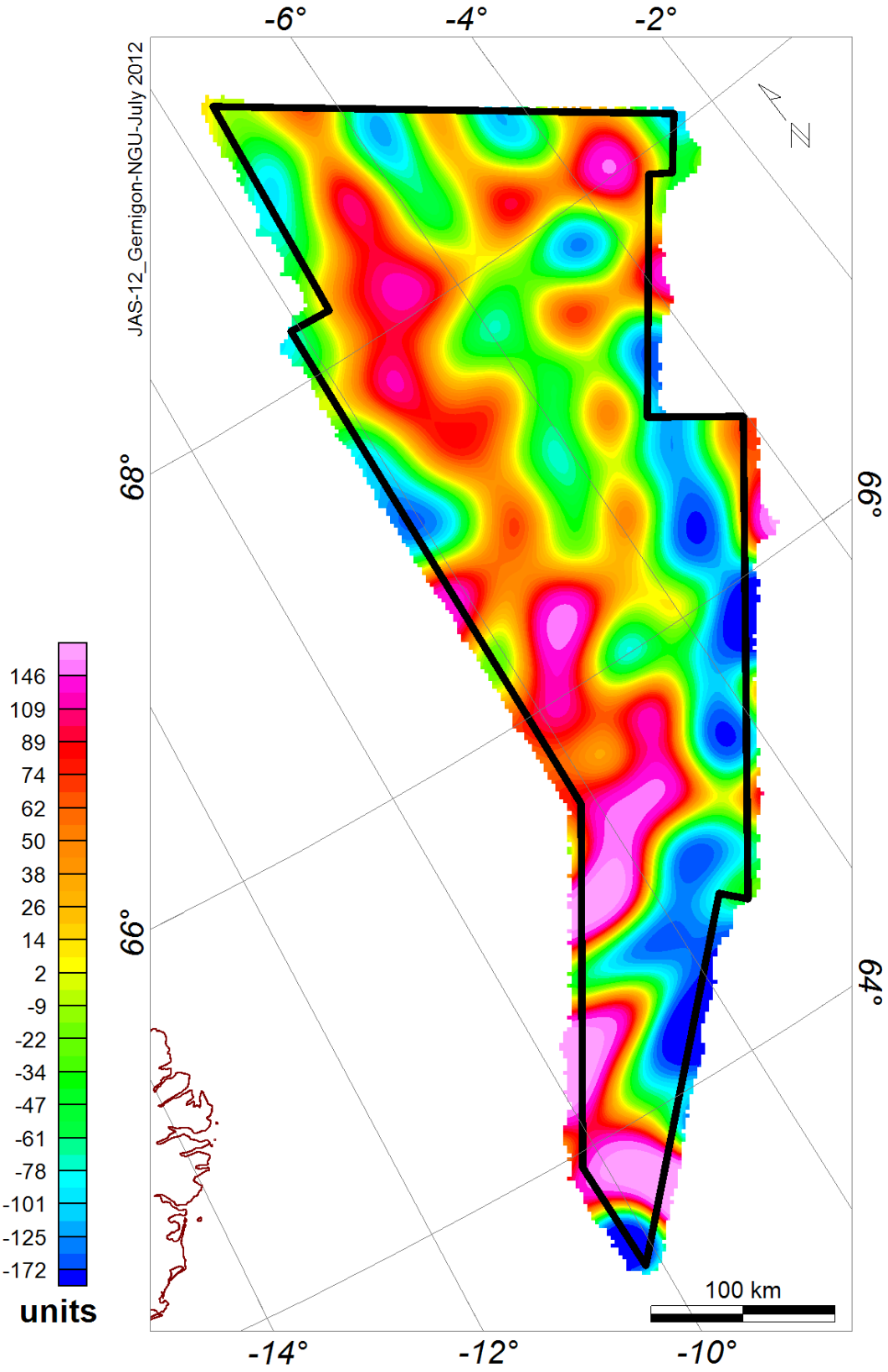

Figure 4.10 Low-pass filtering of the magnetic total field at 50km. This filter smoothes the magnetic signal and emphasizes the distribution of the main magnetic units. In theory, these medium anomalies most likely reflect mid-crustal sources and already illustrate the basin segmentation and complexity.

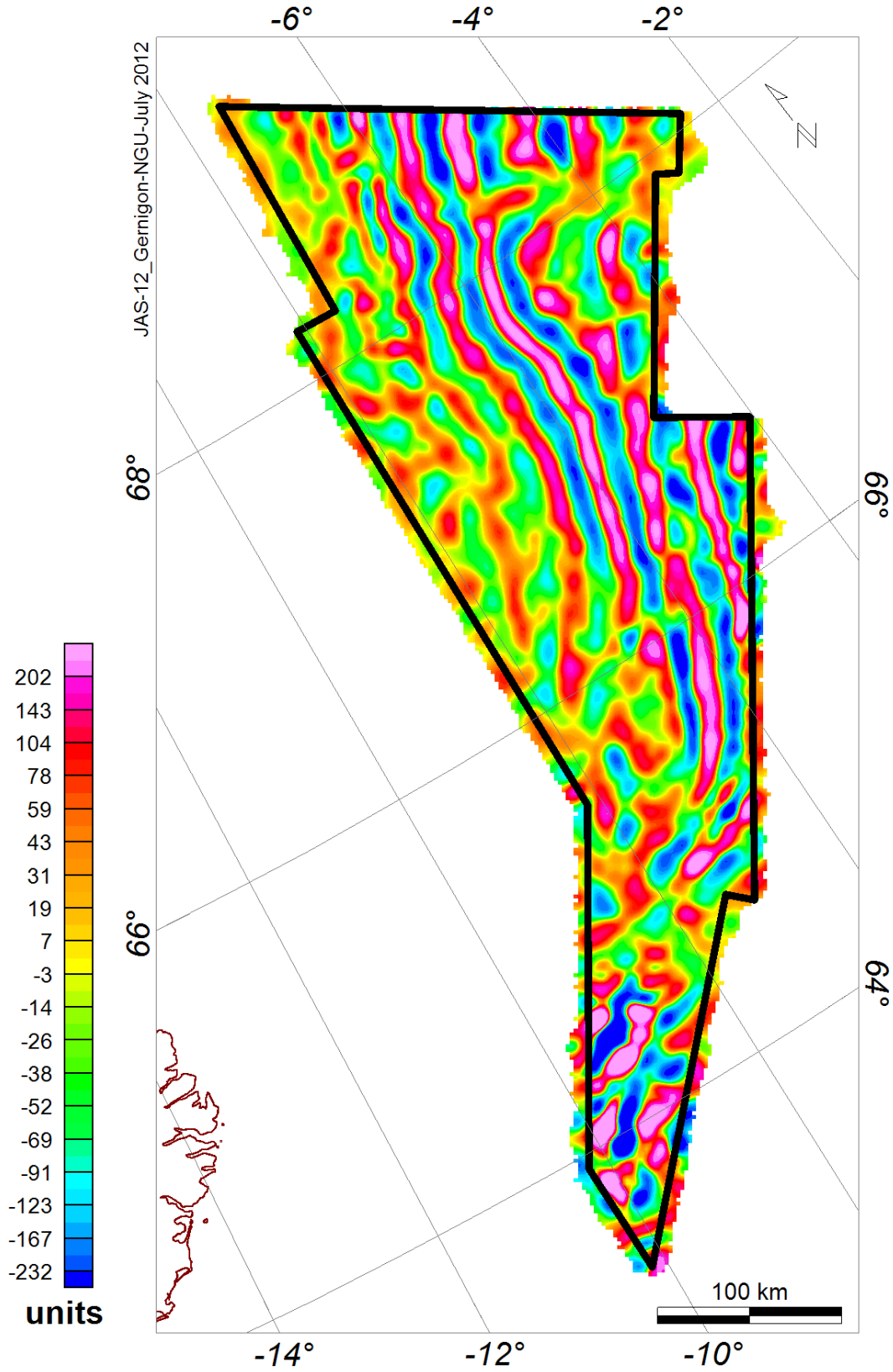

Figure 4.11 Band-pass sampling of the magnetic total field. This filter only considers the wavelengths specified in a certain range. This grid illustrates the anomalies sampled using a high wavelength cut-off of 20 km. According to the spectrum analysis, these anomalies should represent sources located in the 3-5 km depth interval.

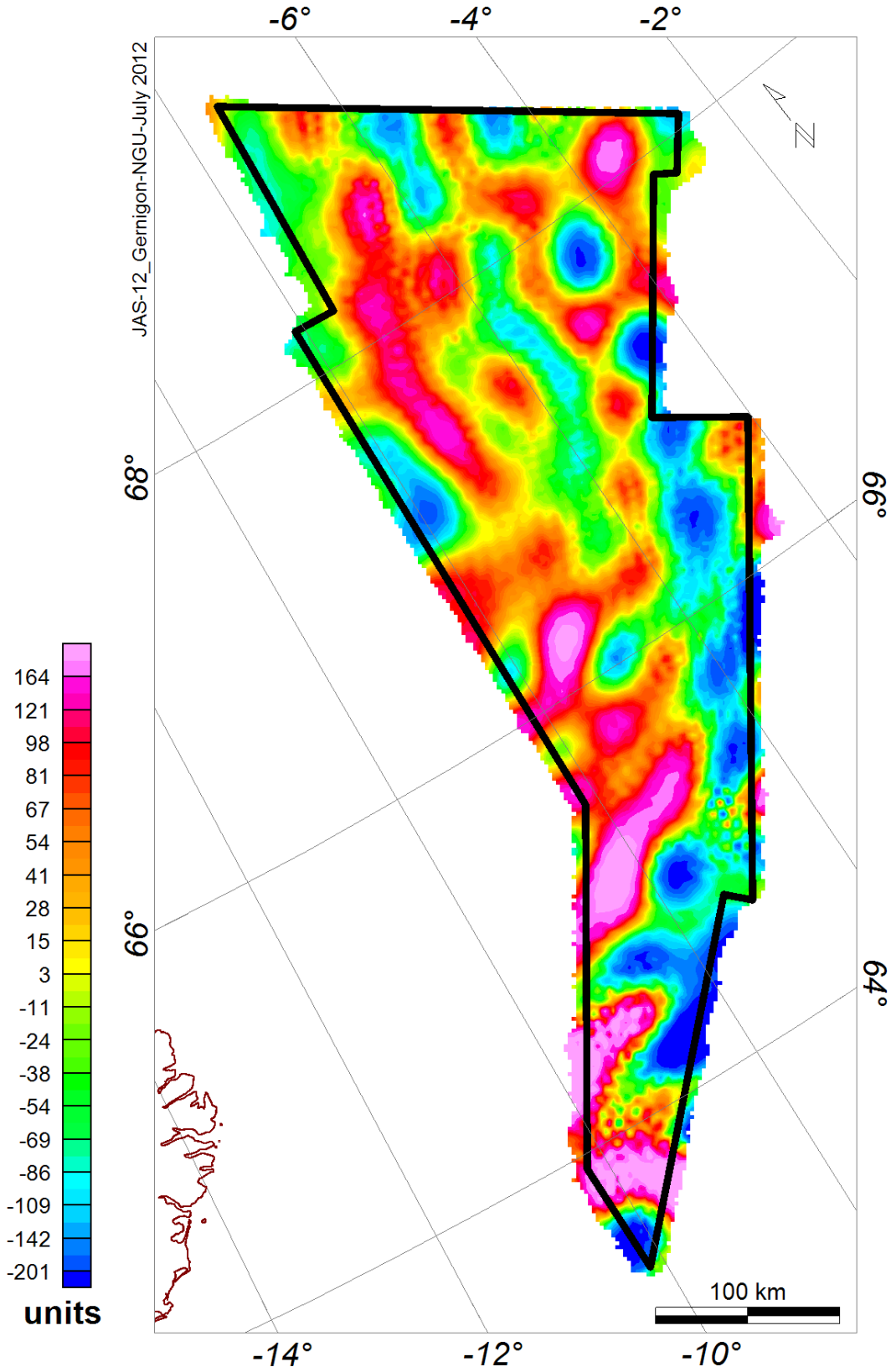

Figure 4.12 Band-pass sampling of the magnetic total field. This filter only considers the wavelengths specified in a certain range. This grid illustrates the residual anomalies after the previous low wavelength cut-off of 40 km and a high wavelength cut-off of 10 km. According to the spectrum analysis, these anomalies should represent both deepest and shallowest anomalies.

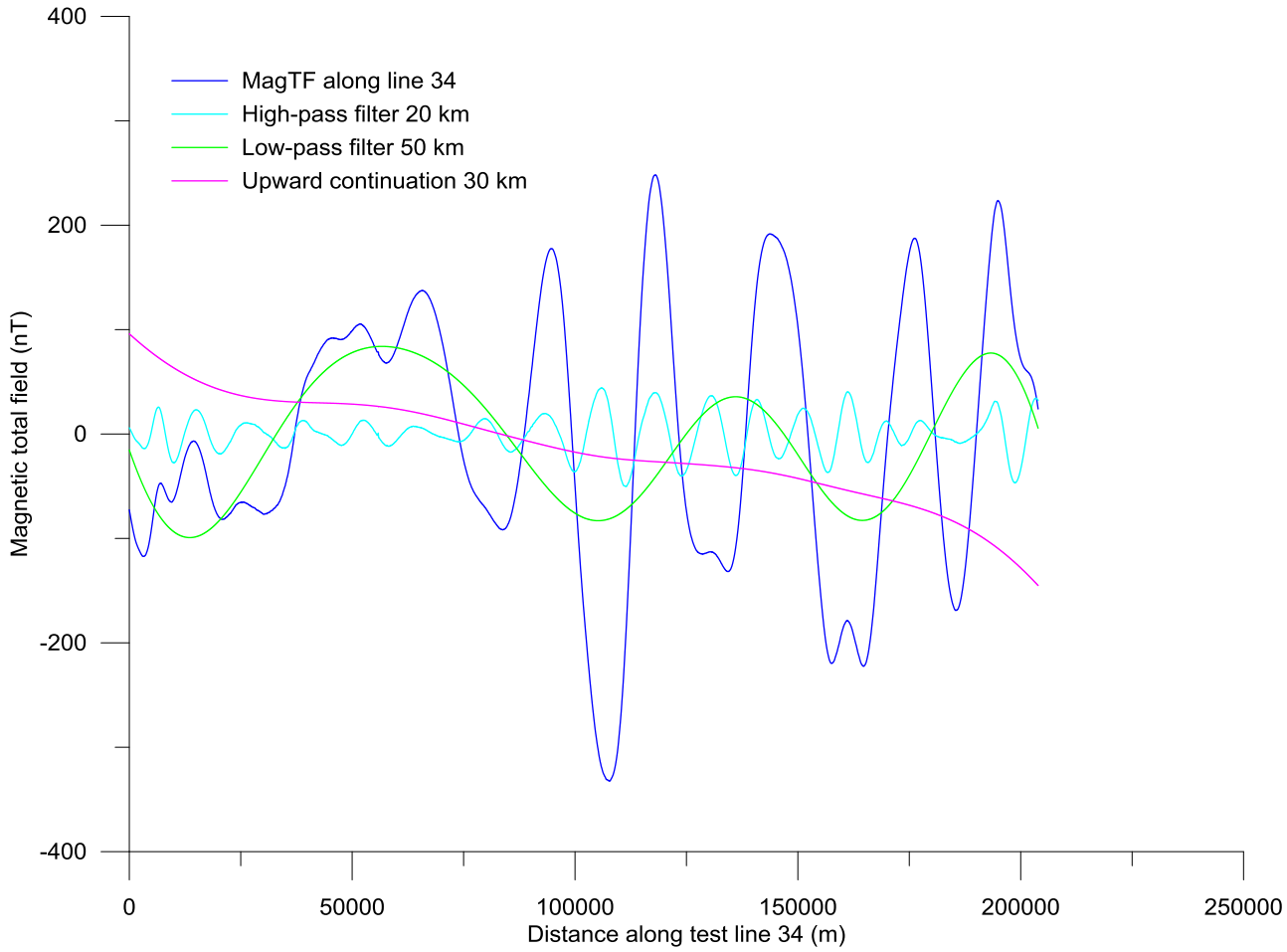

Figure 4.13 Example and comparison of high-pass, low-pass and upward continuation filtering of the magnetic total field (line 34 of the JAS-12 survey).

5 TREND ENHANCEMENT USING STRUCTURAL FILTERS

Laurent Gernigon

The purposes of this chapter are 1) to show the applicability of derivative and normalised filters in investigation of the structural setting along the Norway Basin and surrounding margin (e.g. Jan Mayen microcontinent); 2) to evaluate the images produced by several enhancement techniques for lineaments mapping; 3) to prepare structural and depth to magnetic basement estimation maps (lineament) based on magnetic and gravity data interpretation. Some newly discovered lineaments and features might be subsequently used as a reference for future geological mapping, interpretation or re-interpretation.

5.1 Automatic gain control (AGC)

The automatic gain control filtering (AGC) was applied to convert waveforms of variable amplitudes to a grid that gives an equal emphasis to signals with both low and high amplitudes (Mudge 1991). Like derivative filters, the AGC filter is particularly useful to enhance structural features because it highlights trends with coherent alignments not always apparent in true amplitude data (Fig. 5.1).

5.2 Derivative filters

Derivatives of the magnetic total field and its analytic signal have been computed within this study to enhance short wavelength features and main lineations. Computation of the three orthogonal derivatives, (x, y, z) within potential field modelling is considered as a universally applicable and basic processing step (Thurston and Brown 1994; Nabighian et al. 2005).

5.2.1 Vertical derivatives

Vertical derivatives (VDR) were used to enhance localised near-surface sources and trends, and to improve source resolution, assuming high-quality data (Fig. 5.2). Transformation of potential field data into a derivative map enhances edges or contacts by placing anomaly maxima at the point of the maximum horizontal gradient identified within the x- and y- orientation of the grid. However, the key assumptions made when transforming gravity and magnetic field data into the three orthogonal derivatives are: (1) the potential field measured at the surface is the vertical component of the field; (2) that the lithological contacts giving rise to the anomalies are abrupt, near-vertical, and isolated from other sources. The first assumption is essentially true for gravity and for magnetic data reduced to the pole (Blakely 1995). In reality however, geological contacts are rarely vertical and density and magnetization can vary in all directions in a geological unit.

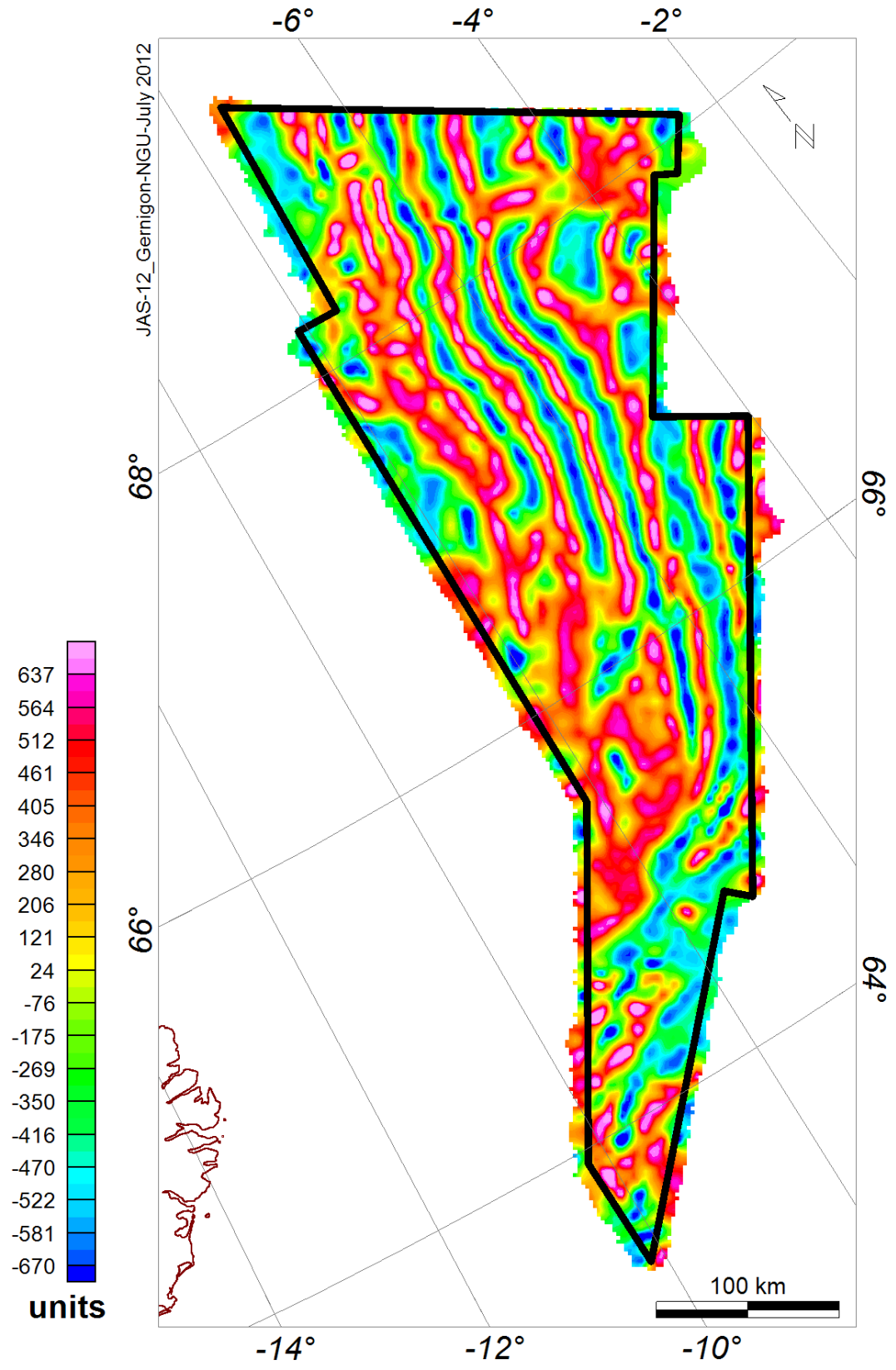

Figure 5.1 Automatic gain control filtering (AGC) of the JAS-12 survey. To highlight the local anomaly details, automatic gain control (AGC) boosts amplitudes in areas with small anomalies, without sacrificing the long-wavelength information. Gain is estimated with a sliding square filter window, centred on each grid node.

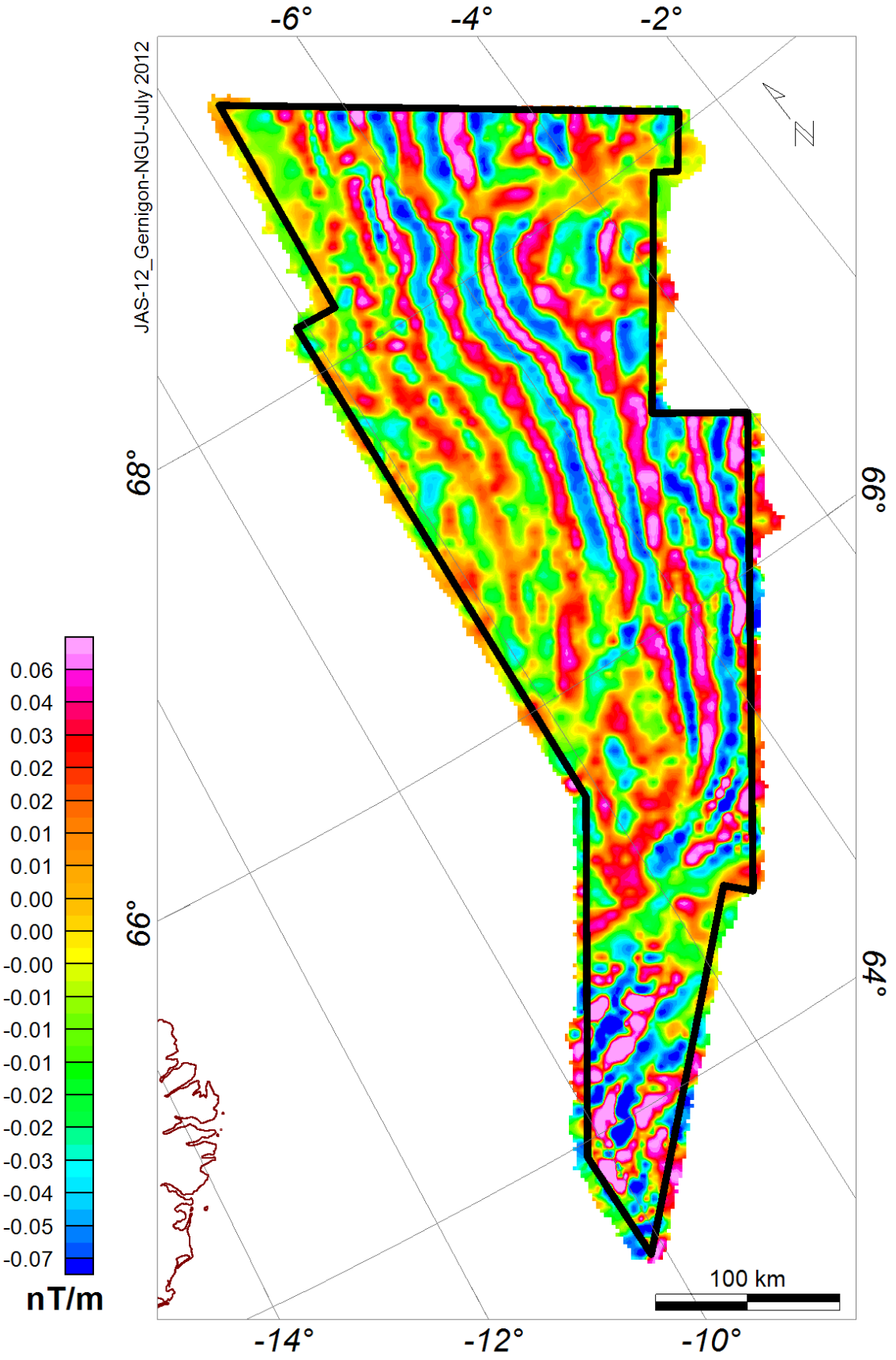

Figure 5.2 Vertical derivative obtained by convolution along the magnetic total field reduced to the pole and gridded with a cell size of 1650m using minimum curvature. The vertical derivative of an anomaly is related to the depth and geometry of the causative body. The gradient operator attenuates broad, more regional anomalies and enhances local, more subtle magnetic responses and as such is sensitive to shallow magnetic source bodies and contacts.

Computation of the second vertical derivative as described by Blakely (1995) can be unstable (Fig. 5.3). The second vertical derivative, or rate of change of the fall-off (rate) of an anomaly, may be considered equivalent to a residualisation of the data and is frequently used as an aid to delineating source bodies. However, because it is a derivative of a derivative (we remind you that the magnetic field is not a harmonic function), this filter emphasizes shallower sources and is also strongly affected by noise. Therefore, it must be treated with some caution when interpreting basement structures.

5.2.2 The horizontal derivatives

The horizontal derivatives (HDR) can be used to predict the locations of major basement or sedimentary structures, igneous bodies and changes in basement grain (Grauch and Cordell 1987; Gunn 1997). Indirectly N-S and E-W directional filters have been found useful to locate suspicious N-W and E-W trending linear anomalies due to remaining levelling errors along the lines and tie-lines of the NB-07 survey (Figs 5.4, 5.5, 5.6).

5.2.3 The terrain slope filter or maximum horizontal derivative filter

Quite similar to the way the first directional derivative defines the slope at any point on the surface, the terrain slope filter has been applied to calculate the slope at any grid node of the JAS-12 (Fig 5.7). Grid files of the terrain slope can produce contour maps that show isolines of constant steepest magnetic slope. The terrain slope filter or total horizontal derivative filter, calculates the slope at any grid node on the surface. For a particular point on the surface, it is based on the direction of steepest descent or ascent of the magnetic field at that point. This means that across the surface, the gradient direction can change. This operation is similar to the way the first directional derivative filter defines the slope at any point on the surface but is more powerful in that it automatically defines the gradient direction at each point on the map.

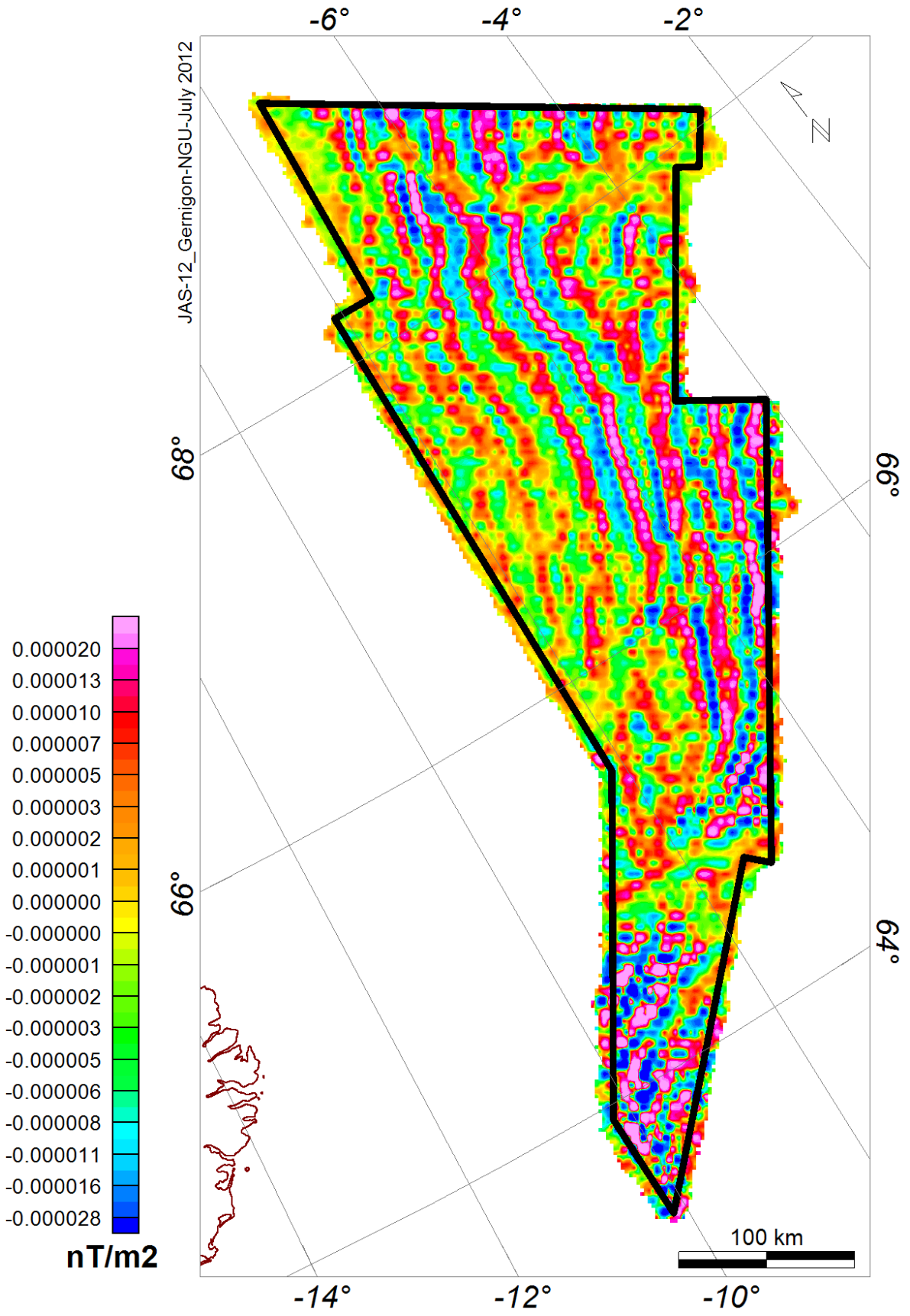

Figure 5.3 Second vertical derivative obtained by convolution along the magnetic total field reduced to the pole. The second vertical derivative can be seen as a regional-residual separation technique because it suppresses long wavelength anomalies related to regional influences. Due to filtering instability (see ringing for example), this dataset must be used with some caution when interpreting basement structures.

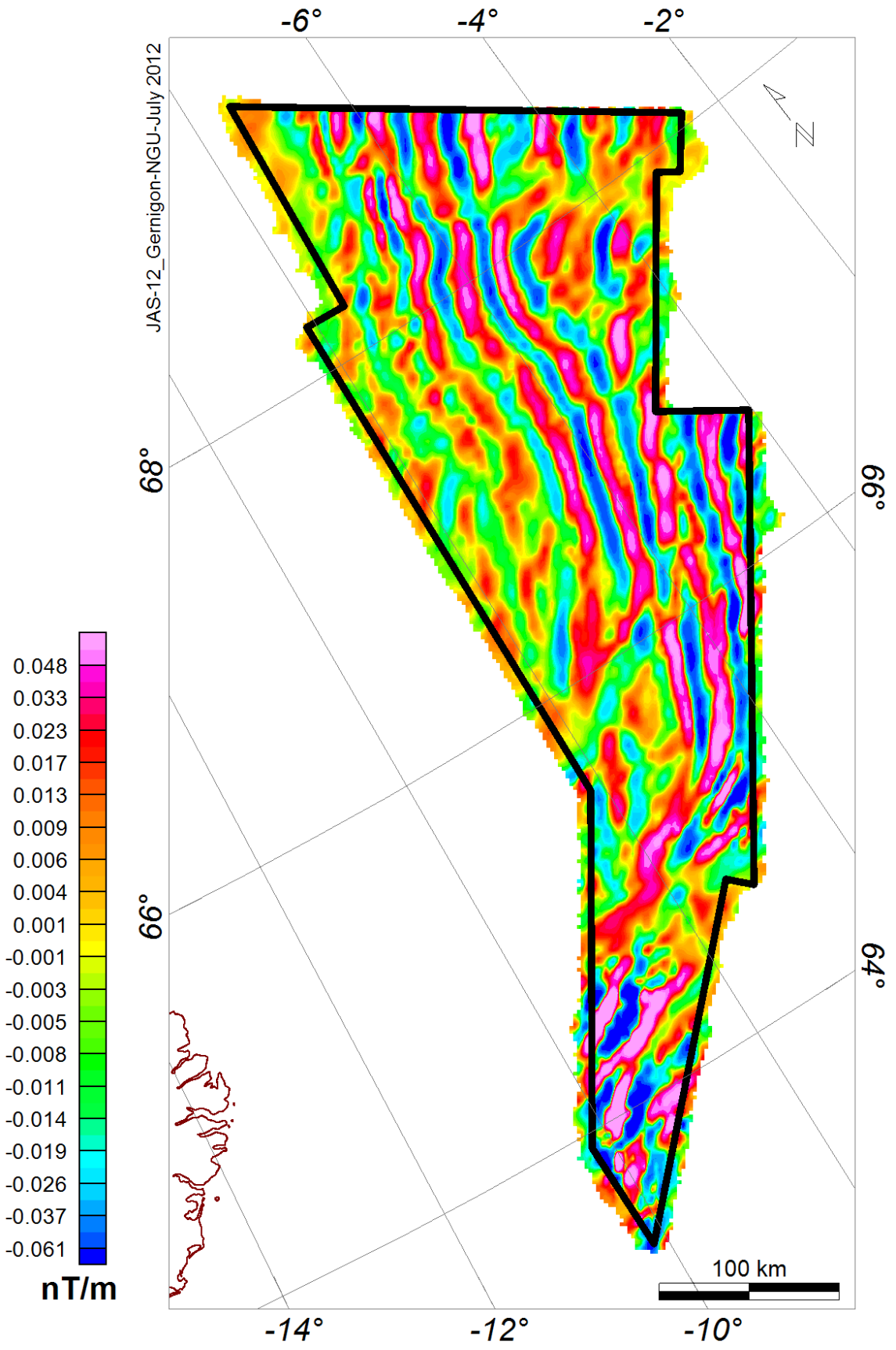

Figure 5.4 Directional horizontal derivatives with the JAS-12 area. The filter enhances the high frequencies along the NW-SE trend.

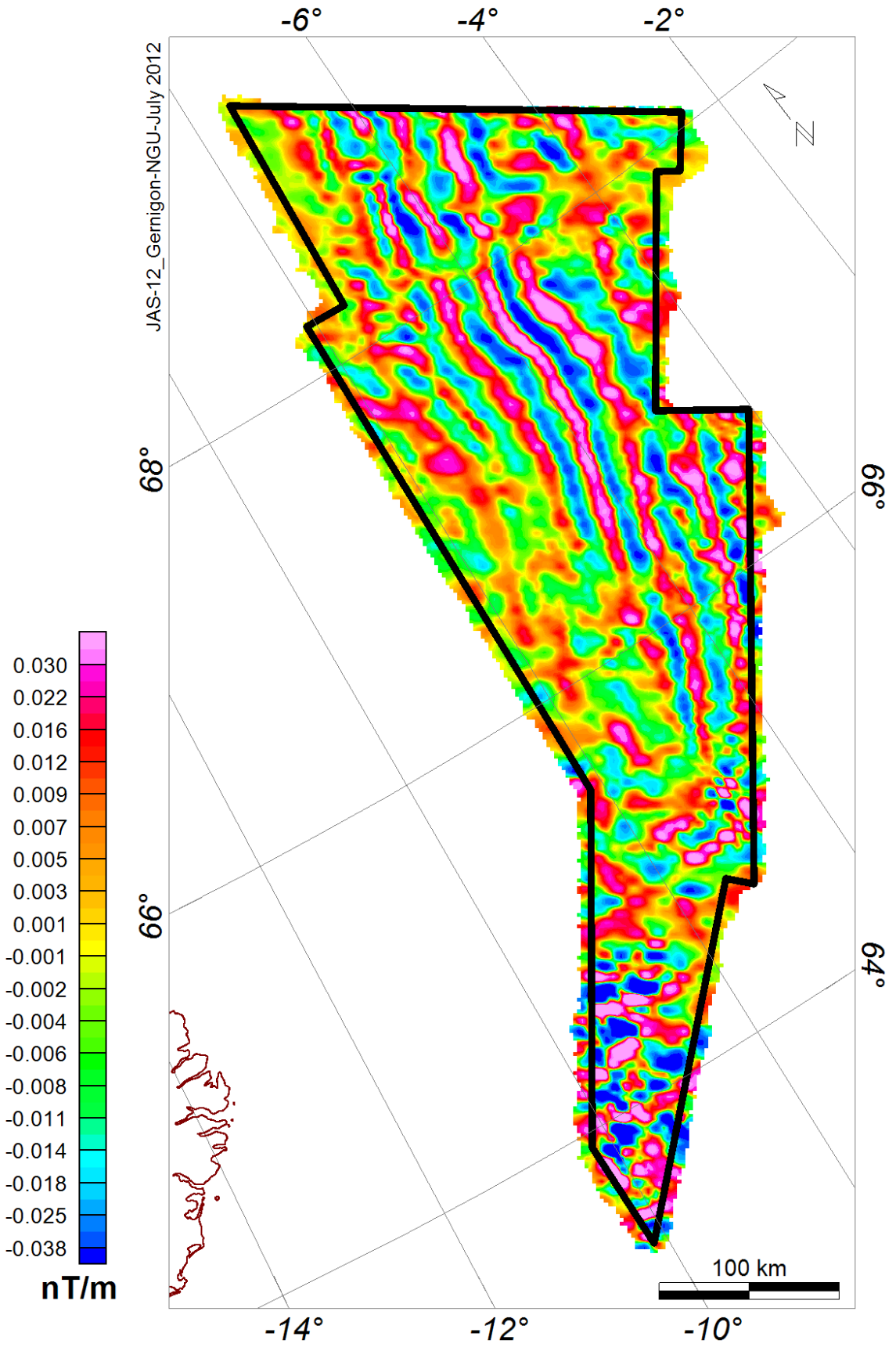

Figure 5.5 Directional horizontal derivatives with the JAS-12 area. The filters enhance the high frequencies along the NE-SW trend.

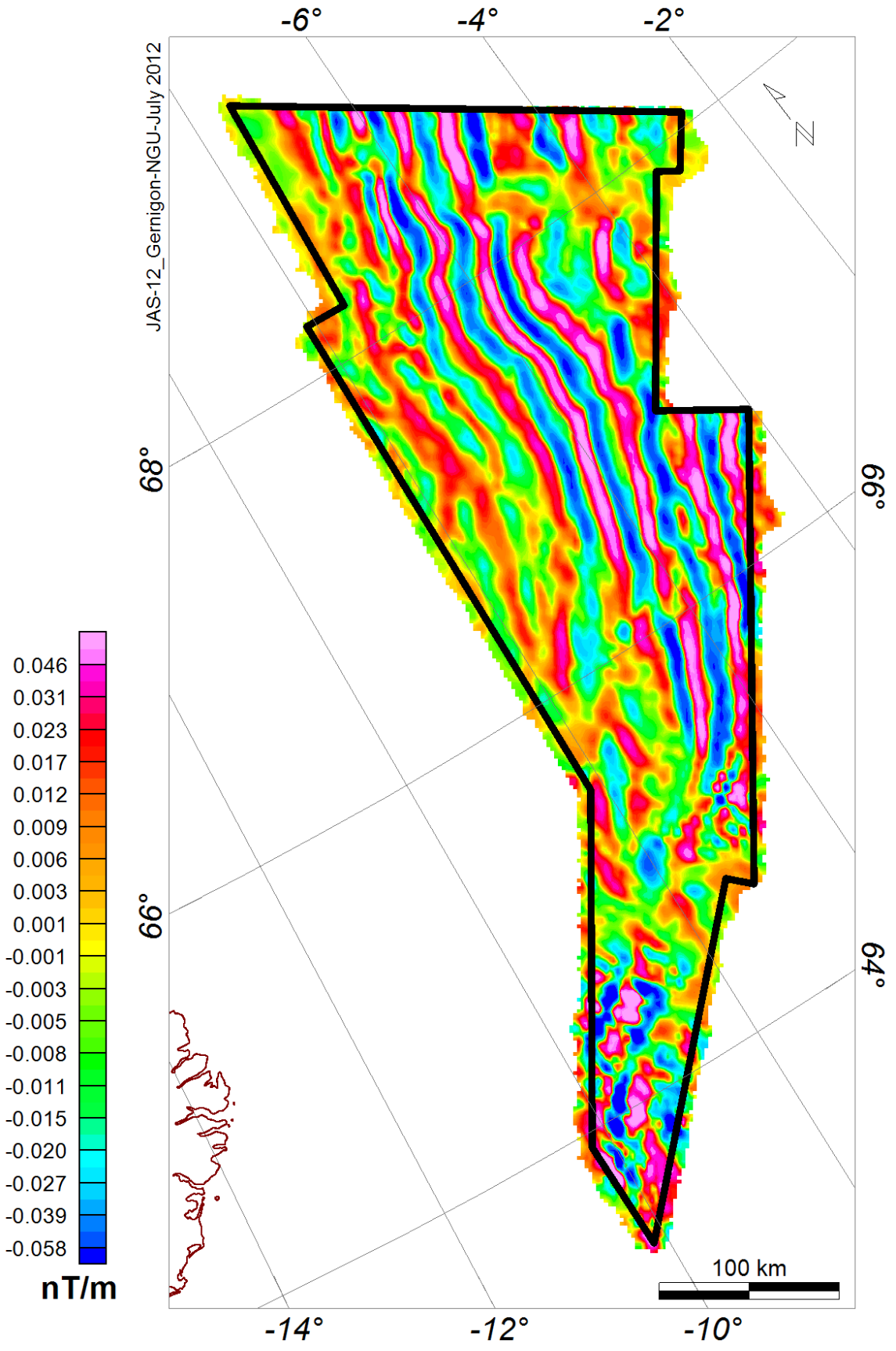

Figure 5.6 Directional horizontal derivatives with the JAS-12 area. The filters enhance the high frequencies along the N-S trend.

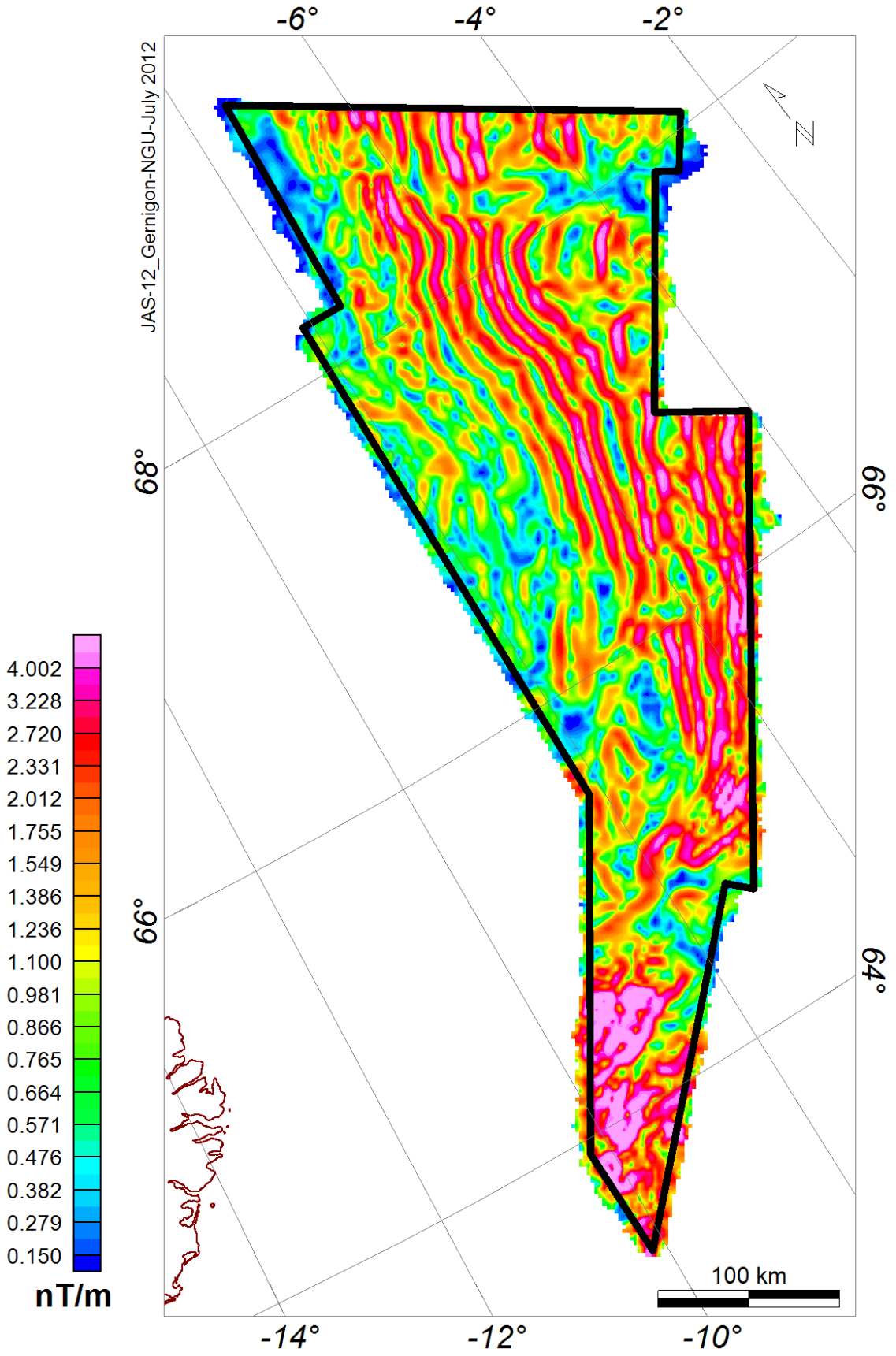

Figure 5.7 Maximum horizontal gradient of the JAS-12 dataset. The maximum horizontal gradient (more properly the maxima of the total horizontal gradient) of the anomaly slope is located near or over the body edge. That is, the horizontal gradient operator in map form produces maximum ridges over edges of magnetic basement blocks and faults or other magnetic bodies. In addition, the horizontal gradient highlights linear features, related to magnetic contacts, in the dataset.

5.3 Analytic signal - 3D total gradient

The concept of analytic signal applied to magnetic anomalies was developed in two dimensions by Nabighian (1972) based on a concept initially proposed by the french Ville in 1948. In two dimensions, the complex analytic signal of the magnetic signal $M(x, y)$ can be expressed as (Thurston and Smith 1997):

$$A(x, y) = |A(x, y)|.\exp(j\varphi)$$

with

$$|A(x, y)| = \sqrt{\left(\frac{\partial M}{\partial x}\right)^2 + \left(\frac{\partial M}{\partial y}\right)^2}$$

and

$$\varphi = \tan^{-1}\left(\frac{\partial M}{\partial y} \middle| \frac{\partial M}{\partial x}\right)$$

|A| is the 2D analytic signal amplitude, φ the local phase. A common theme of the normalized derivatives is the concept of mapping angles (or functions of angles) derived from the gradients of the magnetic intensity.

Using 3D dimensional grid, the amplitude of the analytic signal A of M(x,y,z) is calculated by taking the square root of the sum of the squares of each of the directional first derivatives of the magnetic field.

$$|A(x, y)| = \sqrt{\left(\frac{\partial M}{\partial x}\right)^2 + \left(\frac{\partial M}{\partial y}\right)^2 + \left(\frac{\partial M}{\partial z}\right)^2}$$

The resulting shape of the analytic signal is expected to be centred above the magnetic body (Figs. 5.8, 5.9). This has the effect of transforming the shape of the magnetic anomaly from any magnetic inclination to one positive body-centred anomaly at least in 2D (Nabighian 1972). The analytic signal has been utilized widely for mapping of structures and for determining the depth of magnetic sources (Roest et al. 1992; Pilkington et al. 2000; Florio et al. 2006).

The main advantage of the total gradient over the maximum horizontal gradient is its lack of dependence on dip and magnetization direction, at least in 2D. When interpreting the analytic signal it is assumed that the causative sources are simple near-vertical or step-like geological structures (Roest et al. 1992; Roest and Pilkington 1993, Li, 2006). Therefore, the 2D analytic signal has significant advantages over the simple derivatives and this application has been utilized to map changes in basement structure, fabric and trends. Synthetic modelling has proved that the maxima

of the analytic signal are located over the edge of anomalous sources (Nabighian 1974, 1984, Roest et al. 1992). This simplification of the potential field, however, results in the compromise that the original sign of the gravity and magnetic field is lost. Therefore, it cannot be determined whether the analytic signal anomaly represents a positive or negative density or magnetic susceptibility contrast compared to its surroundings.

However, it should be remind that the total gradient expressed in 3D is not (so) independent of the direction of magnetization (Li 2006), nor does it represent the envelope of both the vertical and the horizontal derivatives over all possible directions of the Earth's field and source magnetization. Thus, despite its popularity, the 3D total gradient is not the correct amplitude of the real analytic signal in 3D. In a recent review, it appears that what is commonly called the analytic signal should be rather called 3D "total gradient" (Nabighian et al. 2005).

In the 3D case, some factors produce offsets that are more difficult to predict than in the 2D case. Such factors primarily include the interference from neighbouring magnetic bodies, or from varying magnetization directions, terrain effects, 3D corners on body edges, or irregular boundaries. Roest et al. (1992) have demonstrated that this is true for any 2D anomaly and suggested their generalization to 3D. However, the data should be interpreted with care in the 3D case (Fig. 5.8). The properties of the analytic signal are strictly valid for isolated 2D bodies and one should use caution in extrapolating the conclusion of the 2D case to the 3D case. For 3D case, the shape and the absolute value of the analytic signal are also dependent on the directions of the magnetization and the Earth's magnetic field. The amount of offset is primarily determined by the depth to the top edge of the boundary below the observation level and by the dip of the boundary and by the directions of magnetization and of the Earth's field. In the most common 3D cases, the locations of the total gradient are always offset from edges of the causative bodies. The best results are obtained for vertical and relatively shallow thick dikes (Li 2006). For the 2D finite dipping step model, the locations of the maxima vary with both burial depth and dipping angle. All these factors become important as the size of study area becomes smaller because the small amounts of offset they cause become more significant. For local scale magnetic surveys, mutual interference from different bodies is the greatest limiting factor of the analytic signal method and this can render the method virtually useless. For large-scale magnetic surveys like the JAS-12 or for shallower depths of causative bodies, the analytic signal method remains nevertheless a useful and fast way of delineating magnetic boundaries in the subsurface (Fig. 5.8).

The technique therefore requires interpretation in conjunction with other geophysical and geological information to maximize its potential. After calibration with known structures or other derived potential field products the analytic signal can be interpreted geologically with better confidence.

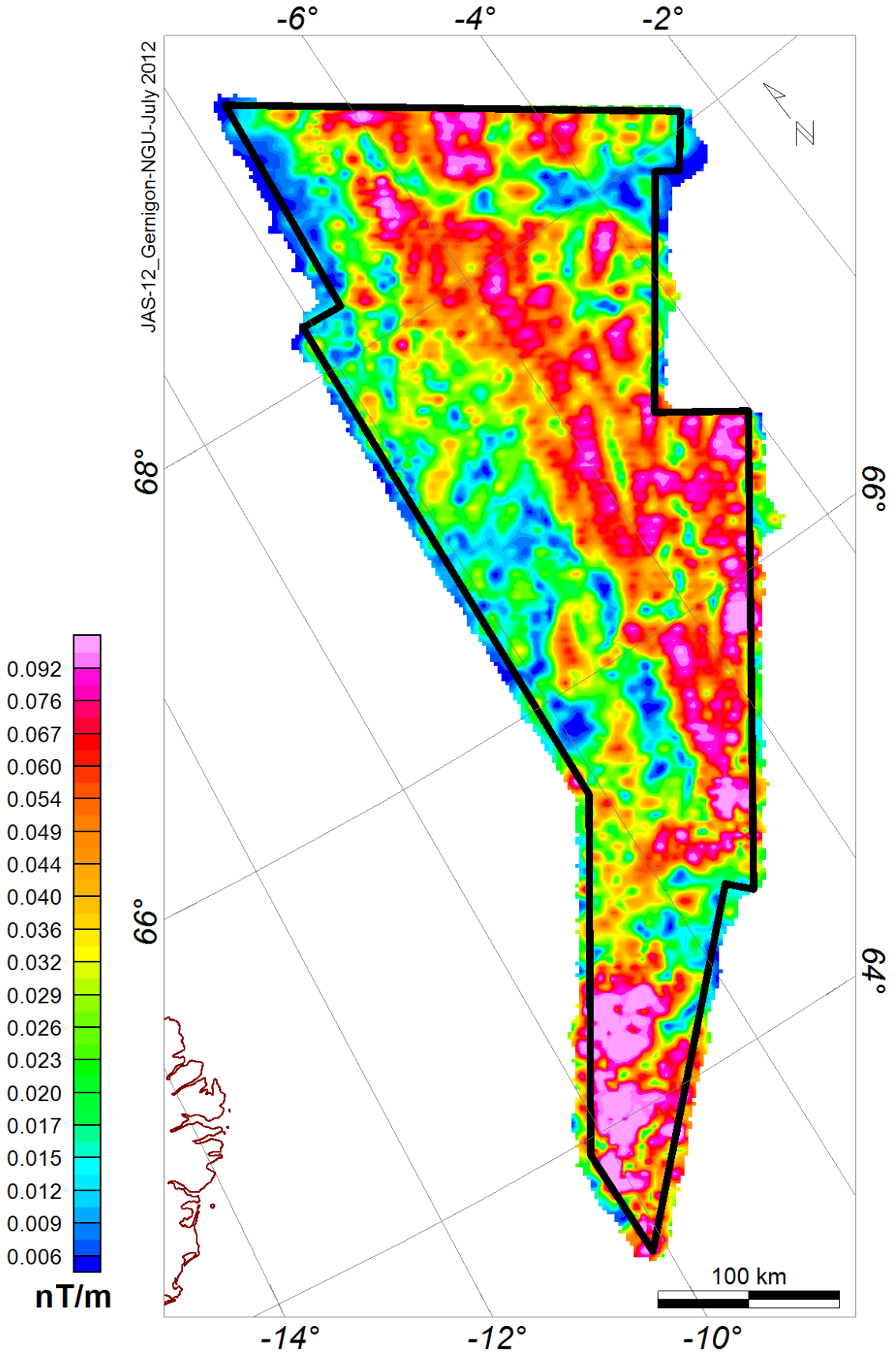

Figure 5.8 Analytic signal of the magnetic total field grid, reduced to the pole (1650x1650m cell size). The 3D analytic signal ("3D total gradient") is the root-sum square of the vertical and horizontal gradients. Like the horizontal gradient, it is used to delineate the edges of bodies or contacts. It has the advantage over the horizontal gradient that it is independent of the dip of the contact, but the disadvantage that it is somewhat less continuous. It is therefore sometimes advantageous to use the two in parallel.

5.4 Tilt derivative (TDR)

The tilt derivative filter (TDR) appears to be a powerful and normalised derivative tool for shape and edge detection (Figs. 5.9, 5.10). It works notably pretty well to identify the magnetic chrons in the Norway Basin. The problems to be overcome in data enhancement using the TDR were to identify and map subtle anomalies attenuated in the dynamic range due to the presence of high amplitude magnetic anomalies, the continuity of individual bodies and the edges of structures.

The TDR is defined in terms of the ratio between the first vertical derivative of the potential field and the total horizontal gradient of the field (Miller and Singh 1994; Verduzco et al. 2004; Cooper and Cowan 2006; Salem et al. 2008).

$$TDR = \tan^{-1}\left[\frac{VDR}{THDR}\right]$$

where VDR and THDR are the first vertical and total horizontal derivatives of the magnetic total field M(x,y), respectively

$$THDR = \sqrt{\left(\frac{\partial M}{\partial x}\right)^2 + \left(\frac{\partial M}{\partial y}\right)^2}$$

and

$$VDR = \frac{\partial M}{\partial z}$$

Its horizontal gradient (derivative) is also defined by:

$$HGTDR = \sqrt{\left(\frac{\partial TDR}{\partial x}\right)^2 + \left(\frac{\partial TDR}{\partial y}\right)^2}$$

The tilt derivative (TDR) is restricted to values in the range from $+\pi/2$ to $-\pi/2$, and can be considered as an expression of the vertical derivative normalized by the total horizontal derivative. This measure has the property of being positive over a source and negative elsewhere (Fig. 5.9). The tilt filter technique tends to enhance mapping of the subtle magnetic anomalies and maximizes the geometrical contrast of the internal basin structure (partly constrained by seismics). The tilt angle was compared with other edge detection measures such as the horizontal gradient, the second vertical derivative and the analytic signal and found to have added some advantage of responding well to both shallow and deep sources in the JAS-12 area. Using synthetic models, Verduzco et al. (2004) showed that the TDR has its zero values close to the edges of the body for RTP fields. The tilt derivative amplitudes can be enhanced using its total horizontal derivative (or local

wavenumber) in which the edge anomalies are prominent and invariant to geomagnetic inclination, thus making this derivative effective for mapping geologic edges.

Combined with its total horizontal derivative, results were particularly useful for the structural interpretation of the JAS-12. The tilt angle results were combined and systematically compared with other filtered datasets (using transparency in Oasis Montaj) to provide a set of interpretative maps presented and discussed later.

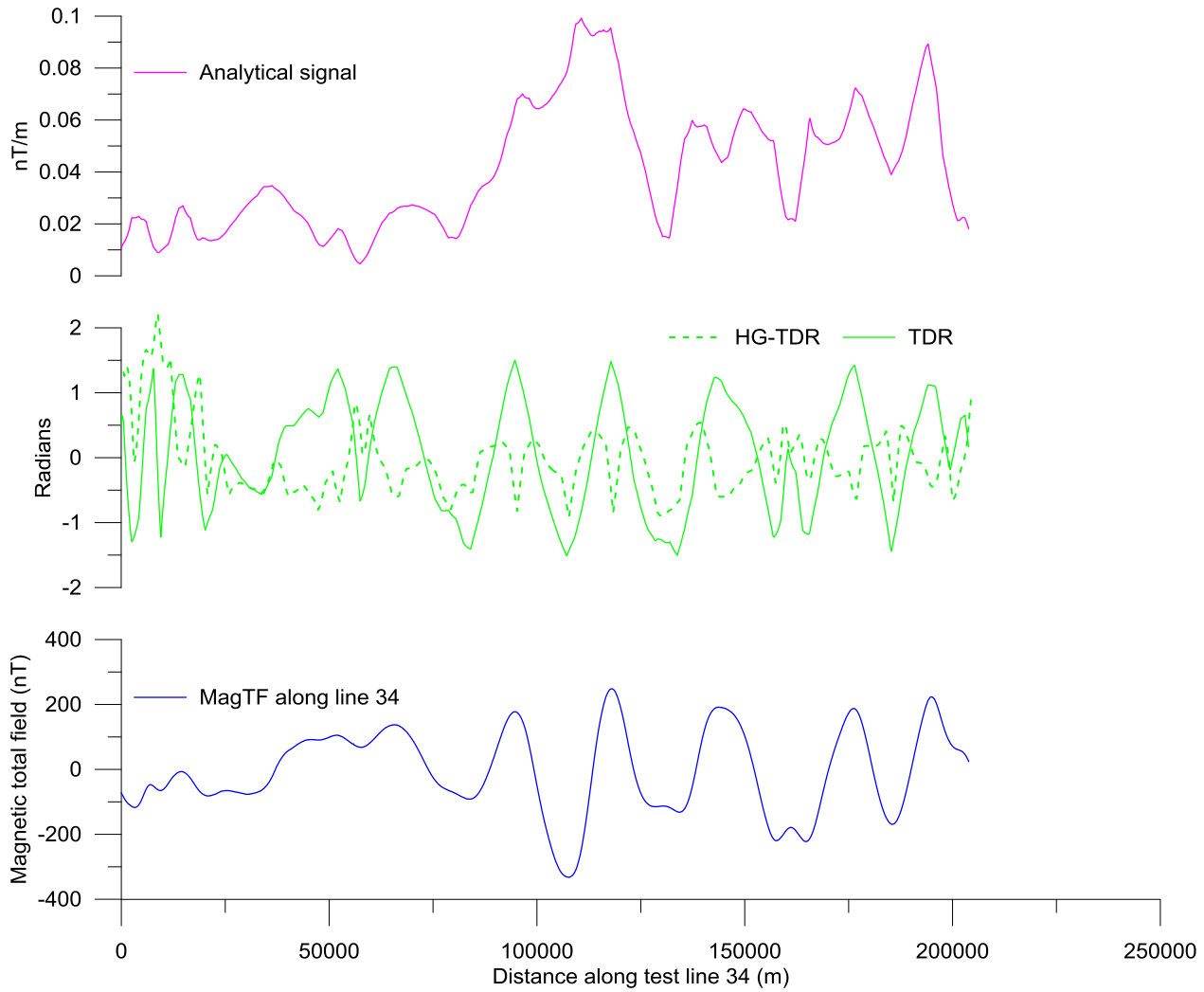

Figure 5.9 TDR and analytical signal filtering along line 34. The TDR filter is particularly effective in identifying subtle anomalies and their edges.

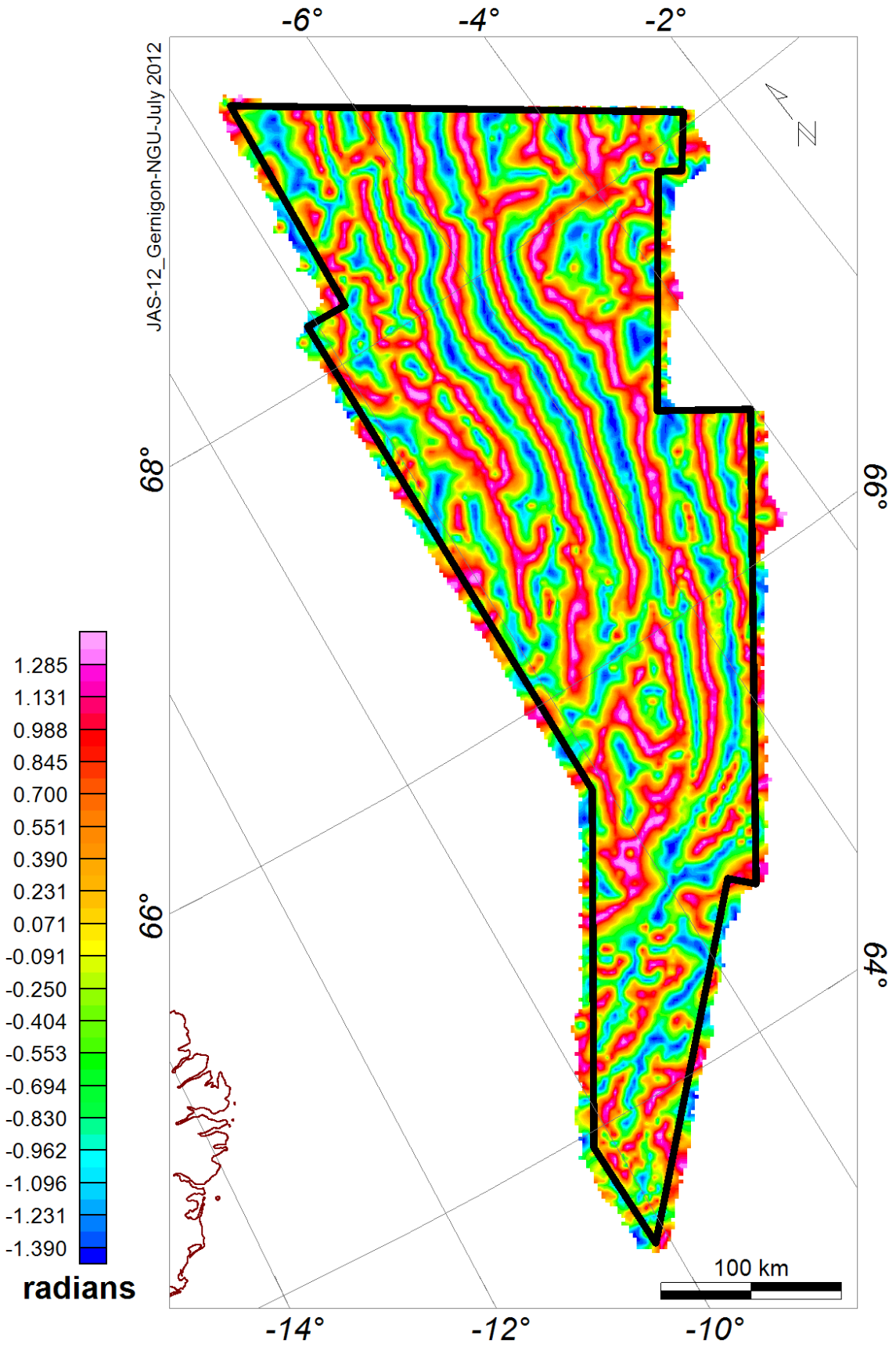

Figure 5.10 Tilt derivative of the magnetic total field. The tilt derivative (TDR) is an alternative method to derive the maximum gradient anomalies associated with magnetic contacts. The result is strongly peaked along the maxima of the horizontal gradient. This display gives a much sharper definition of the magnetic contacts than the horizontal gradient map. For the JAS-12 interpretation, this filter proves to be interesting for mapping and identifying the magnetic chrons.

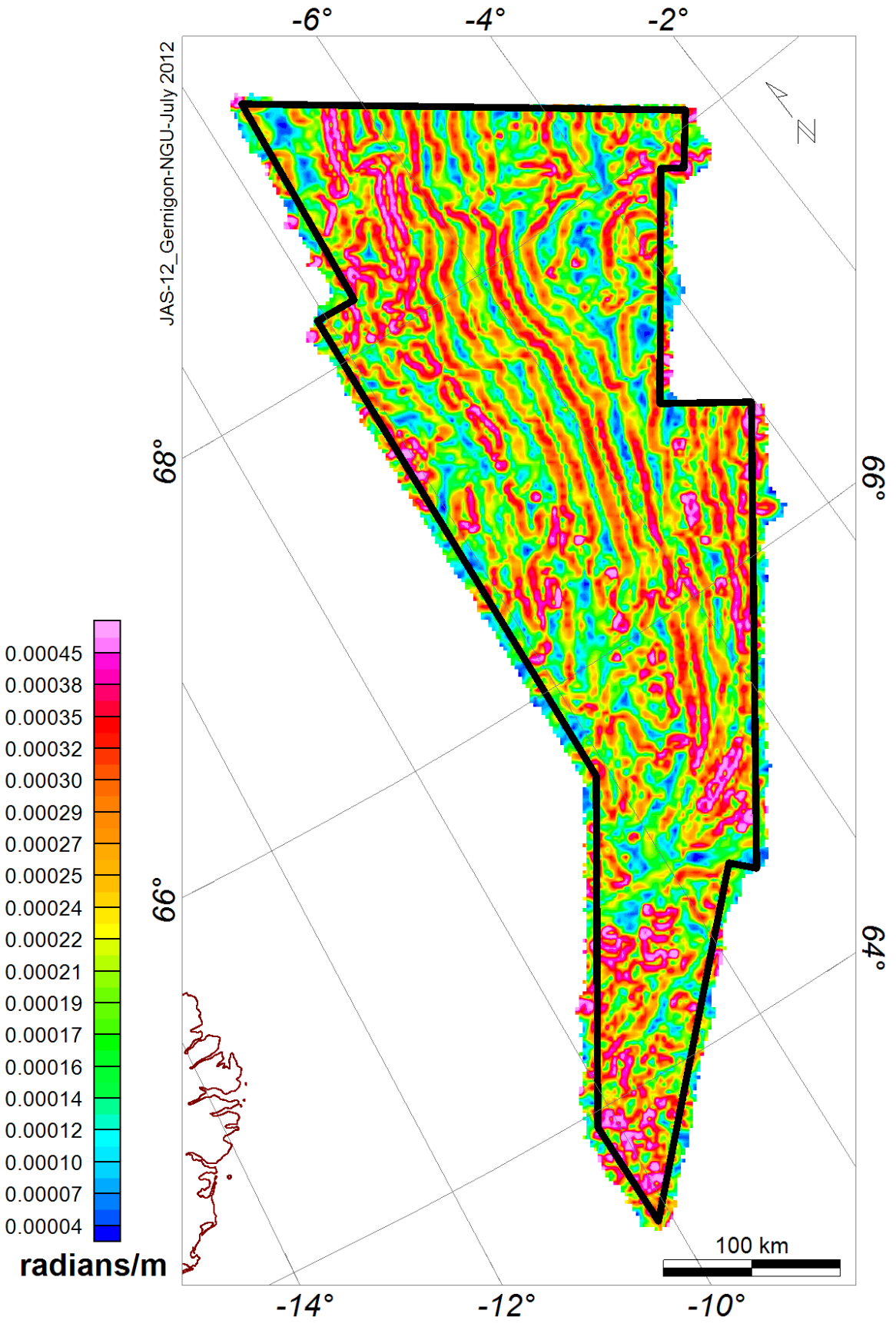

Figure 5.11 Horizontal gradient (derivative) of the tilt derivative (HG-TDR) of the magnetic total field grid (1500x1500), reduced to the pole. The different patterns underline major magnetic units and major lineaments.

5.5 TDX filtering

Cooper and Cowan (2006) and Fairhead and Williams (2006) have modified the tilt derivative so that the total horizontal derivative is now normalized by the vertical derivative (Fig. 5.12). They named it TDX but neither of their papers mentions the origin of the name TDX. Note that the two definitions of TDX are slightly different in the two papers. Fairhead and Williams (2006) use the first vertical derivative in the denominator, whereas Cooper and Cowan (2006) use its absolute value:

$$TDX = \tan^{-1}\left[\frac{THDR}{VDR}\right]$$

where VDR and THDR are the first vertical and total horizontal derivatives, respectively

$$THDR = \sqrt{\left(\frac{\partial M}{\partial x}\right)^2 + \left(\frac{\partial M}{\partial y}\right)^2}$$

$$VDR = \frac{\partial M}{\partial z}$$

The angle defined by the TDX expression is effectively sign(Tilt)×(π/2 - |Tilt|), and like the Tilt is also constrained between +π/2 and -π/2, but has a much sharper gradient over the contact (Cooper and Cowan 2006; Fairhead and Williams 2006).

We also propose a nice combination of the TDX with a Laplacian filter [0,-1,0,-1,4,-1,0,-1,0] applied to the original TDX grid: It can be used to better highlight the inflection points on both edges of the anomalies (Figs. 5.13, 5.14). This filter was used to delineate properly the magnetic chrons in the Norway Basin.

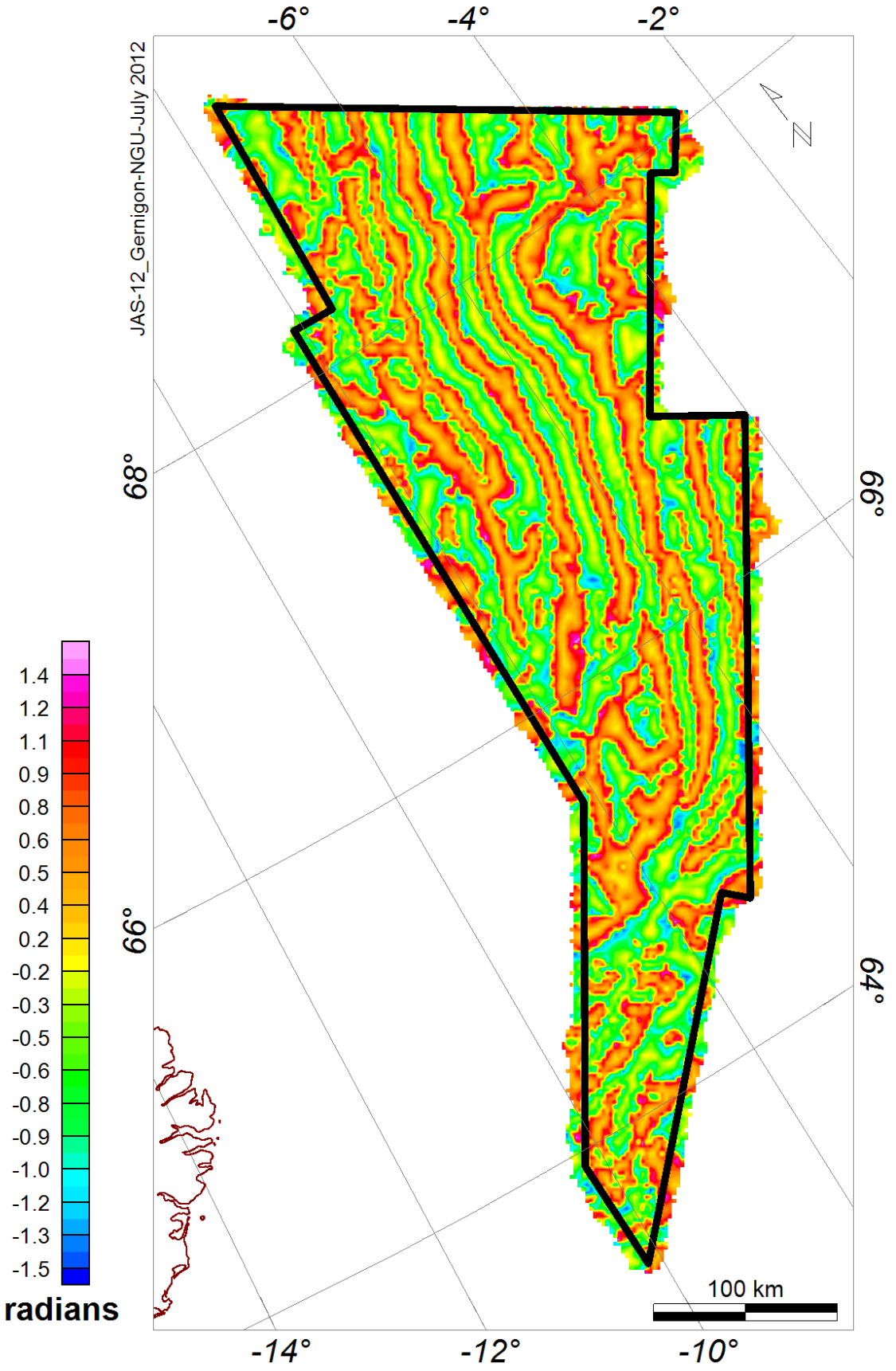

Figure 5.12 TDX filter of the magnetic total field grid (1500x1500m) reduced to the pole. The different TDX patterns highlight major magnetic units and major lineaments.

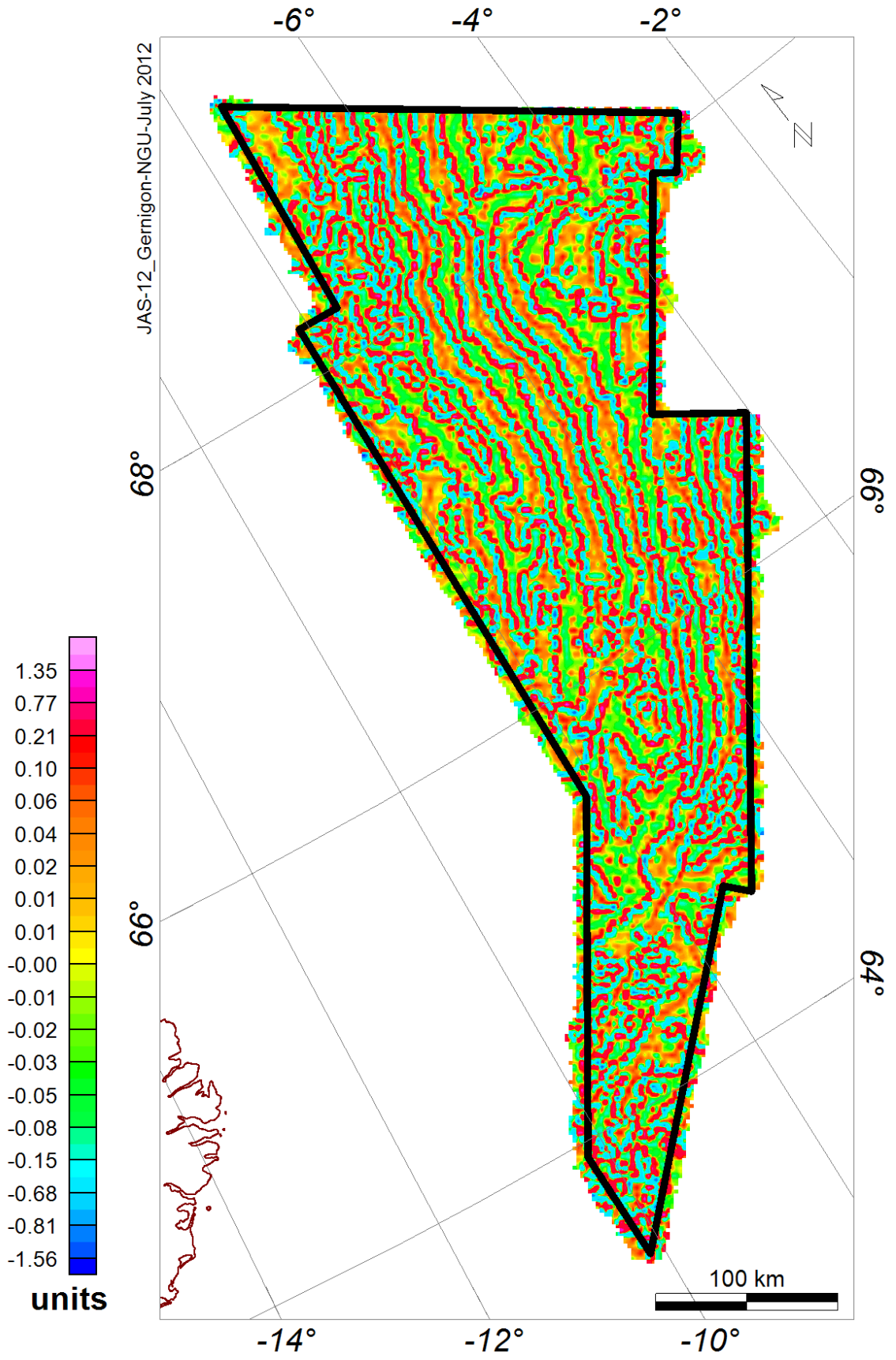

Figure 5.13 2D Laplacian filter [0,-1,0,-1,4,-1,0,-1,0] applied to the TDX of the magnetic total field grid (1650x1650m) reduced to the pole. A Hanning filter [0.06, 0.1, 0.06, 0.1, 0.36, 0.1, 0.06, 0.1, 0.06] has subsequently been applied to smooth the edges. This filtering highlights the main inflection points of the TDX grid.

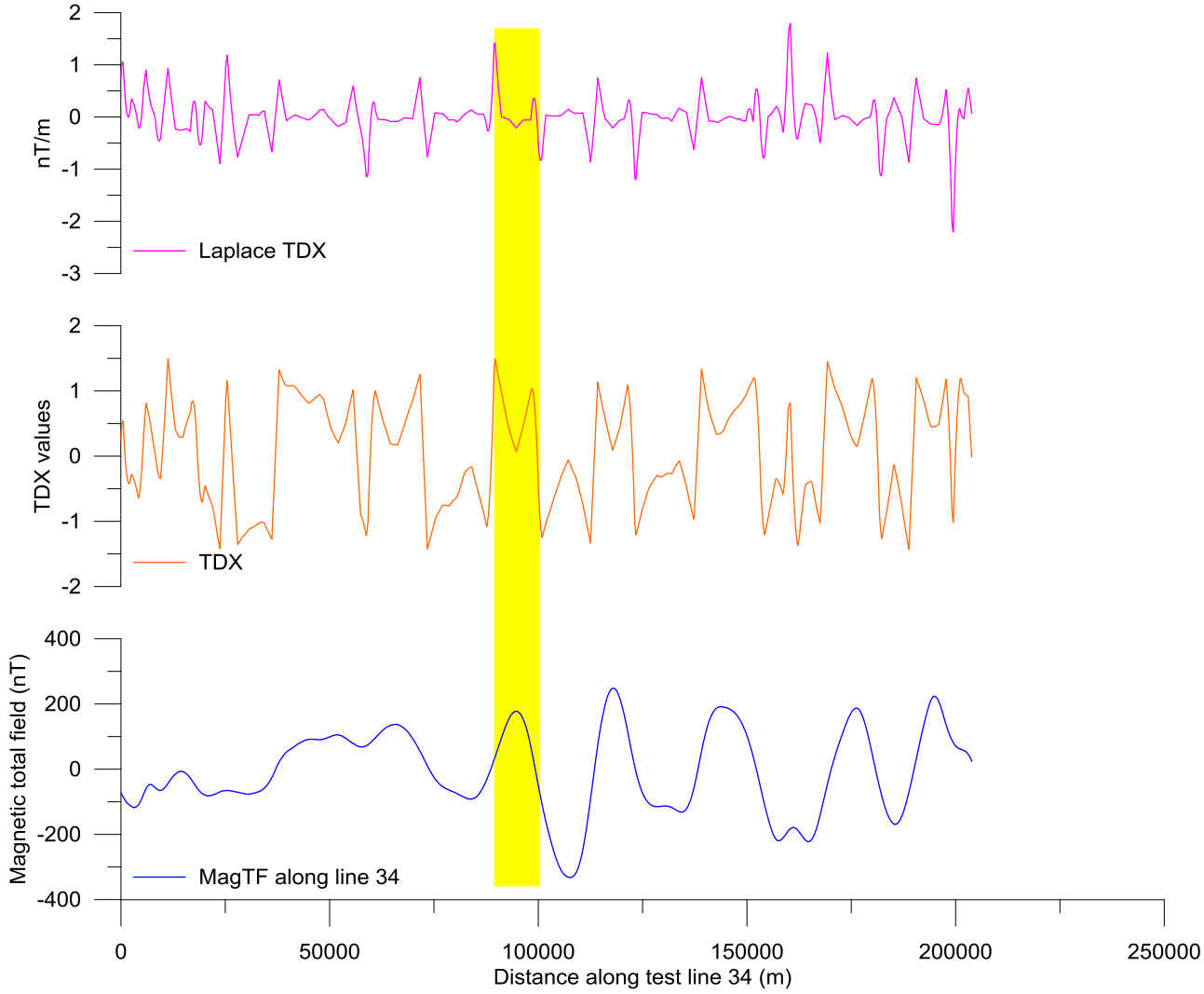

Figure 5.14 Example of different edge detection filters applied to line 34. The TDX filtering highlights the main inflection points of the TDX grid including maximum and minimum for each anomaly. A 3x3 Laplace filter applied to a TDX grid is mostly useful to highlight the points of tangency.

5.6 Pseudogravity

Pseudogravity is the gravity anomaly that would be observed if density contrasts were proportional to magnetization contrasts (Baranov 1957). It is calculated from magnetic observations and is used to compare gravity and magnetic observations to distinguish between the effects of different rock types. Aeromagnetic data are then transformed into pseudogravity data assuming Poisson's relation between gravity and the JAS-12 magnetic total field (Fig. 5.15). Under the assumption that the basement is magnetized uniformly by induction, the pseudogravity field can be attributed to the density (susceptibility) variations along the survey. Under ideal conditions, the pseudogravity field could provide an approximate representation of the basement domains when the sediments are nonmagnetic, whereas the original gravity field may also include variation of density within the sedimentary section and the crust. A pseudogravity transformation might be a useful strategy in

interpreting magnetic anomalies because a comparison with real gravity data could help to build an interpretation of the shape and size of the sources. The Geosoft software was used for performing the Fourier transformation with a filter operator defined by:

$$G(\theta) = \frac{g.\rho/J}{[\sin(Ia) + i\cos(I).\cos(D-\theta)]^2 \times r}$$

With

ρ: density contrast in g/cm^3

g: gravitational constant=$6.670.10^{-8}$

I: Geomagnetic inclination

Ia: Inclination for amplitude correction. Default is 20°. If $|Ia| < |I|$, $|Ia| = |I|$

D: Geomagnetic declination

J: magnetization in Gauss

$\theta = \tan^{-1}(u/v)$ is the wavenumber direction

r is the wavenumber in ground-unit=2πk where k is cycles/ground-units

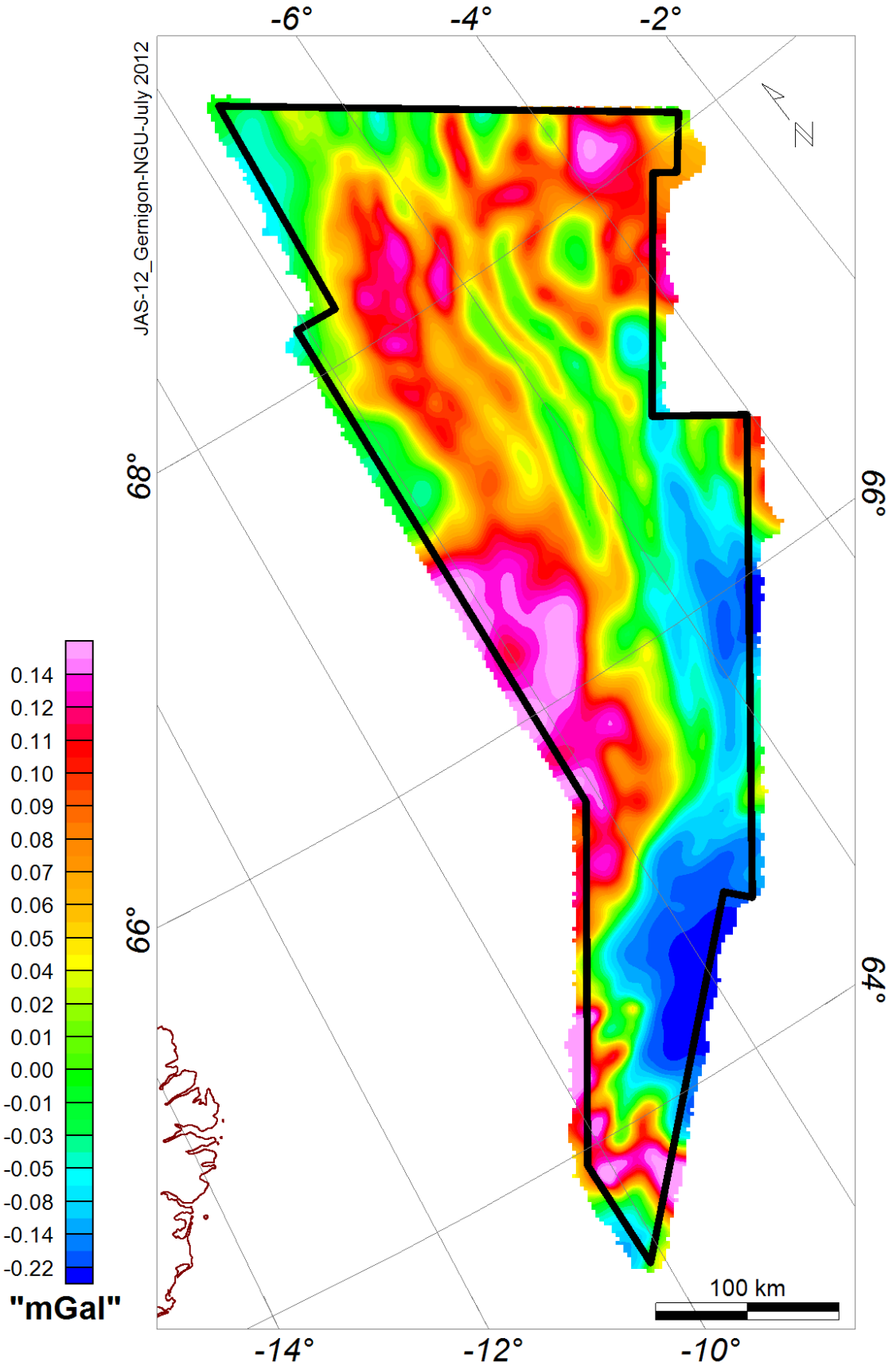

Figure 5.15 Pseudogravity of the JAS-12 survey. The pseudogravity was computed using a density contrast of 1.5 g·cm^{-3} and a magnetization of 3 A/m. *Inclination: 76.47° and declination:-7.61°.*

5.7 Source parameter imaging (SPI) and magnetic sources depth estimation

The source parameter imaging (SPI) technique is another quick method for calculating the "expected" depth to magnetic sources (Thurston and Smith 1997). The SPI methods used the local frequency *f* of the magnetic signal, which is defined as the rate of change of the local phase θ with respect to x.

$$f = \frac{1}{2\pi}\frac{\delta}{\delta x}\theta$$

Where the local phase θ is defined by:

$$\theta = \tan^{-1}\left(\frac{\partial M}{\partial z}\Big/\frac{\partial M}{\partial x}\right)$$

Using the local wavenumber $k = 2\pi f$ and using the differentiation rule

$$\frac{\partial(\tan^{-1}\emptyset)}{\partial x} = \frac{1}{(1+\emptyset^2)}$$

Thurston and Smith (1997) show that the wavenumber k could be linked with the total horizontal gradient $|A|$, formerly called analytic signal and complex derivative filters of the magnetic field.

$$k = \frac{1}{|A|^2}\left(\frac{\partial^2 M}{\partial x \partial z}.\frac{\partial M}{\partial x} - \frac{\partial^2 M}{\partial x^2}.\frac{\partial M}{\partial z}\right) \; with \; |A| = \sqrt{\left(\frac{\partial M}{\partial x}\right)^2 + \left(\frac{\partial M}{\partial z}\right)^2}$$

For a sloping contact, Thurston and Smith (1997) demonstrate that the “local susceptibility” K at the maxima of the local wavenumber can be a function of the total gradient (A), the local wavenumber (k), the local depth (h) and the dip (d) of the contact using the following equation:

$$d = \frac{1}{k} \quad \text{and} \quad K = \frac{|A|}{2kFc\sin d}$$

Using the wavenumber, the phase, the total horizontal gradient at each wavenumber maxima, the local dip, and the “susceptibility" contrasts can be derived. The SPI produces a more complete set of coherent solution points, do not require any windows assumptions and is easier to use (Fig. 5.16). The SPI’s accuracy has been shown to be +/- 20% in tests on real data sets with drill hole control and this accuracy is similar to that of the Euler deconvolution (Thurston and Smith 1997). However, this technique remains relatively simple and assumes that the sources are simply sloping contacts, with infinite depth extend. It also assumes no interferences from adjacent anomalies. This model considers no remanence magnetization.

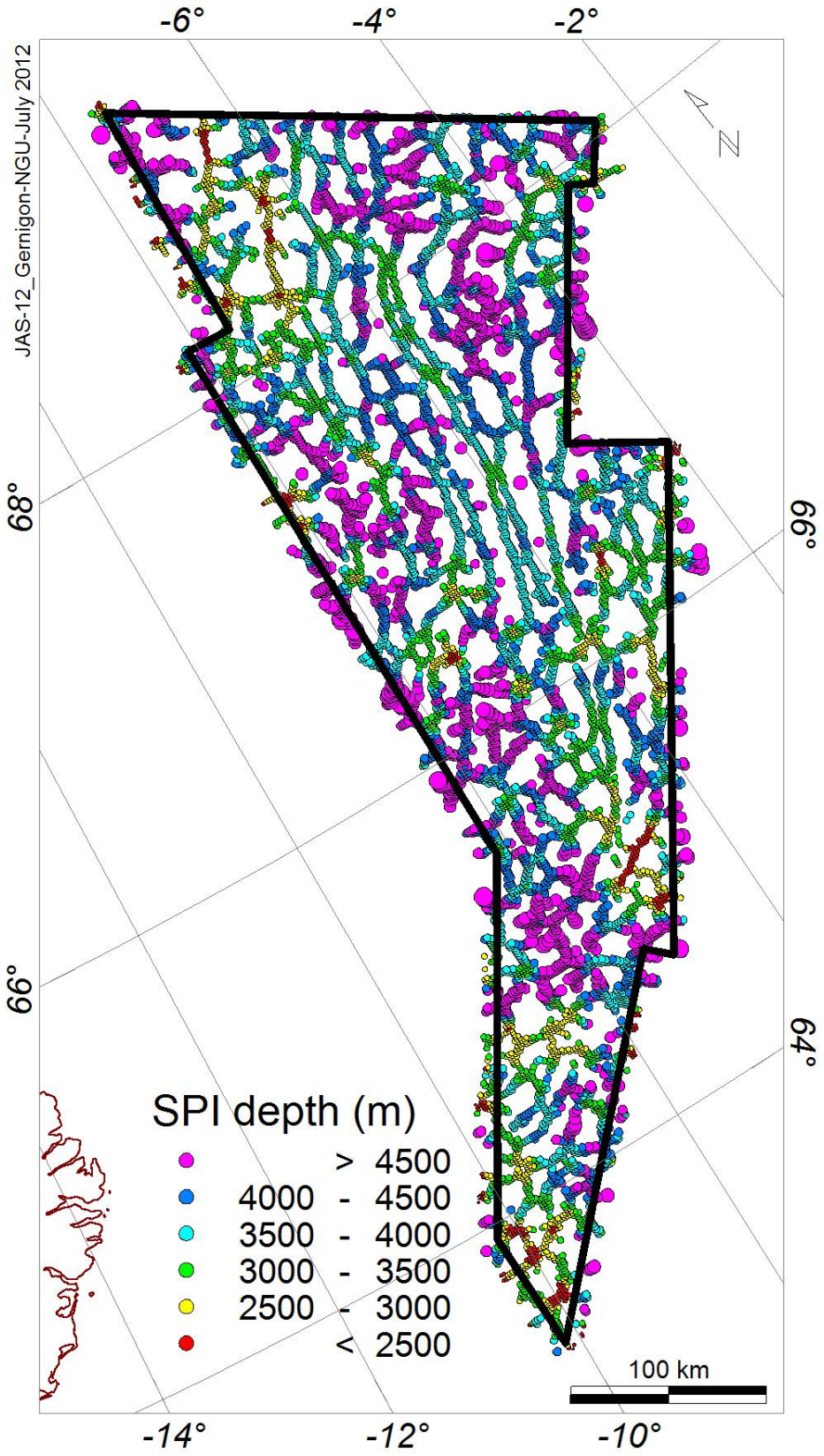

Figure 5.16 Results from the source parameter imaging (SPI) depths plotted on the SPI edge detection grid based on the local wavenumber technique of Thurston and Smith (1997). Depth solutions focus near the maxima of the magnetic anomalies.

6 FINAL MERGE AND COMPARISON WITH PREVIOUS COMPILATION

Aziz Nasuti and Laurent Gernigon

6.1 Merge of the JAS-12 grid with the more recent 2012 NGU compilation

The JAS-12 grid has been merged with the pre-existing and most recent surveys available in the Norwegian Greenland Sea (Table 6.1). In 2012, all the previous surveys have been remerged and locally reprocessed (Nasuti et al., unpublished) to get the final dataset presented in this chapter. Due to survey restriction and confidentiality of the recent Norwegian survey, this final NGU 2012 compilation including the JAS-12 is only available to the NPD representatives.
Outside the JAS-12 survey area, we performed micro-levelling to remove minor ('micro') levelling errors still remaining along parts of some profiles after the statistical levelling of the oldest surveys. To improve the quality, the Geosoft micro-levelling approach using the PGW GX system of the available MAGMAP processing package of the Oasis Montaj (Geosoft 2010a) was used. It proved to be better adapted to preserve geological information for this specific case where the remaining levelling errors are irregularly distributed. The PGW GX system applies a decorrugation process in the frequency domain to isolate the levelling corrections before applying them to the original data. Compared to previous NGU magnetic compilations (Olesen et al. 2010, Gernigon et al. 2012) some of the surveys (Table. 6.1) have been decorrugated to reduce line-to-line levelling errors, which are visible as linear magnetic features parallel to the flight lines. Decorrugation is a frequency domain procedure based on a directional cosine filter. This filter retains anomalies, from gridded data, in the flight line direction only. Then, a Butterworth high-pass filter is set to four times the line spacing to pass wavelengths on the order of two to four line separations. Such a process results from a line-to-line levelling error. Finally, a directional cosine filter is set to pass wavelengths only in the direction of the lines.

Besides the processing of the JAS-12 itself, a test reprocessing of the CCG-73 raw data has been carried out and already presented to Orkustofnun and NPD in Reykjavik in January 2012. The reprocessing of the CCG-73 included a version including the merge of the JM-85 magnetic profiles (non- release data) provided by ISOR, Orkustofnun and NPD in the context of the JAS-12 project (but not implemented at the end in the regional compilation). The main topic was to level the JM-85 ship track profiles acquired together with gravity and seismics during the JM-85 experiment (Gunnarsson et al., 1989) with the old 1973 CGG aeromagnetic profiles in order to get accurate levelled profiles for subsequent modelling.

The CGG-75/JM-85 reprocessing sequence is described as follows:

- The merge and levelling of the JM-85 profiles together with the original CGG corrected from IGRF (approximate date) using a similar approach presented in the previous chapters
- The CGG-73 JM-85 raw data were re-corrected from the IGRF (an approximate date for the acquisition of the CGG-73 was estimated).
- Since the original JM-85 and CGG-73 survey have different altitudes and origins, an upward continuation was first carried out along the JM-85 raw IGRF corrected to simulate and reach

the original CGG-73 sensor elevation (610 m for the CGG-73 flying altitude versus ~0 m for the shiptrack JM-85 dataset)

- Statistical levelling (iterative) was then carried out but after several tests, we decided to remove most of the JM-85 N-S lines, sometime located at the same location as the CGG tie line.
- We kept the JM-85 E-W and NE-SW oriented lines: this corrected some levelling effects.
- Finally we applied the Geosoft microlevelling technique to correct the final noise.
- The final grid merge was not totally satisfactory compared to modern surveys and some mistakes still exist. It is mostly the results of a different quality of recording (altitude difference, and 12 years between the two acquisitions). We also note some imprecision in the JM-85 navigation files simply due to the old navigation system used at that period (see Geco cruise report, Myklebust, 1985).
- The E-W and NE-SW JM-85 lines have been finally levelled and corrected to the CGG altitude level for better correlation (610 m). No downward continuation has been carried out.

The Oasis Montaj GridKnit module was used to merge the JAS-12 grid with the other geophysical surveys characterised by different cell size, projection or grid type (Geosoft 2005d). The blending method merged the grids via standard smoothing functions. Trend removal operations were performed with respect to the regional grid. The maximum trend order has been specified or adjusted automatically based on a fitting tolerance. However, this technique locally "forces" the magnetic trend envelope of the new JAS-12 to be adjusted with the surrounding dataset. Since the surrounding magnetic datasets are partly old has low resolution (Table 6.1) and is less reliable, the merge process could contaminate and reduce the initial right quality at the edge of the JAS-12. For local interpretation and modelling, we consequently recommend using the original JAS-12 grid. The final regional grid can only be provided to partners, which also purchased the regional NGU magnetic datasets.

Year	Area	Operator, Reference	Survey name	Sensor elevation m	Line spacing km	Length km	Reprocessing
1968-1992	Iceland	University of Iceland, Kristjánsson *et al.* 1989; Jónsson *et al.* 1991	UoI-68/92	900-1200	3-6	56.900	-
1969	SW Barents Sea	NGU, Åm 1975	NGU-69	200	4	26.200	Microlevelled
1970	SE Barents Sea	NGU, Åm 1975	NGU-70	200	4-8	22.800	Partly reprocessed Microlevelled
1971	Viking Graben	Fairey, Åm 1973a	Fairey-71a	300	2	11.100	Microlevelled
1971	Shetland Basin	Fairey, Verhoef *et al.* 1996	Fairey-71b	500	7,5	13.500	Microlevelled
1972	Shetland Basin	Fairey, Verhoef *et al.* 1996	Fairey-72	500	5	20.100	Microlevelled
1973	Shetland Basin	Fairey, Verhoef *et al.* 1996	Fairey-73	500	15	32.600	Microlevelled
1973	Vøring Basin	NGU, Åm 1975	NGU-73	500	5	35.000	-
1972	South Russian Barents Sea	MMBS 1992 seminar report, data from Statoil-1972	SEV-72				Partly reprocessed
1972	North Norwegian-Greenland Sea	NRL, Vogt *et al.* 1979	NRL-72	300	7.5	38.500	Microlevelled
1973	South Norwegian-Greenland Sea	NRL, Vogt *et al.* 1979	NRL-73	300	10 (20)	50.600	Partly reprocessed Microlevelled
1973	Denmark Strait	NOO, Vogt *et al.* 1980	NOO-73	160	5.5	60.400	Microlevelled

1974	Norwegian Sea, east of Iceland	NOO, US Naval Oceanographic Office 1982	NOO-74a	160	10	5.500	Microlevelled
1974	Norwegian Sea, SE of Iceland	NOO, US Naval Oceanographic Office 1982	NOO-74b	160	10	2.000	Microlevelled
1974	NE Atlantic, south of Iceland	NOO, US Naval Oceanographic Office 1982	NOO-74c	160	5	22.200	Microlevelled
1974	Norwegian North Sea	NGU, Olesen et al. 1997a	NGU-74	300	2-7	23.000	Microlevelled
1974	East Greenland mainland	GEUS, Larsen 1974	GEUS-74	1820	8	15.200	-
1975	Norwegian North Sea	NGU, Olesen et al. 1997a	NGU-75	300	1-6	19.000	-
1975	North Russian Barents Sea	MMBS 1992 seminar report, data from Statoil-1975	SEV-75				Partly reprocessed Microlevelled
1976	Central Russian Barents Sea	MMBS 1992 seminar report, data from Statoil-1976	SEV-76				Partly reprocessed Microlevelled
1976	Jan Mayen Ridge	CGG/NPD, Compagnie Générale de Géophysique 1977 Navrestad & Jørgensen, 1979	CGG-76	700	5	11.600	Partly reprocessed Microlevelled
1979	East Greenland shelf	GEUS, Larsen & Thorning 1979	GEUS-79	600	8	48.300	-
1983	Greenland Sea	NRL, Verhoef et al. 1996	NRL-83	300	20	13.000	Partly reprocessed Microlevelled
1985	SW Barents Sea	CGG, xx	BAMS-85	200	4	16.900	Partly reprocessed and Microlevelled
1985	Jan Mayen Ridge	Orkustofnun, NPD Eysteinsson and Gunnarsson, 1995; Gunnarsson et al., 1995	JM85	0 ship		3.239	Microlevelled
1985	S of Faroe Islands	NOO, Verhoef et al. 1996	NOO-85	230	3	18.100	Microlevelled
1986	Trøndelag Platform	Hunting, Skilbrei & Kihle 1995	Hunting-86	200	2	57.000	Reprocessed partly and microlevelled
1987	Vøring Plateau	NOO, Verhoef et al. 1996	NOO-87	230	5	16.900	-
1987	NW Barents Sea	NGU, Skilbrei 1991	BSA-87	250	4-8	34.000	Partly reprocessed Microlevelled
1988	Spitsbergen	NGU, Skilbrei 1992	SPA-88	1550	5.5	13.300	Microlevelled
1989	Nordaustlandet	Statoil-1989	SEV89				
1989	Lofoten	NGU, Olesen et al. 2002	LAS-89	250	2	30.000	Microlevelled
1990	Aegir Ridge	NRL, Jung & Vogt 1997	NRL-90	0 ship	6	11.000	-
1991	Olga Basin		SX2				Microlevelled
1991	Svalbard	Amarok/TGS, Breivik & Faleide 2004	SVA-91	900	7.5	27.800	Microlevelled
1993	N. Viking Graben	NGU, 20	Viking-93	150	0.5-2	28.000	Reprocessed totally
1993	Hel Graben- Nyk High	World Geosciences, 21	SPT-93	80	0.75	19.000	-
1994	Vøring Basin	Amarok/TGS, 22	VGVB-94	140	1-3	31.800	-
1994	Nordland Ridge-Helgeland Basin	NGU, Olesen et al. 2002	NAS-94	150	2	36.000	-
1994	S. Viking Graben	Amarok/TGS, 24	VGVG-94	160	0.2	44.800	Partly processed and microlevelled
1995			SAM-95				-
1996	Skagerrak	NGU, Olesen et al. 2004	SAS-96	150	2	42.000	Microlevelled
1997	Southwestern Barents	NGU, Rønning, Stig; Skilbrei, Jan R. 1988	HRAMS				-
1997	Møre Basin	Amarok/TGS, 26	MBAM-97	220	1-2	46.600	Reprocessed totally
1998	Vestfjorden	NGU, Olesen et al. 2002	VAS-98	150	2	6.000	-
2000	Vøring Basin	TGS, Olesen et al. 2007	VBE-AM-00	130	1-4	17.300	Microlevelled
2003	Røst Basin	NGU, Olesen et al. 2007	RAS- 03	230	2	30.000	-
2005	Jan Mayen FZ	NGU, Gernigon et al., 2009	JAS-05	230	5	32.600	Microlevelled
2006	SW Barents Sea	NGU, Gernigon et al., 2006, 2011	BAS-06	230	2-6	30.000	-
2006	SW Barents Sea	NGU, Løvås et al. 2008; Gernigon et al., 2011	NAS-06	230	0.5-1	8955	-
2007	Norway Basin	NGU, Gernigon et al., 2009, 2012	NB-07	230	5	38.500	-
	Norway Basin	NGDC, Maus et al. 2009	NGDC	0 ship		15.200	-
2008	SW Barents Sea	NGU, Brönner et al., 2008; Gernigon and Brönner, 2012	BASAR-08	230	2-5	58.000	-
2009	SW Barents Sea	NGU, Brönner et al., 2010; Gernigon and Brönner, 2012	BAS-09	230	2-5	75.000	-
2010	Central North Sea	NGU, Nasuti et al., 2012	CNAS-10	115	1	82.000	Totally reprocessed

2011	Lofoten	Brönner et al., in prep	LOVAS-11	150	0.5-1	68.000	New data
2011	Stat region (western coast of Norway)	NOATEM *C11089, 2012*	SAS-11	60	0.25-2.5	52.000	New data

Table 6.1 Main characteristics of the offshore aeromagnetic surveys available at the Geological Survey of Norway.

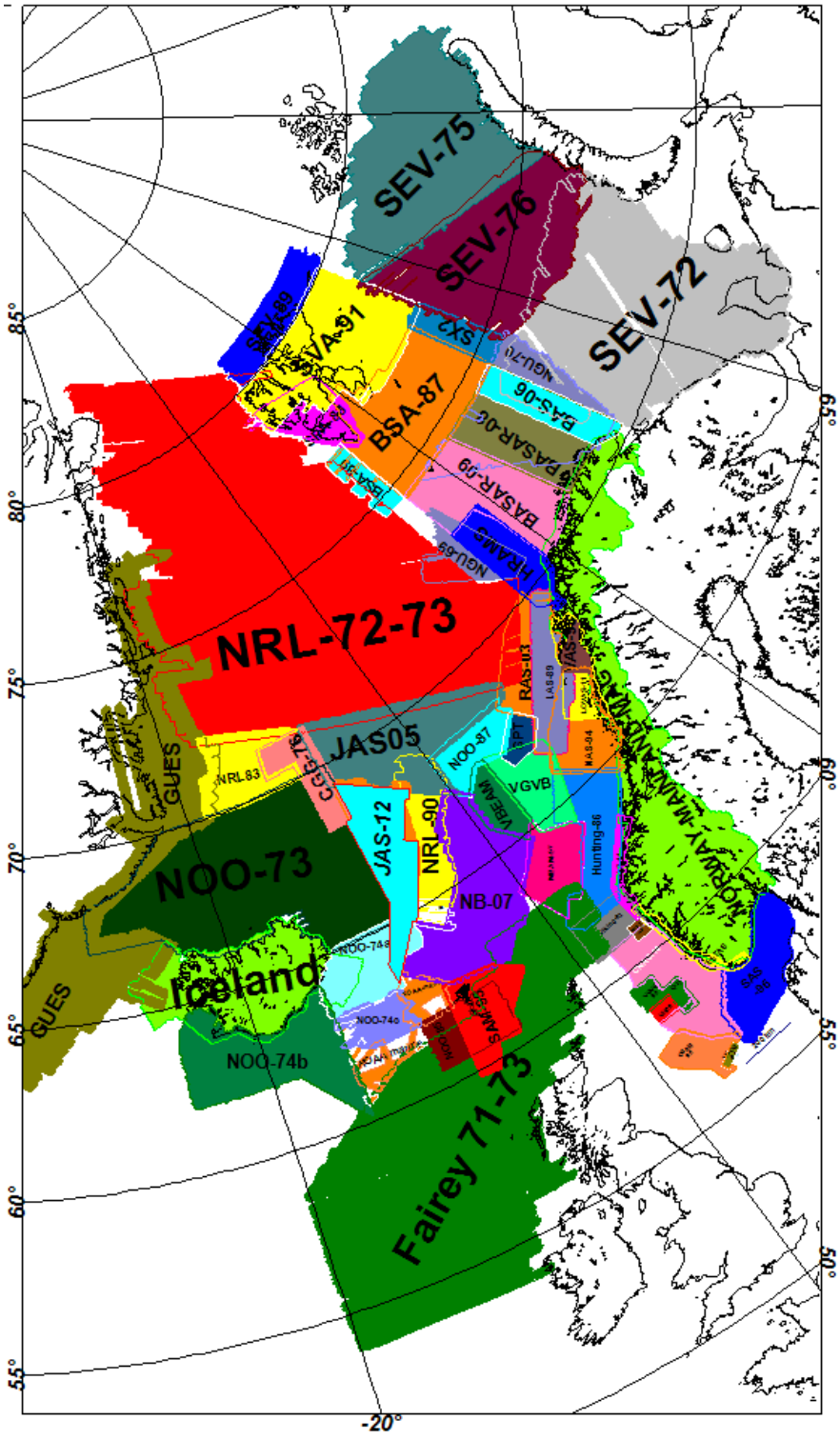

Figure 6.1 Surveys outline of the most recent NGU 2012 compilation (Nasuti et al., unpublished) including the JAS-12 survey (this report).

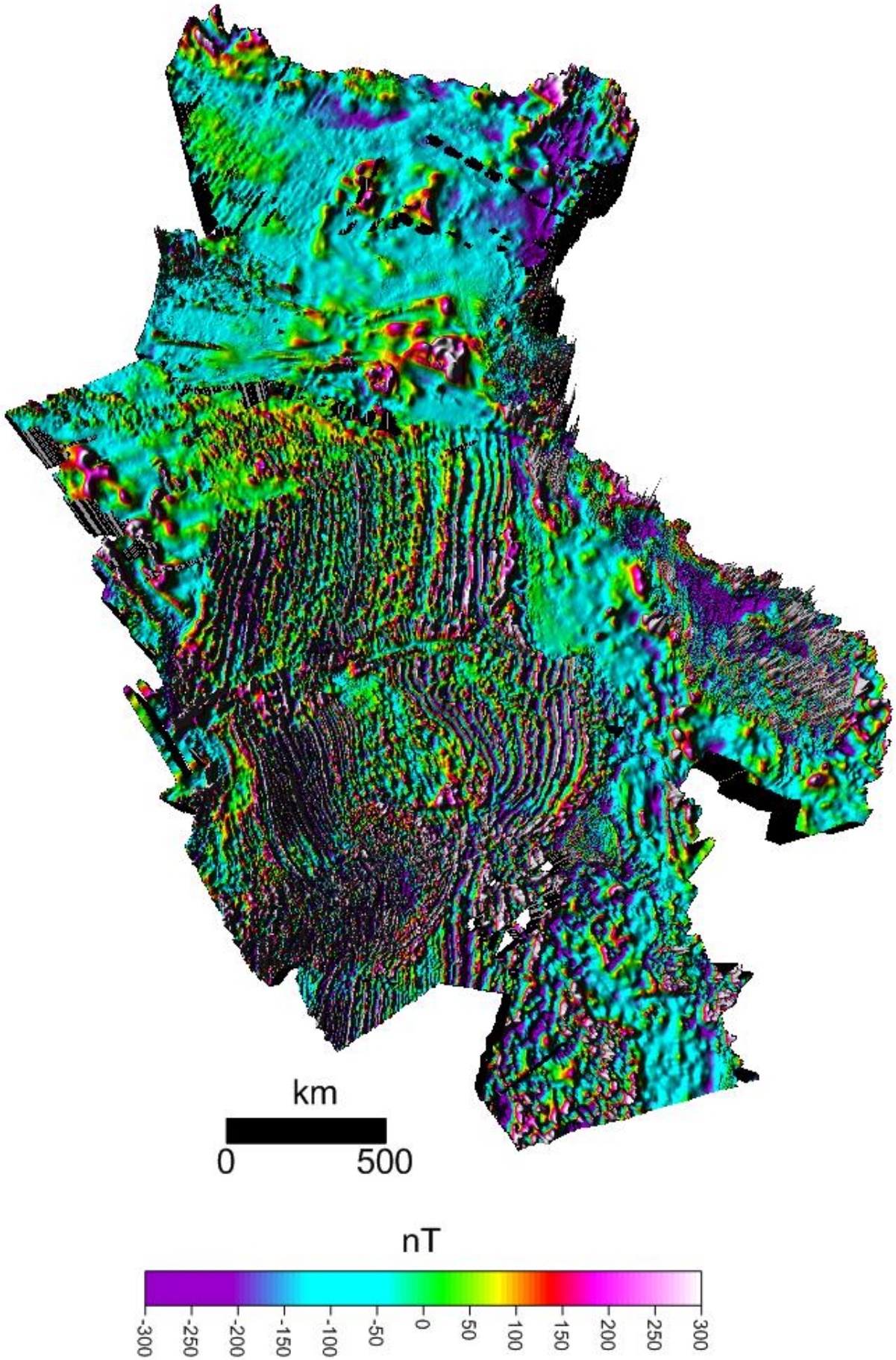

Figure 6.2 3D perspective view of the more recent 2012 NGU compilation including the JAS-12 survey.

6.2 Comparison with other compilations

The Figure 6.3 illustrates the JAS-12 results and the major differences from the previous public domain compilations. Figure 6.3b represents the old compilation of Verhoef et al. (1997) and Figures 6.4c and 6.5d represent the recent releases from the world magnetic anomaly map (Hemant et al. 2007; Maus et al. 2007) and the last CAMP Arctic (Gaina et al. 2011). These compilation are derived from release aeromagnetic surveys (including previous NGU (vintage) work) over land areas, research vessel magnetometer traverses at sea, and observations from earth-orbiting satellites (CHAMP), supplemented by anomaly values "artificially" derived from oceanic crustal ages. The anomaly field is shown at an altitude of 5 km above the WGS84 ellipsoid and gridded at 3 minutes arc spacing (~5.5 km). The A version (Fig. 6.3c) differs in its handling of areas without near-surface data, which are filled with the 5 km downward-continued CHAMP magnetic model. In contrast, the B version (Fig. 6.3d) contains both model data derived from CHAMP, and marine data, with a priority given to the marine. Both versions, when upward-continued to satellite altitude, reproduce the magnetic anomaly field derived from the CHAMP satellite.

These models are particularly suited for inferring large-scale structure and composition of the lithosphere. However, a rapid comparison shows that the JAS-12 survey provides, without surprise, a better resolution both for high and low frequency content (Fig. 6.3). Even anomalies with kilometre wavelengths disappear on the vintage compilation (Fig. 6.3) the contrast is even more obvious if we compare transects extracted along the same profile (Fig. 6.4).

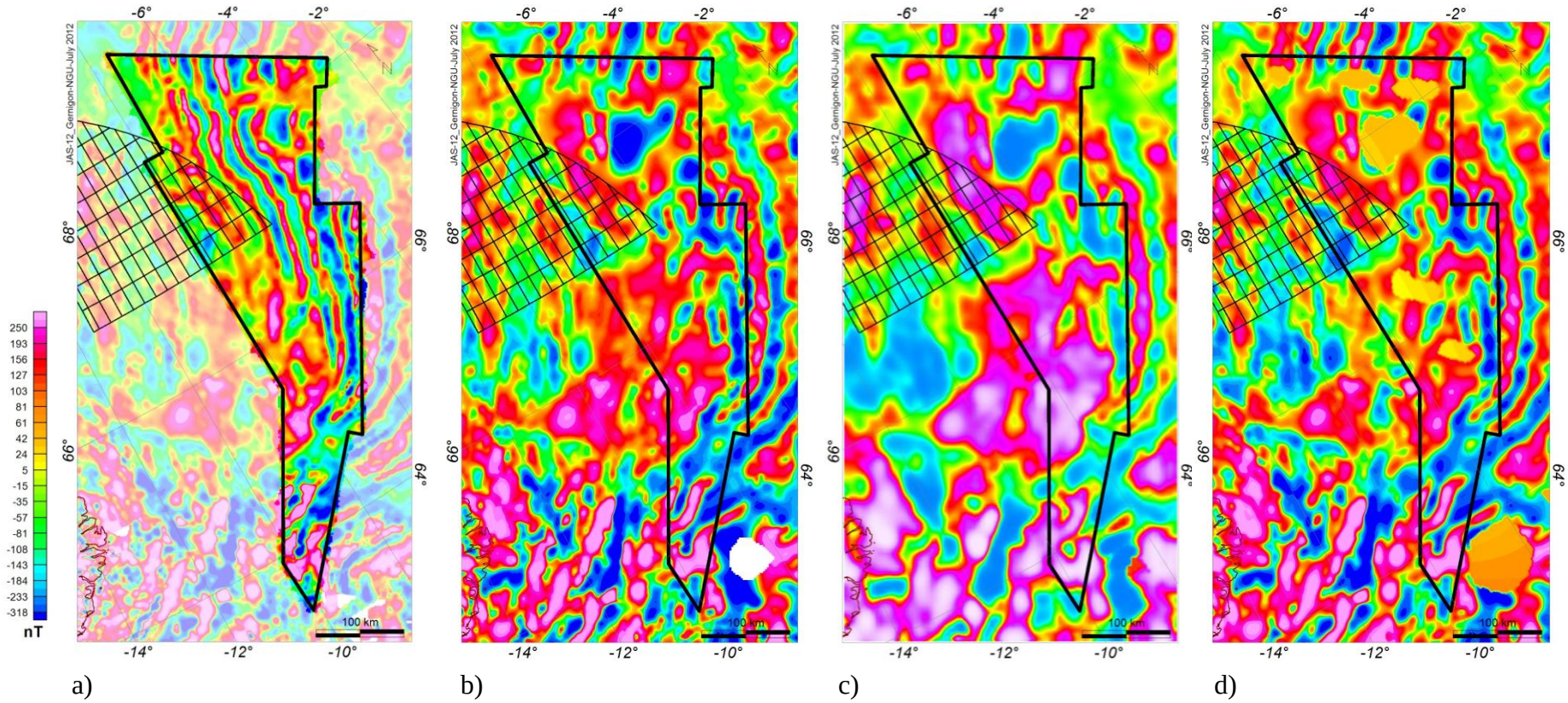

Figure 6.3 NGU final compilation compared with previous public domain compilations. From left to right: a) Outline of the new JAS-12 with the pre-existing NGU compilation (Olesen et al. 2010, Gernigon et al. 2009, 2012) in background (1000x1000m). b) North Atlantic vintage marine compilation form Verhoef et al. (1997) gridded to 1500x1500 m. c) CGMW World magnetic map including satellites CHAMP data version A (3 min of arc spacing)(Hemant et al. 2007) and d) CAMP Arctic compilation (2x2 km upward continued by 2 km) (Gaina et al. 2011). The new JAS-12 compilation (without satellite correction) provides much more details and reliability.

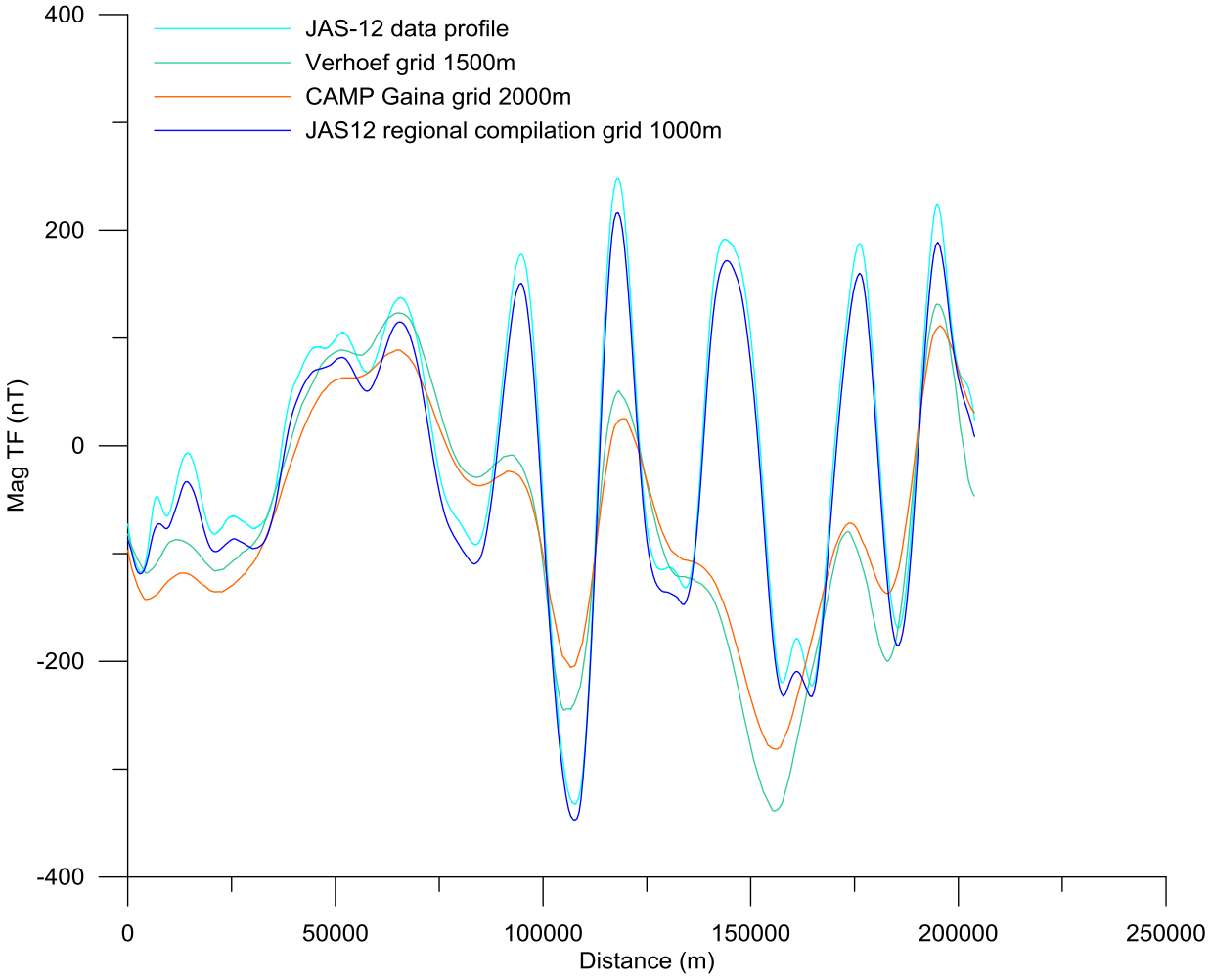

Figure 6.4 Magnetic total field of the new JAS-12 survey compared with other compilations along JAS-12 Line 34. Using profiles, the differences are even more obvious. The JAS-12 clearly provides a significant improvement for short as well as long wavelengths.

7 OTHER DATASETS AND DATA COMPILATION

Laurent Gernigon

7.1 Bathymetry

For regional and more local investigation of the Norway Basin, we had access to and compiled different bathymetric sources (Fig. 7.1; Table 7.1). Our original dataset included the Bathymetry and topography grid of the NE Atlantic compiled by Olesen et al. (2010). This 250x250 m grid represents an updated version of the Dehls *et al.* (2000) compilation using new releases of bathymetric data from the Arctic ocean, IBCAO v. 2.23 (Jakobsson *et al.* 2008) and the world oceans (GEBCO). High-resolution topography data (100x100m) for Norway and the adjacent land areas were supplied by the Norwegian Mapping and Cadastre Authority and the US Geological Survey, respectively.

Covering a large part of the Norwegian-Greenland Sea up to the Arctic regions further north, the recent International Bathymetric Chart of the Arctic Ocean release IBCAO Version 3.0 represents the largest improvement since the first grid published in 1999. It has been considered as the most reliable regional source for the JMMC area. The IBCAO Version 3.0 includes different bathymetric data collected from fishing vessels, data acquired from the US Navy and from research ships of various origins (see complete description in Jakobsson et al., 2012). Built using an improved gridding algorithm, this new grid is a 500 meter spacing, revealing much greater details of the seafloor than the previous IBCAO Version 1.0 (2.5 km) and Version 2.0 (2.0 km). The area covered by multi-beam surveys has increased from 6% in Version 2.0 to 11% in Version 3.0 (Jakobsson et al. 2012).

Unfortunately, the IBCAO3 grid is limited to the south at 64°N and only covers half of the Norway Basin. To extend this regional grid, we have merged the IBCAO3 grid together with the DTU10 Ocean wide Mean Sea Surface provided by the DTU Space National Space institute (Andersen, 2010). The worldwide DTU mean sea surface is the displacement of the sea surface relative to a mathematical model of the Earth and it closely follows the geoid (Andersen and Knudsen 2009; Andersen 2010). The original DTU10 Ocean wide Mean Sea Surface height (relative to the Ellipsoid) has been mapped with a resolution of 1 minute by 1 minute.

We also included and merge in this compilation the two confidential multi-beam surveys provided by NPD, ISOR and Okustofnun at the level of the Jan Mayen Ridge. These high resolution bathymetric surveys included:

- the A8-2008 survey acquired in the Dreki area by the Marine Research Institute of Iceland (HAFRO) (Helgadóttir et al. 2008)
- the North Jan Mayen Ridge A11-2010 survey (Confidential) in accordance to a cooperation agreement between the National Energy Authority of Iceland (NEA),

Norwegian Petroleum Directorate (NPD) and the Marine Research Institute (MRI) (Reynisson and Helgadóttir 2010)

To keep a correct resolution of the regional Jan Mayen grid we have regrided the IBCAO3, the DTU grid and the multi-beam survey together with a grid resolution of 500x500 m.

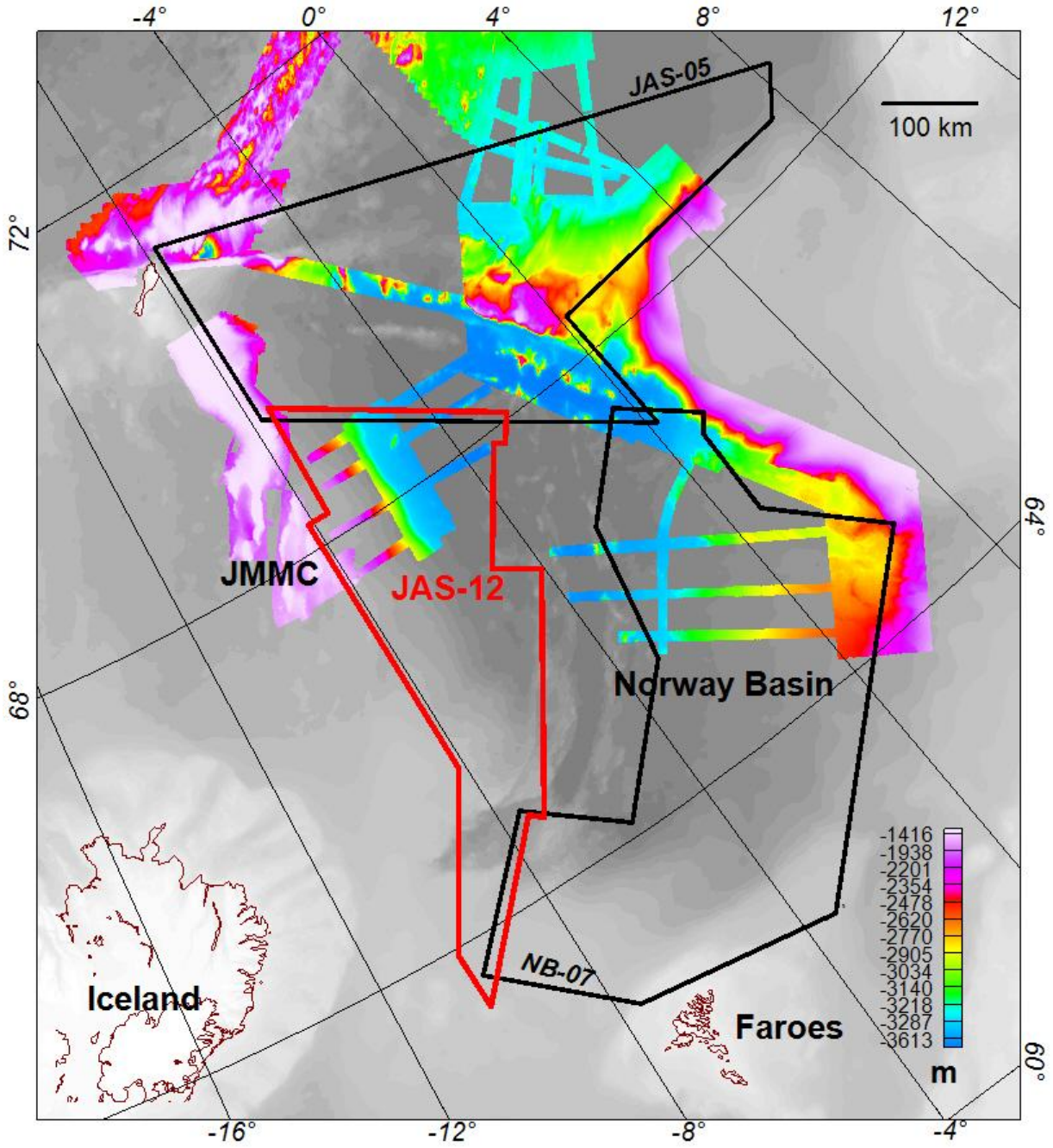

Figure 7.1 Regional and local multi-beam bathymetric dataset, compiled and merged in the vicinity the JAS-12 survey. See text for details.

Survey	Resolution available	references
A8-2008	25 m	Helgadóttir et al. 2008
A11-2010	25m	Reynisson and Helgadóttir 2010 (confidential)
OD 99-2000	25m	NPD, unpublished
NGU 2012 Bathy, onshore topography	250m	Dehls et al. 2000; Olesen et al. 2010
IBCA0 version 3	500 m	Jakobsson et al. 2012
DTU10 Ocean wide Mean Sea Surface	1 minx1min	Anderson and Knudsen 2009; Andersen 2010

Table 7.1 The most recent bathymetric datasets available in the vicinity of the JMMC

7.2 Gravity

We had access to several regional gravity compilations during that JAS-12 project (Table 7.2). The regional NGU compilations of Skilbrei et al. (2002) and Olesen et al. (2010) have been partly used in the present study. This compilation is offshore based on measurements of c. 554 000 km of various shipboard gravity measurement provided by the Norwegian Petroleum Directorate, oil companies, and the Norwegian Mapping Authority (Fig. 7.1). This dataset was merged with previous Geosat and ERS-1 satellite compilations available in the deep-water areas of the Norwegian-Greenland Sea (Laxon and McAdoo 1994; Laxon and McAdoo 1994; Andersen and Knudsen 1998; Andersen and Knudsen, 2010). The surveys have been levelled using the International Standardization Net 1971 (IGSN 71) and the Gravity Formula 1980 for normal gravity. The combined dataset has been interpolated to square cells of 2000 m size using the minimum curvature method (Olesen et al., 2010).

Surveys	Resolution available	references
NGU 2012-DNC08	2000mx2000m	Olesen et al. 2010 Andersen et al. 2008
Arctic Gravity Project	5 mnx5mn	Kenyon et al. 2008
DTU10GRAV	1 mnx1mn	Andersen 2010
Árni Friðriksson Cruise Survey 2012	500mx500 1000mx1000	Solheim 2012
JM 85 shiptrack profiles		Gunnarson et al. 1989; Eysteinsson and Gunnarsson 1995

Table 7.2 The most recent gravity datasets avaible in the vicinity of the JMMC

The 5 minutes x 5 minutes Arctic Gravity Project grid is also freely available (http://earth-info.nga.mil/GandG/wgs84/agp/index.html) and covers most of the JMMC and part of the Norway Basin (Kenyon et al. 2008). However, this grid is too coarse to highlight the main structures of the JMMC in detail.

The DTU10GRAV compilation of the DTU National Space Institute was also used for regional purposes (Andersen, 2010). This compilation is an updated version of the DNSC08GRAV described by Andersen (2010). This global gravity field model shows the gravity variations over the global ocean as mapped by the ERS-2 and ENVISAT satellites (Andersen 2010). On land the field has been augmented with the best available terrestrial gravity field to get a complete global coverage. Improved editing, ocean tide correction and ice retreat at northern latitudes have been considered The DTU10 ocean wide gravity field has been mapped with a resolution of 1 minute by 1 minute. Further information can be obtained on the DTU website http://www.space.dtu.dk.

More recently, we also got access to the Jan Mayen gravity survey acquired during the Árni Friðriksson Cruise during summer 2012 by the Norwegian Mapping Authority (Solheim 2012) (Fig. 7.2). This (confidential) survey covers most of the central and northern Jan Mayen Ridge and partly the southern Jan Mayen Ridge. The density of measurement in the northern part is relatively correct with a line spacing of ~3 km. For regional purpose, we merged this gravity survey with the DTU10 wide gravity survey with a grid spacing of 1500m using the Geosoft grid stitching suture algorithm allowing the DTU10 initial grid to be adjusted properly at the edge of the new Jan Mayen Ridge survey. This method provides smooth blending without over-smoothing high-frequency variations which may occur along the suture path. During the merge, only the coverage of the central and northern Jan Mayen Ridge has been considered due to the proper density of shiptrack measurements. The final result provides a more accurate regional dataset especially at the main bathymetric escarpments that characterise the JMMC.

For this study, we also obtained from ISOR the original shiptrack data acquired by the National Energy Authority of Iceland (NEA, Orkustofnun) and NPD during the Jan Mayen Ridge geophysical survey in 1985 (Gunnarsson et al. 1989; Eysteinsson and Gunnarsson 1995). A comparison of the shiptrack data with the different grid compilations is show on Figure 7.3.

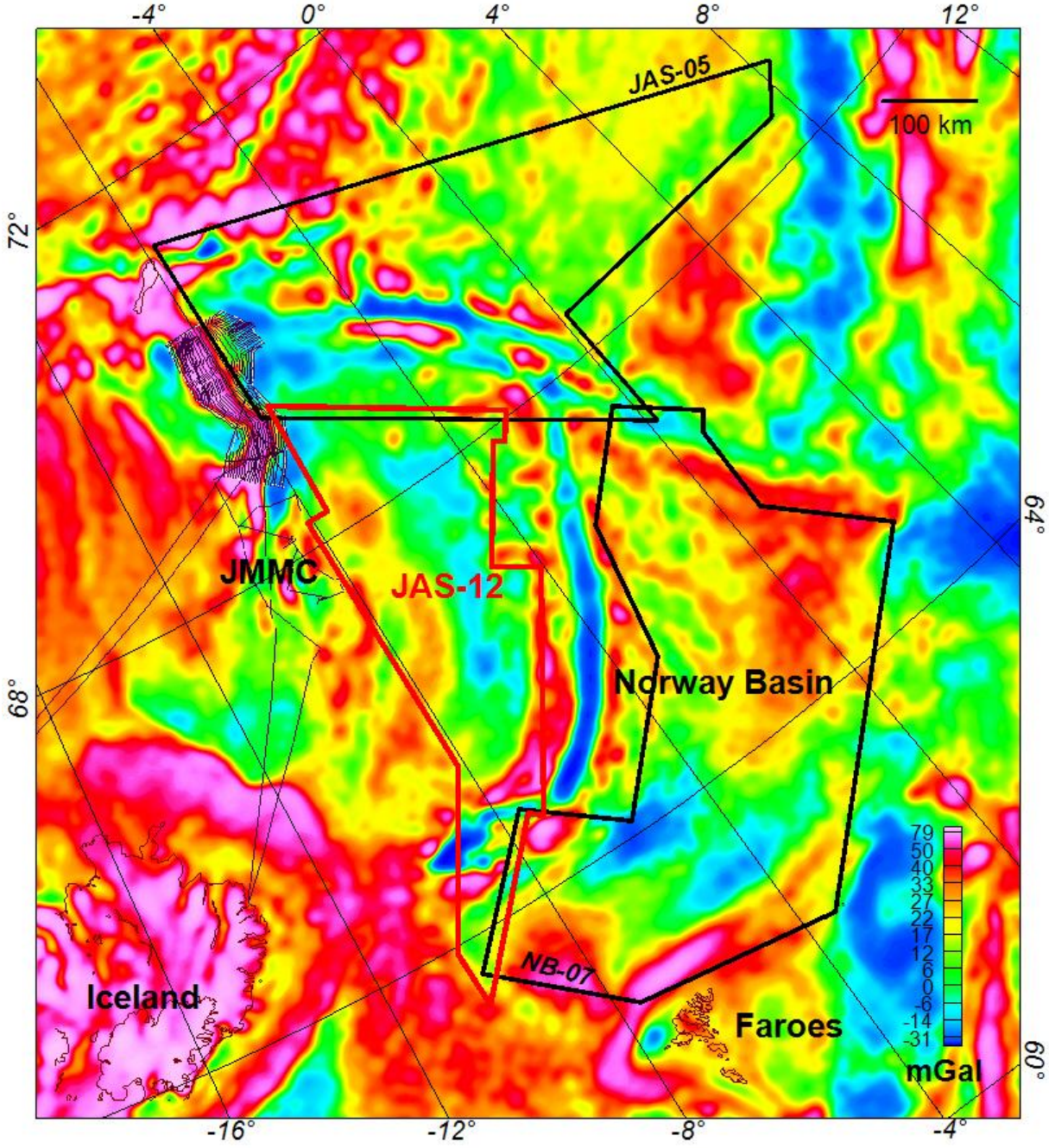

Figure 7.2 Regional gravity (free air) and location of the Árni Friðriksson shiptrack gravity merged with the pre-existing DTU10 compilation.

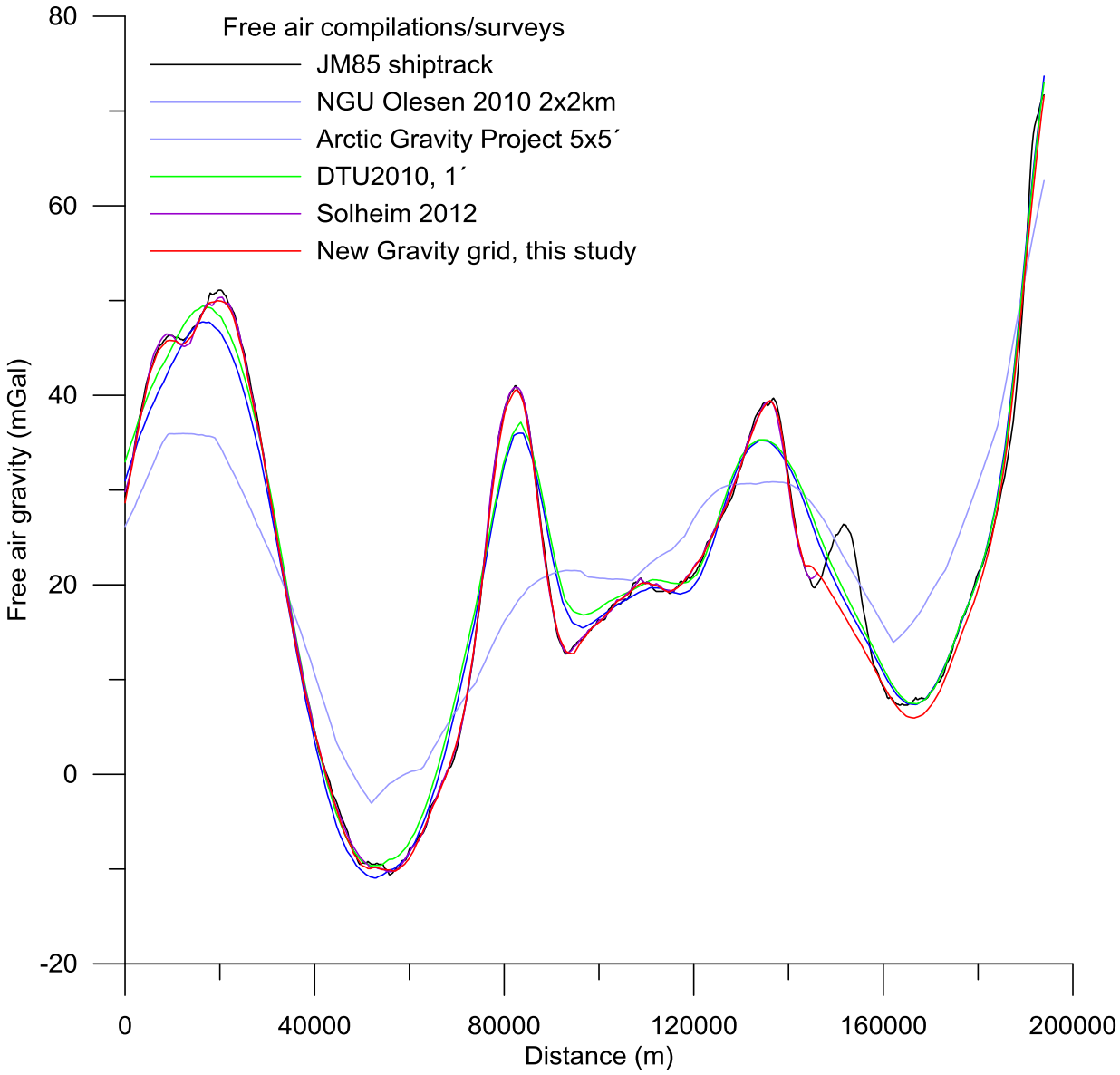

Figure 7.3 Comparison of the different gravity compilations and shiptrack data along the NPD-JM85 profile JM-25-85.

7.3 Seismic reflection/refraction compilation

Seismic reflection profiles provided by the Norwegian Petroleum Directorate were combined with gravity and magnetic data for interpretation and modelling. Some of the old multichannel seismic data available with the study area have already been introduced by Skogseid and Eldholm (1987). We also got access to the Law of Sea seismic transects acquired by the Norwegian Petroleum Directorate between 1996 and 2000 in the Norway Basin (provided by NPD the previous JAS-05 and NB-07 projects). Some of the JM88 seismic sections (Gunnarsson et al. 1989) have been provided by ISOR and NPD. This survey has been acquired by the Norwegian Petroleum Directorate and the National Energy Authority of Iceland in 1988.

It was shot by the University of Bergen and processed by the NEA (see also http://www.nea.is/oil-and-gas-exploration/exploration-areas/datasets/). Some of this data have been reprocessed by Spectrum A.S. These seismic data are only available in two-way travel times. We interpreted and simply converted the seismic sections using a linear velocity versus depth function from sea bottom to top oceanic basement. This model of instantaneous velocity ($Vp=1.9+0.4 \cdot time$) refers to the more recent velocity database (Myhre and Eldholm 1980; Breivik et al. 2006; Engen et al. 2006) for the oceanic part. On the JMMC region, the crustal velocity model has been mostly derived from the more recent OBS data (Breivik et al. 2012) and old ESP/Sonoboy refraction (Johnsen et al. 1988; Johansen 1992) (see JAS-12 interpretation report part B, in prep).

8 CONCLUSION AND PERSPECTIVES

8.1 Acquisition and processing

- The new survey JAS-12 allowed the previous magnetic gaps between the Jan Mayen microcontinent and the Ægir Ridge to be filled.

- The magnetic anomalies coverage of the entire Norway Basin is almost complete now. The new survey reflects the different structure, composition and geodynamic history of the oceanic crust of the Norway Basin and surrounding margins that developed during Eocene-Oligocene time.

- Levelling and microlevelling of the raw data have been completed. Several filtered versions have been calculated.

8.2 Early observations and perspectives

- The tectonic implications of the new survey will be further described in the future JAS-12 interpretation report. Some preliminary interpretations (early potential field model and magnetic chrons interpretation) have been presented at NPD in September 2012 (the archive in the USB stick included this PowerPoint presentation).

- Thank to the new results, we already see that the continent-ocean boundary can be properly identified on the new JAS-12. Oceanic fractures zones are now clearly observed and magnetic chrons from C24b up to C10 can be identified.

- The early results also suggest that subsequent to C22n, the spreading centre accommodated an important Eocene geodynamic adjustment as observed in the previous NB-07 (Gernigon et al. 2008, 2012). In light of the new conjugate survey, the transition from C22n to C20n definitively reflects a significant change in the Norway Basin. The spreading direction changes from NW-SE between C24 and C22 to NNW-SSE after C22n. At the same time a crudely northward-widening fan-shaped magnetic anomaly pattern developed along the active Aegir Ridge. Compared to the previous models, the new dataset clearly shows that the onset of the fan-shaped evolution definitively starts earlier at C22n (49.7-49.0) instead of C18-C17 (40.1-36.6) as previously proposed. This rejects definitively the early hypothesis of Scott et al. (2000) involving several fracture zone to the east of the JMMC. The new data do not show numerous discontinuities. Continental extension of the southern Jan Mayen microcontinent in Eocene time is required to compensate the spreading evolution observed in the eastern part of the Aegir Ridge.

- The new interpretation also confirm that a compensating deformation zone exists between C22 and C13, somewhere in the western part of the Aegir Ridge before the onset of breakup between Greenland and the Jan Mayen microcontinent at C7 (or C13 ?).

- In the future, the JAS-12 survey will be better integrated with previous aeromagnetic surveys to re-evaluate and update more precisely the spreading history of the Norway Basin development between the outer Møre Basin and the JMMC. The JAS-12 survey already provides new magnetic constrains required to refine the plate reconstruction in this area. Precise estimation of the rotation poles requires an initially precise identification and pick of the magnetic chrons. Rotation parameters will be calculated using robust and precise best-fitting techniques and cost function analysis.

- As part of the project, potential field modelling will be also carried out across the JMMC and surrounding oceanic domain.

- On a long term perspective, we suggest the acquisition of new aeromagnetic surveys to refine the vintage datasets still present (>35 years old) to the west and south of the new JAS-12 survey (Fig. 8.1). New surveys with a minimum lines/tie line configuration of 5x20 km will be required in the southern and central part of the JMMC to properly evaluate the structures and volcanism of the microcontinent. Higher resolution could be proposed in the northern part in order to highlight shallower magnetic sources. We recommend waiting at least until 2014/2015 to get better magnetic conditions.

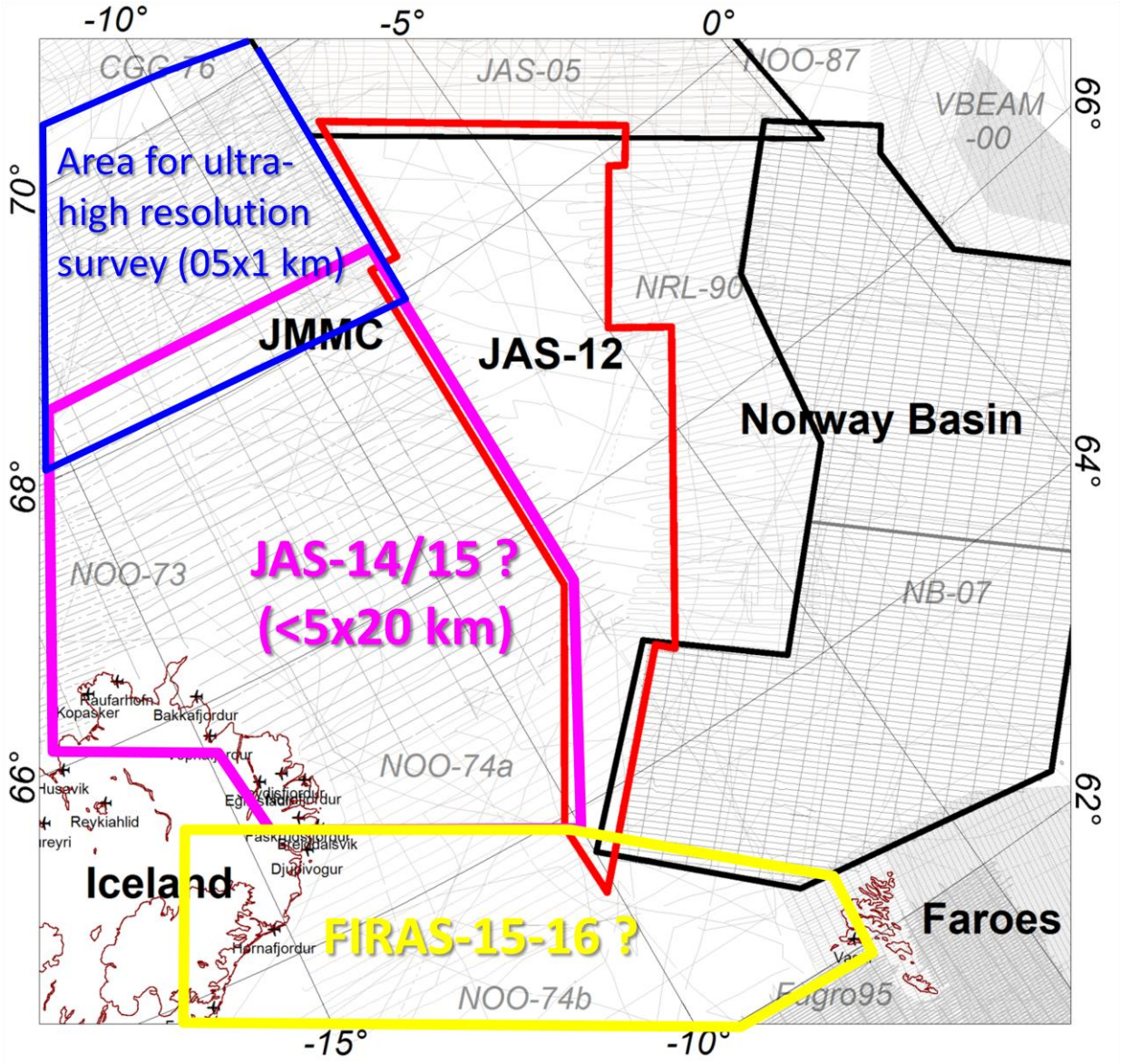

Figure 8.1 Proposal for future aeromagnetic surveys to the west west and south of the JAS-12.

9 ACKNOWLEDGEMENTS

NGU financed the Jan Mayen Aeromagnetic Survey 2012 in collaboration with the Norwegian Petroleum Directorate and the Icelandic National Energy Authority (Orkustofnun). NPD (Morten Sand), Orkustofnun (Thorarinn Sveinn Arnarson) and (ISOR (Anett Blischke) provided a reprocessed versions of the JM88 seismics and new Marine Research Institute (HAFRO) muli-beam bathymetry surveys from the area around the Jan Mayen microcontinent. NPD and Dag Solheim from the Norwegian Mapping Authority (Kartverket) provided access to the Arni Fridriksson cruise 2010 gravity measurements. Blom Geomatics and Fly Taxi Nord provided the aeroplanes and have been in charge of the data acquisition. We express our thanks to these companies, institutions and persons.

10 BIBLIOGRAPHY

Åm, K. 1973: Tolkning av magnetiske og gravimetriske data, Kontinentalsokkelen Stavanger/Stad (59–628N). Norges geologiske undersøkelse Report 1175.

Åm, K. 1975: Aeromagnetic basement mapping north of latitude 62N, Norway. *Norges geologiske undersøkelse Bulletin* **316**, 351-374.

Andersen, O. B. 2010: The DTU10 Gravity field and Mean sea surface. *Second international symposium of the gravity field of the Earth (IGFS2)*, Fairbanks, Alaska.

Andersen, O.B. & Knudsen, P. 2009: DNSC08 mean sea surface and mean dynamic topography models: *Journal of Geophysical Research-Oceans*, **114**, C11001, doi:10.1029/2008JC005179.

Andersen, O.B. & Knudsen, P. 1998: Global marine gravity field from the ERS-1 and Geosat geodetic mission altimetry. *Journal of Geophysical Research-Oceans* **103**(C4), 8129-8137.

Arkani-Hamed, J. 2007: Differential reduction to the pole: Revisited. *Geophysics* **72**(1), L13-L20.

Arkani Hamed, J. 1988: Differential reduction to the pole of regional magnetic anomalies. *Geophysics* **53**, 1592-1600.

Bainbridge, G., Musselman, C., Whitehead, N. & McDonald, N., 2002: Euler 3D Deconvolution (v5.1.5). Processing, analysis and visualization system for 3D inversion of potential field. *Tutorial and user guide*. Geosoft incorporated, 66 pp.

Baranov, V. 1957: A new method for interpretation of aeromagnetic maps: pseudo gravity anomalies. *Geophysics* **22**, 359-383.

Barbosa, V.C.F., Silva, J.B.C. & Medeiros, W.E. 1999: Stability analysis and improvement of structural index estimation in Euler deconvolution. *Geophysics* **64**(1), 48-60.

Barbosa, V.C.F., Silva, J.B.C. & Medeiros, W.E. 2000: Making Euler deconvolution applicable to small ground magnetic surveys. *Journal of Applied Geophysics* **43**(1), 55-68.

Berndt, C., Mjelde, R., Planke, S., Shimamura, H. & Faleide, J.I. 2001b: Controls on the tectono-magmatic evolution of a volcanic transform margin: the Vøring Transform Margin, NE Atlantic. *Marine Geophysical Researches* **22**(3), 133-152.

Berndt, C., Planke, S., Alvestad, E., Tsikalas, F. & Rasmussen, T. 2001: Seismic volcanostratigraphy of the Norwegian Margin: constraints on tectonomagmatic break-up processes. *Journal of the Geological Society* **158**, 413-426.

Bhattacharya, B.K. 1966: Continuous spectrum of the total magnetic field anomaly due to rectangular prismatic body. *Geophysics* **31**, 97-121.

Blakely, R.J. 1995: Potential Theory in Gravity and Magnetic Applications. *Cambridge University Press*, 461 pp.

Blakely, R.J. & Simpson, R.W. 1986: Approximating edges of source bodies from magnetic or gravity anomalies. *Geophysics* **51**, 1494-1498.

Blakely, R.J., Wells, R.E., Yelin, T.S., Madin, I.P. & Beeson, M.H. 1995: Tectonic Setting of the Portland-Vancouver Area, Oregon and Washington - Constraints from Low-Altitude Aeromagnetic Data. *Geological Society of America Bulletin* **107**(9), 1051-1062.

Blystad, P., Brekke, H., Færseth, R.B., Larsen, B.T., Skogseid, J. & Tørudbakken, B. 1995: Structural elements of the Norwegian continental shelf, Part II. The Norwegian Sea Region. *Norwegian Petroleum Directorate Bulletin* **8**, 0-45.

Breivik, A.J., Mjelde, R., Faleide, J.I., & Murai, Y. 2012: The eastern Jan Mayen microcontinent volcanic margin. *Geophysical Journal International* **188**, 798-818.

Breivik, A., Faleide, J.I. & Mjelde, R. 2008: Neogene magmatism northeast of the Aegir and Kolbeinsey ridges, NE Atlantic: Spreading ridge mantle plume interaction? G-Cube. Geochemistry *Geophysics* Geosystem **9(2),** Q02004, doi:10.1029/2007GC001750.

Breivik, A.J., Mjelde, R., Faleide, J.I. & Murai, Y. 2006: Rates of continental breakup magmatism and seafloor spreading in the Norway Basin-Iceland plume interaction. *Journal of Geophysical Research-Solid Earth* **111**(B7), B07102, doi:10.1029/2005JB004004.

Breivik, A.J., & Faleide, J.I. 2004: Geophysical Atlas of the Barents Sea, Integrated Seismic, Gravity and Magnetic Interpretation. *VBPR and TGS-NOPEC Report*, Oslo (Confidential).

Breivik, A.J., Verhoef, J. & Faleide, J.I. 1999: Effect of thermal contrasts on gravity modeling at passive margins: Results from the western Barents Sea. *Journal of Geophysical Research-Solid Earth* **104**(B7), 15293-15311.

Briggs, I.C. 1974: Machine contouring using minimum curvature. *Geophysics* **39**, 39-48.

Brönner, M., Gernigon, L., Pascal, C., Koziel, J., & Marello, L., 2010: Barents Sea Aeromagnetic Remapping 2009 (BASAR-09): Acquisition and processing report and preliminary interpretation of the SW Barents Sea. Geological Survey of Norway (NGU) Report no. 2010.056, 210 pp.

Brönner, M., Gernigon, L., Ebbing, J., Olesen, O., Roberts, D., Barrére, C., & Koziel, J., 2009, Barents Sea Aeromagnetic Remapping BASAR-08: Acquisition, processing and interpretation. Geological Survey of Norway (NGU) Report no. 2009.020, 150 pp.

Burg, J.P. 1975: Maximum Entropy Spectral Analysis. *Stanford University*. PhD thesis, unpublished.

Cande, S.C. & Kent, D.V. 1995: Revised calibration of the geomagnetic polarity timescale for the Late Cretaceous and Cenozoic. *Journal of Geophysical Research* **100**(B4), 6093-6095.

Cannat, M. 1996: How thick is the magmatic crust at slow spreading oceanic ridges? *Journal of Geophysical Research-Solid Earth* **101**(B2), 2847-2857.

Cannat, M., Mevel, C., Maia, M., Deplus, C., Durand, C., Gente, P., Agrinier, P., Belarouchi, A., Dubuisson, G., Humler, E. & Reynolds, J. 1995: Thin Crust, Ultramafic Exposures, and Rugged Faulting Patterns at Mid-Atlantic Ridge (22-Degrees 24-Degrees-N). *Geology* **23**(1), 49-52.

Carlson, R.L. & Herrick, C.N. 1990: densities and porosities in the oceanic-crust and their variations with depth and Age. *Journal of Geophysical Research-Solid Earth and Planets* **95**(B6), 9153-9170.

Christensen, N.I. & Mooney, W.D. 1995: Seismic velocity structure and composition of the continental crust: A global view. *Journal of Geophysical Research* - Solid Earth **100**, 9761-9788.

Clark, D.A. 1997: Magnetic petrophysics and magnetic petrology: aids to geological interpretation of magnetic surveys. *AGSO Journal of Australian Geology and Geophysics* **17**(2), 83-103.

Cochran, J.R. & Karner, G.D. 2007: Constraints on the deformation and rupturing of continental lithosphere of the Red Sea: the transition from rifting to drifting. *In G.D. Karner, G. Manatschal and L.M. Pinheiro (eds) Imaging, Mapping and Modelling Continental Lithosphere Extension and Breakup*. Geological Society, London, Special Publications **282**, 265-289.

Compagnie Générale de Géophysique. 1977: Norwegian Petroleum Directorate, Aeromagnetic Survey Jan Mayen Area, Interpretation Report. 23 pp.

Cooper, G.R.J. & Cowan, D.R. 2006: Enhancing potential field data using filters based on the local phase. *Computers & Geosciences* **32**(10), 1585-1591.

Dehls, J.F., Olesen, O., Bungum, H., Hicks, E., Lindhom, C.D., & Riis, F. 2000: Neotectonic Map, Norway and Adjacent Areas, 1:3 Mill. Trondheim, Geological Survey of Norway.

Dobrin, M. & Savit, C. 1988: Introduction to geophysical prospecting. 4th edition. *McGraw-Hill*, 867 pp.

Eldholm, O. & Grue, K. 1994: North-Atlantic volcanic margins - dimensions and production-rates. *Journal of Geophysical Research-Solid Earth* **99**(B2), 2955-2968.

Engen, O., Frazer, L.N., Wessel, P., & Faleide, J.I. 2006: Prediction of sediment thickness in the Norwegian-Greenland Sea from gravity inversion. *Journal of Geophysical Research-Solid Earth*, **111**, B11, B11403, doi:10.1029/2005JB003924.

Eysteinsson, H., & Gunnarsson, S. 1995: Maps of gravity, bathymetry and magnetics fro Iceland and Surroundings. *Reykjavik, Orkustofnun (National Energy Authority)*, 39 pp.

Ferraccioli, F., Gambetta, M., & Bozzo, E., 1998, Microlevelling procedures applied to regional aeromagnetic data: an example from the Transantarctic Mountains (Antarctica). *Geophysical Prospecting*, 46, 177-196.

Fairhead, J.D. & Williams, S.E. 2006: Evaluating normalized magnetic derivatives for structural mapping, *SEG 2006 New Orleans Annual meeting*, New Orleans, USA.

Fichler, C., Rundhovde, E., Olesen, O., Sæther, B.M., Rueslåtten, H., Lundin, E. & Doré, A.G. 1999: Regional tectonic interpretation of image enhanced gravity and magnetic data covering the mid-Norwegian shelf and adjacent mainland. *Tectonophysics* 306(2), 183-197.

FitzGerald, D., Reid, A. & McInerney, P. 2004: New discrimination techniques for Euler deconvultion. *Computers & Geosciences* **30**(5), 461-469.

Fjellanger, E., Surlyk, F., Wamsteeker, L.C. & Midtun, T. 2005: Upper Cretaceous basin-floor fans in the Vøring Basin, Mid Norway Shelf. *In B. Wandas et al. (eds.) Onshore-Offshore Relationships on the North Atlantic Margin*. Norwegian Petroleum Society, Special Publication, 12, 135-134.

Florio, G., Fedi, M., & Pasteka, R. 2006: On the application of Euler deconvolution to the analytic signal. *Geophysics* **71**, L87-L93.

Gaina, C., Werner, S.C., Saltus, R., Maus, S., & GROUP, C.-H. 2011: Circum-Arctic mapping project: new magnetic and gravity anomaly maps of the Arctic. *In Spencer, A.M., A.F. Embry, D.L.Gautier, A.V. Stoupakova and K. Sørensen (eds). Arctic Petroleum Geology*. Geological Society, London, Memoirs **35**, 39-48.

Gaina, C., Gernigon, L., & Ball, P. 2009: Palaeocene-Recent plate boundaries in the NE Atlantic and the formation of the Jan Mayen microcontinent. *Journal of the Geological Society*, 166, 601-616.

Gardner, G.H.F., Gardner, L.W. & Gregory, A.R. 1984: Formation velocity and density -The diagnostic basics for stratigraphic traps. *Geophysics* **39**, 770-780.

Geosoft 2004: OASIS Montaj v 6.0 Mapping and processing system, The core software platform for working with large volume spatial data. *Quick start tutorials. Geosoft Incorporated*, 258 pp.

Geosoft 2005a: Montaj grav/mag interpretation, processing, analysis and visualization system for 3D inversion of potential field data for Oasis Montaj v6.1, *Tutorial and user guide. Geosoft Incorporated*, 65 pp.

Geosoft 2005b: Montaj *Geophysics* Levelling System, processing and enhancing geophysical data extension for Oasis Montaj v6.2. Tutorial and user guide. *Geosoft Incorporated*, 68 pp.

Geosoft 2005c: Montaj MAGMAP filtering-2D Frequency Domain Processing of Potential Field Data Extension for Oasis montaj v.6.1. *Geosoft Incoporated*, 66 pp.

Geosoft 2005d: Montaj GridKnit, Grid extension for OASIS Montaj v6.1, Tutorial and user guide. *Geosoft Incorporated*, 27 pp.

Gernigon, L., & Brönner, M. 2012b: Late Palaeozoic architecture and evolution of the southwestern Barents Sea: insights from a new generation of aeromagnetic data. *Journal of the Geological Society* **169**, 449-459.

Gernigon, L., Gaina, C., Olesen, O., Ball, P.J., Peron-Pinvidic, G., & Yamasaki, T., 2012: The Norway Basin revisited: From continental breakup to spreading ridge extinction. Marine and Petroleum Geology **35**, p. 1-19.

Gernigon, L., Brönner, M., Fichler, C., Lovas, L., Marello, L., & Olesen, O. 2011: Magnetic expression of salt diapir-related structures in the Nordkapp Basin, western Barents Sea. *Geology* **39**, 135-138.

Gernigon, L., Olesen, O., Koziel, J., & Lynum, R., 2008: Norway Basin aeromagnetic survey NB-07 - acquisition, processing and interpretation. Geological Survey of Norway (NGU) Report 2008.052. Geological Survey of Norway (NGU), p. 216.

Gernigon, L., Olesen, O., Ebbing, J., Wienecke, S., Gaina, C., Mogaard, J.O., Sand, M., & Myklebust, R., 2009: Geophysical insights and early spreading history in the vicinity of the Jan Mayen Fracture Zone, Norwegian-Greenland Sea. *Tectonophysics* **468**, 185-205.

Gernigon, L., Olesen, O. & Continental Shelf *Geophysics* team 2007: Challenging the Established Truths. *Geoexpro* **4**, 40-44.

Gernigon, L., Marello, L., Mogaard, J.O., Werner, S.C. & Skilbrei, J.R. 2007b: Barents Sea Aeromagnetic Survey BAS-06 - Acquisition-processing report and preliminary interpretation. Geological Survey of Norway (NGU) Report 2007.035, 142 pp.

Gernigon, L., Le Gall, B. & Ringenbach, J. C. 1999. Imagerie sismique et géométrie 2D-3D des complexes magmatiques paléocènes associés à la marge volcanique de Norvège (Bassins de Møre et Vøring) (Seismic imaging and 2D/3D geometries of magmatic complexes in the Mid-Norway margin (Møre and Vøring Basins). Oceanic margins and magmatism. Special meeting of the Geological Society of France (SGF), Villefranche sur Mer, France, 15-17 November.

Grant, F.S. & Dodds, J. 1972: MAGMAP FFT processing system development notes. Paterson Grants and Watson Limited.

Grauch, V.J.S. & Cordell, L. 1987: Limitations of determining density or magnetic boundaries from the horizontal gradient of gravity or pseudogravity Data. *Geophysics* **52**(1), 118-121.

Gudlaugsson, S.T., Gunnarsson, K., Sand, M., & Skogseid, J. 1988: Tectonic and volcanic events at the Jan mayen Ridge microcontinent. *In A.C. Morton and L.M. Parson (eds) Early Tertiary Volcanism and the Opening of the NE Atlantic*. Geological Society, London, Special Publications **39**, 85-93.

Gunnarsson, K., Sand, M., & Gudlaugsson, S.T. 1989: Geology and hydrocarbon potential of the Jan Mayen Ridge, Oljedirektoret (Norwegian Petroleum Directorate) and Orkustofnun (Icelandic National Energy Authority), OD-89-91 (Norwegian Petroleum Directorate) or OS-89036/JHD-07 (Orkustofnun), 156 pp.

Gunn, P.G. 1997: Quantitative methods for interpreting aeromagnetic data: a subjective review. *AGSO Journal of Australian Geology and Geophysics* **17**(2), 105-113.

Hagevang, T., Eldholm, O. & Aalstad, I. 1983: Pre-23 magnetic anomalies between Jan Mayen and Greenland-Senja Fracture Zones in the Norwegian Sea. *Marine Geophysical Researches* **5**, 345-363.

Hathaway, D.H., Wilson, R.M. & Reichmann, E.J. 1999: A synthesis of solar cycle prediction techniques. *Journal of Geophysical Research-Space Physics **104**(A10)*, 22375-22388.

Helgadóttir, G. et al. 2008: Preliminary results from the 2008 Marine Research Institute multi-beam survey in the Dreki area, with some examples of potential use, Marine Research Institute, Iceland Exploration Conference Reykjavík, Iceland.

Hemant, K., Thebault, E., Mandea, M., Ravat, D. & Maus, S. 2007: Magnetic anomaly map of the world: merging satellite, airborne, marine and ground-based magnetic data sets. *Earth and Planetary Science Letters* **260**(1-2), 56-71.

Hsu, S.K. 2002: Imaging magnetic sources using Euler's equation. *Geophysical Prospecting* **50**(1), 15-25.

Huang, H.P. 2008: Airborne geophysical data leveling based on line-to-line correlations. *Geophysics*, **73**, F83-F89.

Jakobsson, M., Mayer, L., Coakley, B., Dowdeswell, J.A., Forbes, S., Fridman, B., Hodnesdal, H., Noormets, R., Pedersen, R., Rebesco, M., Schenke, H.W., Zarayskaya, Y., Accettella, D., Armstrong, A., Anderson, R.M., Bienhoff, P., Camerlenghi, A., Church, I., Edwards, M., Gardner, J.V., Hall, J.K., Hell, B., Hestvik, O., Kristoffersen, Y., Marcussen, C., Mohammad, R., Mosher, D., Nghiem, S.V., Pedrosa, M.T., Travaglini, P.G., & Weatherall, P. 2012: The International Bathymetric Chart of the Arctic Ocean (IBCAO) Version 3.0. *Geophysical Research Letters* 39, L12609, doi:10.1029/2012GL052219,

Jakobsson, M., & Macnab, R. 2006: A comparison between GEBCO sheet 5.17 and the International Bathymetric Chart of the Arctic Ocean (IBCAO) version 1.0. *Marine Geophysical Research* **27**, 35-48.

Jolley, D.W. & Bell, B.R. 2002a. The evolution of the North Atlantic Igneous Province and the opening of the NE Atlantic rift. *In D.W. Jolley and B.R. Bell (eds) The North Atlantic Igneous Province: stratigraphy, tectonic, volcanic and magmatic processes*. Geological Society, London, Special Publications **197**, 1-13.

Jolley, D.W. & Bell, B.R. 2002b. Genesis and age of the Erland Volcano, NE Atlantic Margin. In D.W. Jolley and B.R. Bell (eds.) *The North Atlantic Igneous Province: stratigraphy, tectonic, volcanic and magmatic processes*. Geological Society, London, Special Publications 197, 95-110.

Jolley, D.W., Clarke, B. & Kelley, S. 2002c: Paleogene time scale miscalibration: Evidence from the dating of the North Atlantic igneous province. *Geology* 30(1), 7-10.

Johansen, J.M. 1992: Modellering av det magnetiske anomalifeltet over Jan Mayen Ryggen: Oslo, Universitetet i Oslo. Mater thesis, 111 pp.

Johansen, B., Eldholm, O., Talwani, M., Stoffa, P.L., & Buhl, P. 1988: Expanding spread profile at the northern Jan Mayen Ridge. *Polar Research* **6**, 95-104.

Johnson, G.L. & Heezen, B.G. 1967: The morphology and evolution of the Norwegian-Greenland Sea. *Deep-Sea Research* **14**, 755-771.

Jónsson, G., Kristjansson, L., & Sverrisson, M. 1991: Magnetic Surveys of Iceland. *Tectonophysics* **189**, 229-247.

Jung, W.Y. & Vogt, P.R. 1997: A gravity and magnetic anomaly study of the extinct Aegir Ridge, Norwegian Sea. *Journal of Geophysical Research-Solid* Earth **102**(B3), 5065-5089.

Karson, J.A. & Brooks, C.K. 1999: Structural and magmatic segmentation of the Tertiary East Greenland volcanic rifted margin. *In C. Mac Niocaill and P.D. Ryan (eds.) Continental Tectonics*. Geological Society of London, Special Publications, 164, 313-338.

Kenyon, S., Forsberg, R., & Coakley, B. 2008. New Gravity Field for the Arctic: EOS, Transactions American Geophysical Union **89**, p. 289.

Kodaira, S., Mjelde, R., Gunnarsson, K., Shiobara, H., & Shimamura, H., 1998: Structure of the Jan Mayen microcontinent and implications for its evolution: *Geophysical Journal International* **132**, 383-400.

Keating, P. & Pilkington, M. 2004: Euler deconvolution of the analytic signal and its application to magnetic interpretation. *Geophysical Prospecting* **52**(3), 165-182.

Kodaira, S., Mjelde, R., Gunnarsson, K., Shiobara, H., & Shimamura, H. 1998: Structure of the Jan Mayen microcontinent and implications for its evolution: *Geophysical Journal International* **132**, 383-400.

Kristjánsson, L., Jónsson, G., & Sverrisson, M., 1989: Magnetic Surveys at the Science Institute. Documentation to Accompany a Colored Map of total-field anomalies in Scale 1:1 000 000, and computer diskettes of survey data, Science Institute, University of Iceland, RH01.89.

Kristjánsson, L. & Jónsson, G. 1998: Aeromagnetic results and the presence of an extinct rift zone in western Iceland. *Journal of Geodynamics* **25**(1-2), 99-108.

Kuvaas, B. & Kodaira, S. 1997: The formation of the Jan Mayen microcontinent: the missing piece in the continental puzzle between the Møre-Vøring Basins and East Greenland. *First Break* **15**(7), 239-247.

Larsen, H.C., & Thorning, L. 1979: Project Eastmar: Acquisition of High Sensitivity Aeromagnetic Data off East. Grønlands. *Geologiske Undersøkelse Report* 100, x pp.

Larsen, H.C. 1974: Airborne Geophysical Survey in the Central East Greenland., *Grønlands Geologiske Undersøkelse Report no.* 75, x pp.

Laxon, S. & McAdoo, D. 1994: Arctic-Ocean Gravity-Field Derived from Ers-1 Satellite Altimetry. Science **265**(5172), 621-624.

Løvås, L., Mogaard, J.O., Olesen, O., Koziel, J., & Lynum, R. 2006: Southern Nordkapp Basin Aeromagnetic Survey 2006 (SNS-06). Data acquisition and processing report. *Geological Survey of Norway (NGU) Report* 2006.089, 50 pp.

Lundin, E. & Doré, A.G. 2002: Mid-Cenozoic post-breakup deformation in the 'passive' margins bordering the Norwegian-Greenland Sea. *Marine and Petroleum Geology* **19**(1), 79-93.

Luyendyk, A.P.J. 1997: Processing of airbone magnetic data. *AGSO Journal of Australian Geology and Geophysics **17***(2), 31-38.

Mari, J.-L., Glangeaud, F. & Coppens, F. 2001: Traitement du signal pour géologues et géophysisiens-Techniques de base **2**. *Editions Technip*, 268 pp.

Marson, I. & Klingele, E.E. 1993: Advantages of using the vertical gradient of gravity for 3-D interpretation. *Geophysics* **58**(11), 1588-1595.

Mauring, E., Beard, L.P., Kihle, O. & Smethurst, M.A. 2002: A comparison of aeromagnetic levelling techniques with an introduction to median levelling. *Geophysical Prospecting* **50**(1), 43-54.

Mauring, E. & Kihle, A. 2006: Leveling aerogeophysical data using a moving differential median filter. *Geophysics* **71**(1), L5-L11.

Maus, S., Barckhausen, U., Berkenbosch, H., Bournas, N., Brozena, J., Childers, V., Dostaler, F., Fairhead, J.D., Finn, C., von Frese, R.R.B., Gaina, C., Golynsky, S., Kucks, R., Luhr, H., Milligan, P., Mogren, S., Muller, R.D., Olesen, O., Pilkington, M., Saltus, R., Schreckenberger, B., Thebault, E., & Tontini, F.C. 2009: EMAG2: A 2-arc min resolution Earth Magnetic Anomaly Grid compiled from satellite, airborne, and marine magnetic measurements: *Geochemistry Geophysics Geosystems* **10**, 1525-2027.

Maus, S., Sazonova, T., Hemant, K., Fairhead, J.D. & Ravat, D. 2007: National Geophysical Data Center candidate for the World Digital Magnetic Anomaly Map. *Geochemistry Geophysics Geosystems* **8**, 1029/2007.

Mendel, V., Munschy, M. & Sauter, D. 2005: MODMAG, a MATLAB program to model marine magnetic anomalies. *Computers & Geosciences* **31**(5), 589-597.

Meyer, R., van Wijk, J.W. & Gernigon, L., 2007: An integrated geophysical and geochemical model for North Atlantic Igneous Province magmatism. *In G.R. Foulger and D.M. Jurdy (eds.) Plates, plumes, and planetary processes.* Geological Society of America Special Paper **430**, 525-552 pp.

Miller, H.G. & Singh, V. 1994: Potential-field tilt - a new concept for location of potential-field sources. Journal of Applied *Geophysics* **32**(2-3), 213-217.

Milligan, P.R. & Gunn, P.J. 1997: Enhancement and presentation of airbone geophysical data. *AGSO Journal of Australian Geology and Geophysics* **17**(2), 63-75.

Mjelde, R., Raum, T., Murai, Y. & Takanami, T. 2007: Continent-ocean-transitions: Review, and a new tectono-magmatic model of the Vøring Plateau, NE Atlantic. *Journal of Geodynamics* **43**(3), 374-392.

Mosar, J., Lewis, G. & Torsvik, T.H. 2002: North Atlantic sea-floor spreading rates: implications for the Tertiary development of inversion structures of the Norwegian-Greenland Sea. *Journal of the Geological Society of London* **159**, 503-515.

Mudge, C. 1991: New developments in resolving details in aeromagnetic data. *Exploration Geophysics* **23**, 277-284.

Myhre, A. & Eldholm, A. 1980: Sedimentary and crustal velocities in the Norwegian-Greeland Sea. *Journal of Geophysical Research* **86**(B6), 5012-5022.

Myklebust, R. 1985: Final report and processing of marine gravity and magneticdata-Jan Mayen, Volume xx, GECO A.S, p. 18.

Nabighian, M.N. 1972: The analytic signal of two-dimensional magnetic bodies with polynomial cross-sections ; Its properties and use for automated anomaly interpretation. *Geophysics* 37, 505-517.

Nabighian, M.N., Grauch, V.J.S., Hansen, R.O., LaFehr, T.R., Li, Y., Peirce, J.W., Phillips, J.D. & Ruder, M.E. 2005: 75th Anniversary - The historical development of the magnetic method in exploration. *Geophysics* **70**(6), 33nd-61nd.

Navrestad, T., & Jørgensen, F. 1979: Aeromagnetic investigations of the Jan Mayen Ridge. *In Torvanger, O., J. Bleie, O. Eldholm, S.Fønstelien, Y. Kristoffersen, H.C. Rønnevik, E. Sundor, and T.O. Vorren (eds), Norwegian Sea Symposium 1979*, Norsk Petroleumsforening (NPF).

Nasuti, A., Aarset, M., Brönner, M., Koziel, J., & Lauritsen, T. 2012: Central North Sea Aeromagnetic Survey 2010 (CNAS-10) data acquisition and processing. Geological Survey of Norway (NGU) Report 2012.023, 34 pp.

Northwest Geohysical Associates Incorporation 2006: GM-SYS Gravity and Magnetic Modelling software. Users Guide v 4.10, 110 pp.

Nunns, A. 1982: The structure and evolution of the Jan Mayen Ridge and surroundings regions. *In J.S. Watkins and C.L. Drake (eds), Studies in Continental Margin Geology*. American Association of Petroleum Geologists memoir **34**, 193-208.

Olesen, Brönner, M., Ebbing, J., Gellein, J., Gernigon, L., Koziel, J., Lauritsen, T., Mykelbust, R., Pascal, C., Sand, M., Solheim, A., & Usov, S. 2010: New aeromagnetic and gravity compilations from Norway and adjacent areas - methods and applications, *In Vining, B.A., and S.C. Pickering (eds), Petroleum Geology: From mature basins to new frontiers*. Proceedings of the 7th Petroleum Geology Conference. Geological Society of London, 559-586.

Olesen, O., Ebbing, J., Lundin, E., Mauring, E., Skilbrei, J.R., Torsvik, T.H., Hansen, E.K., Henningsen, T., Midbøe, P. & Sand, M. 2007: An improved tectonic model for the Eocene opening of the Norwegian-Greenland Sea: Use of modern magnetic data. *Marine and Petroleum Geology* **24**(1), 53-66.

Olesen, O., Gernigon, L., Ebbing, J., Mogaard, J.O., Pascal, C. & Wienecke, S. 2006: Interpretation of aeromagnetic data along the Jan Mayen Fracture Zone, JAS-05. *Geological Survey of Norway (NGU) Report* 2006.018. 162 pp.

Olesen, O., Lundin, E., Nordgulen, O., Osmundsen, P.T., Skilbrei, J.R., Smethurst, M.A., Solli, A., Bugge, T. & Fichler, C. 2002: Bridging the gap between the onshore and offshore geology in Nordland, northern Norway. *Norwegian Journal of Geology* **82**(4), 243-262.

Olesen, O., Gellein, J., Håbrekke, H., Kihle, O., Skilbrei, J.R., & Smethurst, M. 1997a: Magnetic anomaly map Norway and adjacent ocean areas, scale 1:3 million. Norges geologiske undersøkelse (NGU), Trondheim, Norway.

Pilkington, M., Miles, W.F., Ross, G.M. & Roest, W.R. 2000: Potential-field signatures of buried Precambrian basement in the Western Canada Sedimentary Basin. *Canadian Journal of Earth Sciences* **37**(11), 1453-1471.

Planke, S. & Eldholm, O. 1994: Seismic Response and Construction of Seaward Dipping Wedges of Flood Basalts - Vøring Volcanic Margin. *Journal of Geophysical Research-Solid Earth* **99**(B5), 9263-9278.

Press, W.H., Teukolsky, S.A., Vetterling, W.T. & Flannering, B.P. (eds), 2002: Numerical recipes in C++. The art of Scientific Computing Second Edition. Cambridge University Press, 972 pp.

Ravat, D. 1996: Analysis of the Euler method and its applicability in environmental magnetic investigations. *Journal of Environmental and Engineering Geophysics* **1**, 229-238.

Ravat, D., Whaler, K.A., Pilkington, M., Sabaka, T. & Purucker, M. 2002: Compatibility of high-altitude aeromagnetic and satellite-altitude magnetic anomalies over Canada. *Geophysics* **67**(2), 546-554.

Reid, A.B., Allsop, J.M., Granser, H., Millett, A.J. & Somerton, I.W. 1990a: Magnetic Interpretation in 3 Dimensions Using Euler Deconvolution. *Geophysics* **55**(1), 80-91.

Reeves, C. 2005: Aeromagnetic surveys: principles, practice and interpretation, Geosoft, p. 150.

Reynisson, P., & Helgadóttir, G. 2010: Multibeam echosounder and sub-bottom profiler acquisition on the Jan Mayen ridge in the Norwegian Economic Zone, with Icelandic research vessel Árni Friðriksson: A project for the National Energy Authority/Norwegian Petroleum Directorate. *Marine Research Institute report*, pp. 21 (Confidential).

Riddihough, R. 1986: Interpretation of Gravity and magnetic anomalies for non specialists, *In A.K. Goodacre (ed.), Canadian Geophysical Union short course*, 361 p.

Roest, W.R. & Pilkington, M. 1993: Identifying remanent magnetization effects in magnetic data. *Geophysics* **58**(5), 653-659.

Roest, W.R., Verhoef, J. & Pilkington, M. 1992: Magnetic interpretation using the 3-D analytic signal. *Geophysics* **5**(1), 116-125.

Rønning, S. & Skilbrei, J.R. 1998: HRAMS97-1 Southwestern Barents Sea High Resolution Aeromagnetic Survey 97-98. Geological Survey of Norway (NGU) Report no. 98.131.

Rønning, S. & Skilbrei, J.R. 1998: HRAMS97-1 Southwestern Barents Sea High Resolution Aeromagnetic Survey 97-98 (Area A). Geological Survey of Norway (NGU) Report no. 98.132.

Salem, A., Williams, S., Fairchild, D.G., Smith, R. & Ravat, D. 2008: Interpretation of magnetic data using tilt-angle derivatives. *Geophysics* **73**(1), 1-10.

Solheim, D. 2012: Gravity report: Árni Friðriksson Cruise, 2010, Norwegian Mapping Authority report, p. 18.

Saunders, A.D., Fitton, J.G., Kerr, A.C., Norry, M.J. & Kent, R.W. 1997: The North Atlantic Igneous Provinces. *In J.J. Mahoney and M.F. Coffin (eds) Large Igneous Provinces: continental, oceanic, and planetary flood volcanism*. American Geophysical Union, Geophysical Monograph **100**, pp. 45-93.

Silva, J.B.C. & Barbosa, V.C.F. 2003: 3D Euler deconvolution: Theoretical basis for automatically selecting good solutions. *Geophysics* **68**(6), 1962-1968.

Skilbrei, J.R., Olesen, O., Osmundsen, P.T., Kihle, O., Aaro, S. & Fjellanger, E. 2002: A study of basement structures and onshore-offshore correlations in Central Norway. *Norwegian Journal of Geology* **82**(4), 263-279.

Skilbrei, J.R., & Kihle, O. 1995: Reprocessing and Interpretation of the Hunting 1986 Aeromagnetic Data. *Geological Survey of Norway (NGU) Report* 95.026.

Skilbrei, J.R. 1992: Preliminary Interpretation of Aeromagnetic Data from Spitsbergen, Svalbard Archipelago (76-Degrees-79-Degrees-N) - Implications for Structure of the Basement. *Marine Geology* **106**, 53-68.

Skilbrei, J.R. 1991: Interpretation of Depth to the Magnetic Basement in the Northern Barents Sea (South of Svalbard). *Tectonophysics* **200**, 127-141.

Skogseid, J. & Eldholm, O. 1987: Early Cenozoic crust at the Norwegian continental-margin and the conjugate Jan-Mayen Ridge. *Journal of Geophysical Research-Solid Earth and Planets* **92**(B11), 11471-11491.

Skogseid, J., Planke, S., Faleide, J.I., Pedersen, T., Eldholm, O. & Neverdal, F., 2000: NE Atlantic continental rifting and volcanic margin formation. *In A. Nøttvedt et al. (eds) Dynamics of the Norwegian margin*. Geological Society Special Publications **167**, 295-326.

Smith, W.H.F. & Sandwell, D.T. 1997: Global sea floor topography from satellite altimetry and ship depth soundings. *Science* **277**, 1957-1962.

Spector, A. & Grant, F.S. 1970: Statistical models for interpreting aeromagnetic data. *Geophysics* 35(2).

Stavrev, P. & Reid, A. 2007: Degrees of homogeneity of potential fields and structural indices of Euler deconvolution. *Geophysics* **72**(1), L1-L12.

Storey, M., Duncan, R.A. & Tegner, C. 2007: Timing and duration of volcanism in the North Atlantic Igneous Province: Implications for geodynamics and links to the Iceland hotspot. Chemical Geology **241**(3-4), 264-281.

Talwani, M. & Eldholm, O. 1977: Evolution of the Norwegian-Greenland Sea. *Geological Society of America Bulletin* **88**, 969-999.

Thompson, D.T. 1982: EULDPH: A new technique for making computer-assisted depth estimates from magnetic data. *Geophysics* **47**, 31-37.

Thurston, J.B. & Brown, R.J. 1994: Automated source-edge location with a new variable pass-band horizontal-gradient operator. *Geophysics* **59**(4), 546-554.

Thurston, J.B. & Smith, R.S. 1997: Automatic conversion of magnetic data to depth, dip, and susceptibility contrast using the SPI (TM) method. *Geophysics* **62**(3), 807-813.

Tisseau, J. & Patriat, P. 1981: Identification des anomalies magnétiques sur les dorsales à faible taux d´expansion: méthode des taux fictifs. *Earth and Planetary Science Letters* **52**, 381-396.

Unternehr, P. 1982: Etude structurale et cinèmatique de la Mer de Norvége et du Groenland-Evolution du microcontinent de Jan Mayen. *Phd Thesis, Université de Brest*, Brest, 227 pp.

Verduzco, B., Fairhead, J.D., Green, C.M. & MacKenzie, C. 2004: The meter reader-New insights into magnetic derivatives for structural mapping. *The Leading Edge* **23**, 116-119.

Verhoef, J., Roest, W.R., Macnab, R., Arkani-Hamed, J. & Members of the Project Team, 1997: Magnetic anomalies of the Arctic and North Atlantic Oceans and adjacent land areas. *Geological Survey of Canada Open File* 3125

Ville, J. 1948: Théorie et applications de la notion de signal analytique. *Cables et Transmissions* **2A**, 61-74.

Vine, F.J. & Matthews, D.H. 1963: Magnetic anomalies over oceanic ridge. *Nature* 199, 947-949.

Vogt, P.R., Taylor, P., Kovacs, L.C., & Johnson, G.L. 1979: Detailed aeromagnetic investigation of the Arctic Basin. *Journal of Geophysical Research* **84**, 1071-1089.

Vogt, P.R., Ostenso, N.A. & Johnson, G.L. 1970: Magnetic and bathymetric data bearing on sea-floor spreading north of Iceland. *Journal of Geophysical Research* **75**, 903-920.

Vogt, P.R. 1986. Geophysical and geochemical signatures and plate tectonics. *In B. Hurdle (ed.). The Nordic Seas*. Springer-Verlag, New York, 411-662.

Vogt, P.R., Johnson, G.L. & Kristjansson, L. 1980: Morphology and magnetic anomalies north of Iceland. *Journal of Geophysics* **47**, 67-80.

Wegener, A., 1924: The Origins of Continents and Oceans. New York, Methuen, p. 212.

Winograd, S. 1978: On Computing the Discrete Fourier Transform. *Mathematics of Computation* **32**(141), 175-199.

11 LIST OF FIGURES

12 ANNEXE

CHANNEL	DESCRIPTION
LINE_NUMBER	Line name TGS system
LONGITUDE_WGS84	Longitude, WGS84, °.
LATTITUDE_WGS84	Latitude, WGS84, °.
XUTM29, YUTM29	Projected coordinates, UTM29N WGS84, m.
ALT_RADAR_mV	Radar Altitude, miniVolt.
ALT_RADAR_m	Radar Altitude, m.
ALT_RADAR_foot	Radar Altitude, foot.1 foot = 0.3048 meters
ALT GPS_m	GPS Altitude, m.
GEOID_ALT	Altitude geoid- ONLY IN THE NGU DATABASE
PFI	GPS parameter ONLY IN THE NGU DATABASE
HDOP	GPS parameter ONLY IN THE NGU DATABASE
GPSSatellites	Numbers of GPS satellites (it seem)
X_MAG1	X fluxgate (This is fluxgate sensor parallel to transverse axis of aircraft)- ONLY IN THE TGS DATABASE
Y_MAG2	Y fluxgate (This is fluxgate sensor parallel to longitudinal axis of aircraft)- ONLY IN THE TGS DATABASE
Z_MAG3	Z fluxgate (This is fluxgate sensor parallel to vertical axis of aircraft)- ONLY IN THE TGS DATABASE
Raw1, Raw2	Measured magnetic field (1, 2 sensors), nT- ONLY IN THE TGS DATABASE
MAGFIELD1, MAGFIELD2	Compensated magnetic field (1, 2 sensors), nT - ONLY IN THE TGS DATABASE
MAGFIELD_RAW	Magnetic field raw (average (MAGFIELD1 + MAGFIELD2)/2)
BaseMag_NAME	Base station Measured magnetic variations, nT+NAME of the station **
Dirunal_DV	Diurnal deviation
Comp2_HP1c	Result of High pass filtering of COMP2 (cut-off length – 1 c), nT. For QC.
Comp2_D4	Result of 4-Differences filtering of COMP2, nT. For QC.
MAGTIME	Mag time NGU system
Date_YYMM	Date (year, month)
Date_DD	Date (day of the month)
JDay	Julian day (day of the year)
UTCTIME	Time
	LEVELLING CHANNELS
MAGFIELD_RAW_naudy	Magnetic field raw +Naudy filter 5FID=50m
MAG_LAG	Lag correction channel (lag shift=-5 FID=50m)+interpolation
IGRF_FIELD	IGRF field along each profiles (nT)
I	Inclination (degree)
D	Declination (degree)

MAG_LAG_IGRFcorr	MAG_LAG corrected from IGRF field
Mag_tie_corr	Copy of MAG_LAG_IGRFcorr
CROSS_LEVEL	Miss-tie value (LINE_LEVEL - TIE_LEVEL
CROSS_DIFF	Miss-tie value (LINE_LEVEL - TIE_LEVEL)
CROSS_GRAD	Miss-tie value (LINE_LEVEL - TIE_LEVEL
mag_tie_corr_ItLEVELLING_It5	Levelling channel of the magnetic total field after 5 iteration, using inversion (Iterative level Geosoft)
Difference_with_without_LEV	Difference between mag_tie_corr_ItLEVELLING_It5 and Mag_tie_corr (Statistical leveling errors)
dcor_noise	Microlevelling decorrugation noise level
miclevGeosoft	Microlevelled magnetic channel
JAS12_MAG_TF_FINAL	**Copy of miclevGeosoft. Final JAS-12 magnetic total field corrected (leveling and microlevelling). Channel used for filtering in the JAS-12 report.**

Table 12-1: Description of the Geosoft database channels

JAS12_PHASE1_TGS_DATABASE
JAS12_PHASE2_NGU_DATABASE

L570 NGU database=Line 58 TGS reflight in 2012 for calibration

**

BaseMag NGU: RORVIK
BaseMag TGS: Leirvogur Magnetic Observatory, Iceland.

Note that in the merged database, some columns include dummies because the channels were no present in one or the other database

The end.